

**Version for ASAS Release 2  
July 2, 2019**

**ICE, CLOUD, and Land Height Satellite  
(ICESat-2) Project**

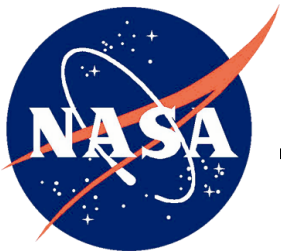
**Algorithm Theoretical Basis Document  
(ATBD)  
for  
Ocean Surface Height**

**Prepared By:  
ICESat2 Science Definition Team Ocean Working Group**

**Contributors**

**James Morison  
David Hancock  
Suzanne Dickinson  
John Robbins  
Leeanne Roberts  
Ron Kwok  
Steve Palm  
Ben Smith  
Mike Jasinski  
Bill Plant  
Tim Urban**

**/Code:**



---

**Goddard Space Flight Center  
Greenbelt, Maryland**

## **Abstract**

This document describes the theoretical basis of the ocean processing algorithms and the products that are produced by the ICESat-2 mission. It includes descriptions of the parameters that are provided in each product as well as ancillary geophysical parameters, which are used in the derivation of these ICESat-2 products.

***ICESat-2 Algorithm Theoretical Basis Document for Ocean Surface Height (ATL12)***

***Release 002***

**Release Date 01 October 2019**

## **CM Foreword**

This document is an Ice, Cloud, and Land Height (ICESat-2) Project Science Office controlled document. Changes to this document require prior approval of the Science Development Team ATBD Lead or designee. Proposed changes shall be submitted in the ICESat-II Management Information System (MIS) via a Signature Controlled Request (SCoRe), along with supportive material justifying the proposed change.

In this document, a requirement is identified by “shall,” a good practice by “should,” permission by “may” or “can,” expectation by “will,” and descriptive material by “is.”

Questions or comments concerning this document should be addressed to:

ICESat-2 Project Science Office

Mail Stop 615

Goddard Space Flight Center

Greenbelt, Maryland 20771

***ICESat-2 Algorithm Theoretical Basis Document for Ocean Surface Height (ATL12)***

***Release 002***

## **Preface**

This document is the Algorithm Theoretical Basis Document for the processing open ocean data to be implemented at the ICESat-2 Science Investigator-led Processing System (SIPS). The SIPS supports the ATLAS (Advance Topographic Laser Altimeter System) instrument on the ICESat-2 Spacecraft and encompasses the ATLAS Science Algorithm Software (ASAS) and the Scheduling and Data Management System (SDMS). The science algorithm software will produce Level 0 through Level 4 standard data products as well as the associated product quality assessments and metadata information.

The ICESat-2 Science Development Team, in support of the ICESat-2 Project Science Office (PSO), assumes responsibility for this document and updates it, as required, as algorithms are refined or to meet the needs of the ICESat-2 SIPS. Reviews of this document are performed when appropriate and as needed updates to this document are made. Changes to this document will be made by complete revision.

Changes to this document require prior approval of the Change Authority listed on the signature page. Proposed changes shall be submitted to the ICESat-2 PSO, along with supportive material justifying the proposed change.

Questions or comments concerning this document should be addressed to:

Tom Neumann, ICESat-2 Project Scientist  
Mail Stop 615  
Goddard Space Flight Center  
Greenbelt, Maryland 20771

### Change History Log

Revision Level	Description of Change	SCoRe No.	Date Approved
	ATL12 ATBD "ICESat-2_Ocean_atbd_07022019" is ICESat2_JMdraft_Ocean_atbd_06262019.docx changes and edits up through July 2, 2019		

***ICESat-2 Algorithm Theoretical Basis Document for Ocean Surface Height (ATL12)***

***Release 002***



## Table of Contents

Abstract.....	2-i
CM Foreword .....	ii
Preface .....	iv
Change History Log .....	v
List of TBDs/TBRs .....	vii
Table of Contents .....	8
List of Figures .....	12
List of Tables .....	15
1.0 INTRODUCTION.....	17
2.0 OVERVIEW AND BACKGROUND INFORMATION.....	19
2.1 Open Ocean Background .....	20
2.2 The Importance of Waves.....	22
2.2.1 Waves and Reflectance.....	22
2.2.2 Waves and Sea State Bias .....	24
2.2.3 ICESat2 Height Statistics and Sea State Bias.....	30
3.0 Open Ocean Products.....	38
3.1 Open Ocean Surface Height (ATL12/L3A) .....	38
3.1.1 Height Segment Parameters .....	39
3.1.2 Input from IS-2 Products.....	41
3.1.3 Corrections to height (based on external inputs).....	41
3.2 Gridded Sea Surface Height - Open Ocean (ATL19/ L3B) .....	43
3.2.1 Grid Parameters .....	43
4.0 ALGORITHM THEORY.....	47
4.1 Introduction.....	47
4.2 ATL12: Finding the surface-reflected photon heights in the photon cloud .....	47
4.2.1 Selection of Signal Photon Heights .....	49
4.2.2 A Priori Sea State Bias Estimation and Significant Wave Height .....	53
4.3 ATL12: Correction and Interpretation of the Surface Height Distribution .....	54

4.3.1	Separating the Uncertainty due to Instrument impulse response .....	54
4.3.2	Characterizing the Random Sea Surface .....	57
4.3.3	Maximum Likelihood Versus Expectation Maximization .....	58
4.4	Calculation of Uncertainty.....	58
4.5	ATL19: Gridding the DOT and SSH.....	59
5.0	Algorithm Implementation .....	60
5.1	Outline of Procedure.....	60
5.2	Input Parameters .....	60
5.2.1	Parameters Required from ICESat-2 Data .....	60
5.2.2	Parameters Required from Other Sources .....	63
5.2.3	Control Parameters for ATL12 Processing .....	63
5.3	Processing Procedure .....	63
5.3.1	Coarse Surface Finding and Setting of Segment Length.....	63
5.3.2	Processing Procedure for Classifying Ocean Surface Photons, Detrending, and Generating a Refined Histogram of Sea Surface Heights .....	66
5.3.3	Processing to Characterize Long Wavelength Waves, Dependence of Sample Rate on Long Wave Displacement, and <i>A Priori</i> Sea State Bias Estimate	71
5.3.4	Processing Procedure for Correction and Interpretation of the Surface Height Distribution .....	75
5.3.5	Applying a <i>priori</i> SSB Estimate.....	91
5.3.6	Expected Uncertainties in Means of Sea Surface Height.....	91
5.4	Ancillary Information .....	93
5.4.1	Solar Background Photon Rate and Apparent Surface Reflectance (ASR) 93	
5.4.2	Additional Ancillary Data.....	93
5.5	Output Parameters .....	95
5.6	Synthetic Test Data .....	98
5.7	Numerical Computation Considerations .....	104
5.8	Programmer/Procedural Considerations .....	104
5.9	Calibration and Validation.....	104
6.0	Browse Products .....	105

6.1	Data Quality Monitoring .....	105
6.1.1	Line plots (each strong beam) .....	105
6.1.2	Histograms (each strong beam) .....	105
7.0	Data Quality .....	106
7.1	Statistics .....	106
7.1.1	Per orbit statistics .....	106
8.0	TEST DATA .....	109
8.1	In Situ Data Sets.....	109
8.2	Simulated Test Data .....	109
9.0	CONSTRAINTS, LIMITATIONS, AND ASSUMPTIONS .....	110
9.1	Constraints .....	110
9.2	Limitations .....	110
9.3	Assumptions.....	111
10.0	References.....	112
	ACRONYMS .....	114
	GLOSSARY .....	115
	APPENDIX A: ICESat2 Data Products .....	116
	APPENDIX B: Sea State Bias Computations for a Photon Counting Lidar.....	121
	APPENDIX C: Expectation-Maximization (EM) Procedure .....	127
11.0	References.....	129



## List of Figures

<u>Figure</u>	<u>Page</u>
Figure 1 - Characteristics of an idealized distribution .....	51
Figure 2. Geodetic height.....	53
Figure 3. Reflectance as modeled .....	55
Figure 4. Typical Gram-Charlier distribution .....	56
Figure 5. Trochoidal shape of surface waves .....	57
Figure 6. Short wave MSS & standard deviation MSS.....	58
Figure 7. Simulated surface displacement and MSS.....	59
Figure 8. Height due to long-waves & MSS.....	59
Figure 9. Height due to long-waves & probability .....	60
Figure 10. Surface return heights from MABEL .....	64
Figure 11. ATL 12 processing block diagram.....	78
Figure 12 Coarse, smoothed, and fine histograms .....	82
Figure 13. Block diagram for the ATL19 gridding.....	89
Figure 14. Coarse, smoothed, final Mabel histograms .....	98
Figure 15. Instrument impulse response histogram .....	104
Figure 16. Probability density functions of the synthetic SSH .....	105
Figure 17. Synthesized received probability density functions .....	106
Figure 18. Single-sided spectra of the received PDFs .....	110
Figure 19. Single-sided spectrum of impulse response .....	110
Figure 20. Single-sided amplitude spectra of the Wiener filters .....	111
Figure 21. Single-sided amplitude spectra of the surface PDF .....	112
Figure 22. PDF of SSH and calculated PDF for 8000 photons.....	114
Figure 22. PDF of SSH and calculated PDF for 800 photons.....	116





## **List of Tables**

<u>Table</u>	<u>Page</u>
Table 1 Reflectance.....	61
Table 2 Input parameters (Source: ATL03).....	62
Table 3 Input parameters (Source: ATL09) .....	92
Table 4 Control Parameters - Surface Finding.....	94
Table 5 Control Parameters for Refined Surface Finding and Analysis.....	96
Table 6 Output (See Appendix A for full product specifications).....	124
Table 7 ATL12 Output Variables for per Orbit Statistics.....	135
Table 8 ATL12 Test Data .....	138



## **1.0 INTRODUCTION**

This ATBD will cover the retrieval of Sea Surface Height (SSH) from ICESat2 ATLAS laser returns. For the purpose of this early draft, the levels of spatial and temporal averaging to be included are still to be definitively decided, as is the amount of high-level data processing to produce gridded fields of SSH and such things as Dynamic Ocean Topography (equal to SSH minus the geoid).

Other ICESat2 ATBDs describe the products for ice sheets, vegetation, sea ice and inland water, the latter two having close relations with the ocean ATBD. Technical ATBDs include orbit and attitude calculations, corrections for atmospheric path-length delays, and corrections for changes in the surface heights due to tidal effects; these other data are needed to convert ranges into absolute surface heights with respect to the geoid.

This document will address sampling the ice-free world ocean, but not ice-covered or inland waters, because the ICESat-2 sampling scheme is different for the open ocean, generally sampling strong beams only, and because the defining characteristics, (e.g., well developed surface waves) are unique to the open ocean. It will include coastal ocean waters. Because of the increasing seasonal variation in the sea ice cover, the boundary between the open-ocean and ice-covered ocean domains will vary seasonally. This ATBD will share some considerations and features with the sea ice ATBD (surface finding algorithm, concern for tides and the geoid) and the vegetation and inland water ATBD (concern with waves in large bodies of inland water). We consider as input data level 2 photon heights for each of the three strong beams along the satellite track along with the required navigation information. (In certain ocean regions near land or sea ice, the weak beams may be also be active. In these cases the weak beam data over the ocean should be processed the same way as the strong beams.) As output, the processing to be described will produce ATL12/L3A (Appendix A), the height of the open ocean surface at a length scales between 70 m (100 Hz) and 7 km (1 Hz), determined by an adaptive surface finding algorithm. Output will include estimates of height distributions (decile bins), significant wave height, surface slope, and apparent reflectance.

Section 2 provides an overview of the ocean altimetry issues,

Section 3 discusses the ocean products the parameters that reside in each product as well as ancillary geophysical parameters, of interest to science users, which are used in the derivation of these ICESat-2 products.

Section 4 provides a theoretical description of the algorithms used in the derivation of the ocean products.

Section 5 describes the specific implementations of the algorithms that are relevant to the development of the processing code. Included here are both algorithmic details and some software architecture details on throughput optimization and computational loading.

Section 6 provides the processing requirements for data quality monitoring and control. These are provided to users as quality assessments of the individual parameters on

each file and to provide criteria for automatic quality control to facilitate timely distribution of the product to the users. Summary statistics or images are provided that allow users to easily evaluate (or Browse) whether the data would be useful and of adequate quality for their research, and as needed to aid in the quick approval or disapproval of products prior to public distribution.

Section 7 describes the testing and validation procedures that are planned.

## 2.0 OVERVIEW AND BACKGROUND INFORMATION

The Advanced Topographic Laser Altimeter System (ATLAS) consists of both LIDAR and altimetry subsystems that will fly on the dedicated platform comprising the mission referred to as ICESat2, the Ice, Cloud, and Land Height Satellite. The following subsections discuss the basic concepts of how ATLAS works and the Level 2 data that we will turn into sea surface height. It then describes the basic properties of the sea surface and how these relate to processing the ICESat2 data.

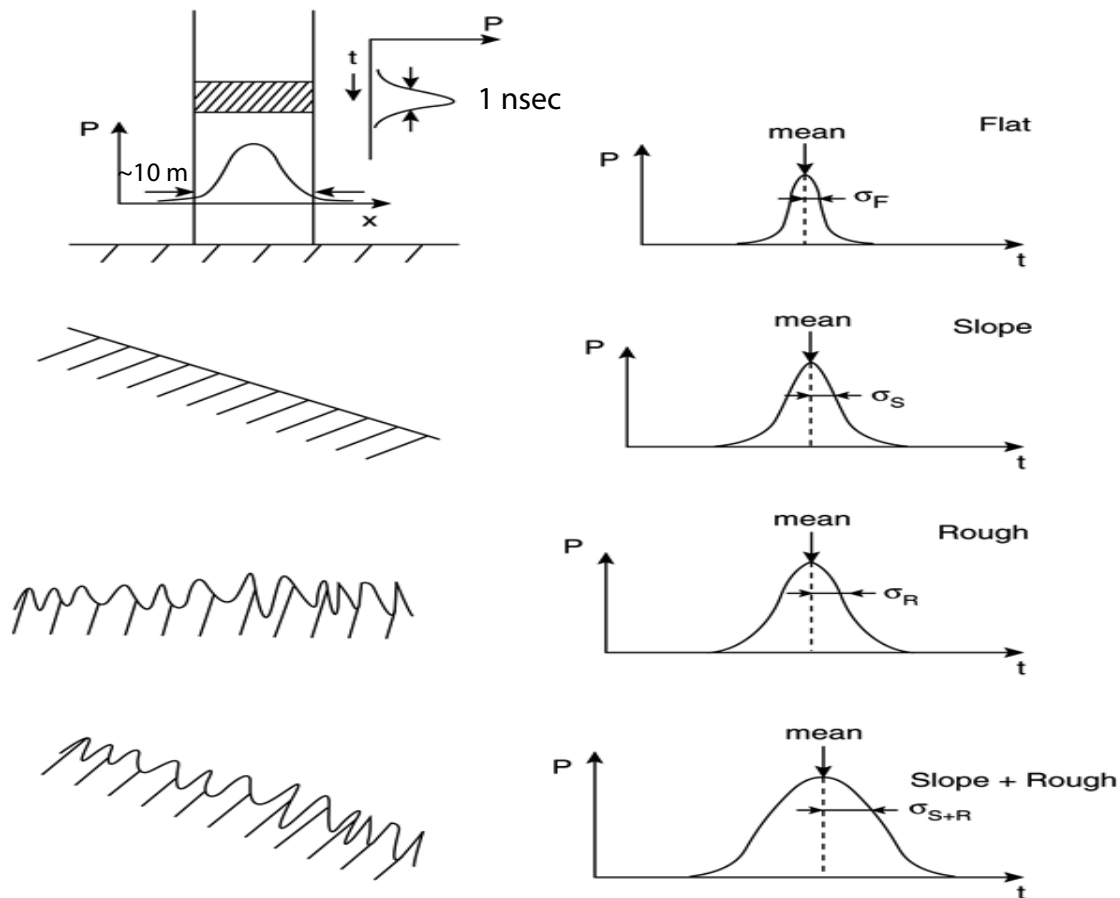


Figure 1 - Characteristics of an idealized distribution of ATLAS return photon arrival times assuming a Gaussian instrument impulse response and a reflective surface with Gaussian roughness. In general surface slope and roughness both broaden the return distribution. For the open ocean the slope effect is likely negligible compared the effect of roughness due to surface waves. An important complication is that surface waves produce a non-Gaussian surface due to their broad troughs and narrow peaks.

The primary purpose of the ATLAS instrument on the ICESat2 mission is to detect surface height changes. With respect to the ocean, these represent Sea Surface Height (SSH). By way of technical history, the predecessor of ICESat2 ATLAS, the ICESat GLAS instrument, used a laser altimeter to measure the range to the surface. Ranges were determined from the measured time between transmission of the laser pulse and detection of the pulse reflected from the surface and received by the instrument. The GLAS laser footprint diameter on the surface due to beam spreading was nominally 70 m, and the duration of the transmitted pulse was 4 ns.

The ICESat2 ATLAS instrument will sample at a higher rate, 10 kHz with 1-2 ns pulse width, with a smaller intrinsic footprint, ~10 m (Fig. 1), and will rely on detecting the range traveled by individual photons. Experience with MABEL suggests that the instrument impulse response distribution, due largely to the variation in transmit times for the photons of each pulse, will be non-Gaussian with significant skewness. Consequently, four points will be measured on the out going pulse distribution and these will be part of the ICESat2 raw data stream. The distribution of receive times of the surface-reflected photons, and hence photon heights, will be broadened by the distribution of surface heights within the footprint as depicted in Figure 1 for an idealized Gaussian distribution of photon return times or heights. Photon return-times will be digitized in 200 ps (3 cm) range bins. However, the origination time of a photon within a pulse is unknown, and the uncertainty in the time of flight of a single photon will be between 1 and 1.5 ns RMS (30-45 cm flight time) due mostly to the laser pulse width, with smaller contributions from other effects within the instrument. This time uncertainty corresponds to between 15 and 22 cm RMS in range.

Return photon arrivals will be aggregated at a scale depending on the surface type being over flown. Over the open ocean, short segment aggregates will be retrieved at 100 Hz (100 pulses over 70 m of track) and long segment aggregates retrieved up to 1 Hz (10,000 pulses over 7 km corresponding to 25 times the atmospheric sample rate. In contrast, to ensure adequate detection of leads, over sea ice return photons may be taken at the maximum rate of 10 kHz (each pulse every 0.7m).

## **2.1 Open Ocean Background**

Over distances of cm to a few hundred meters, the sea surface is roughened by waves and ocean swell, but over distances of many km, the sea surface is almost flat. Nevertheless, surface slopes and long-wavelength undulations are present, caused by variations in Earth's gravity field represented by the geoid, ocean currents, and variations in atmospheric pressure and seawater density. Satellite radar altimeters have shown remarkable success in measuring sea-surface height and tracking changes in circulation and mean sea level. However, the major satellite radar altimeters, TOPEX/Poseidon/Jason do not go beyond about 62° latitude, and thus miss the sub-Arctic seas and southern parts of the Southern Ocean that are critical to the global overturning circulation and the fate of

sea ice in the ice covered Arctic Ocean. ICESat2 over the open ocean will cover this gap between the temperate lower-latitude ocean and the sea ice covered regions of the Arctic and Antarctic

As discussed above, the distribution of ICESat photon return times, or apparent heights from Level 2 processing, will be determined by the mean SSH, the mean surface slope and a surface roughness within the footprint. Among these, the effect of sea surface slope on the photon height distributions should be small compared to the effect of roughness due to surface waves. For the aggregation scales above, the SSH is the sum of the geoid height (fixed in time and on the order of meters amplitude), the dynamic ocean topography (DOT, on the order of centimeters to tens of centimeters amplitude) associated with mean surface currents, tides (mainly diurnal to semidiurnal periods with amplitudes of up to meters), and sea surface atmospheric pressure (SAP, as much as 10s of cm). As a first approximation, SSH can be estimated as the mean of the distribution of photon heights within a vertical window about the ellipsoid or an approximated canonical sea surface height (e.g., 30 m from the estimated geoid) and over the along track aggregation scales to be decided as above.

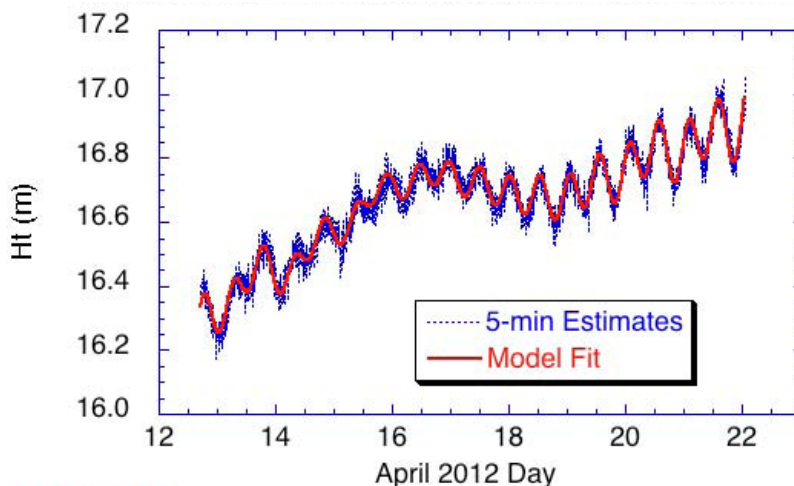


Figure 2. Geodetic height measured with a geodetic grade dual-frequency GPS with PPP processing at a drifting ice camp near the North Pole plotted with an *ad hoc* model of ocean tides and longer variations assumed due to the geoid and DOT variations. The geoid variations over the 60 km drift are estimated to be 60 cm, tides 10 cm peak to peak, and DOT only a few cm.

However, the special and rapidly varying nature of the sea surface pose challenges with the interpretation and aggregation of meaningful SSH from ICESat2 photon heights. It is useful to outline these issues here, keeping in mind that the magnitude of the most sought after components of the SSH signal, changes in DOT and mean SSH, are significantly smaller than most of the other components of SSH.

Tides, Medium-Frequency Changes in Circulation and

Aliasing: ICESat2 will complete one orbit of the

earth in about 1.5 hours. The repeat period is under discussion but has mainly settled on 91 days. More importantly, many of the most important areas and times to oceanographers are prone to being stormy and overcast. Thus, it is likely that ICESat will only get good surface returns infrequently over large and important regions of the open ocean. Tides and medium to high-frequency changes in circulation will seriously alias into slowly sampled regions, making aggregation into valid long-term means difficult. At some point in ICESat2

ocean processing this will have to be addressed. This can be done by referencing the photon heights to the SSH predicted by a model such as the Ocean Model of Circulation and Tides (OMCT) as used for dealiasing gravity data from the Gravity Recovery and Climate Experiment (GRACE). Essentially, the predicted tidal and circulation contributions to SSH are subtracted from each ICESat2 height observation, the residual is averaged monthly and similarly averaged model result is added back in. Only the error in the modeled response is aliased. This procedure may be beyond the scope of Level 3 data, but the same ocean model could be used to more narrowly and accurately define the photon height band that needed to be considered in selecting true ocean surface photon returns.

The Geoid, Narrowing the Window on Photon Returns, and Measuring Mean DOT: ICESat2 photon heights will be heavily influenced by the geoid. An example of this for the Arctic Ocean near the North Pole (Fig. 2) shows changes in SSH associated with geoid height variations of about 1 cm per km of horizontal distance. Given the potentially patchy and temporally sparse character of ICESat2 ocean returns, the variations in the geoid from a geoid model (e.g., EGM2008 or an improvement thereon using GOCE and GRACE data) should be extracted from the basic height data to allow meaningful spatial means of SSH to be made. The spatial resolution of these geoid corrections is an important issue affecting the smaller DOT and SSH signals.

Surface Atmospheric Pressure and the Inverse Barometer Effect: Changes in surface atmospheric pressure a short time scales directly cause an inverse deflection of SSH. As with tides, ocean circulation changes, and the geoid, these direct pressure disturbances at the time and place of each ICESat2 photon retrieval should be estimated and removed from estimated SSH before aggregation to avoid spatial and temporal aliasing. This will require bringing atmospheric reanalysis products or direct SAP observations into the processing stream. Knowledge of the likely inverted barometer effect will also help in narrowing the range of return photon heights and thus identifying photons returning from the sea surface.

## **2.2 The Importance of Waves**

### **2.2.1 Waves and Reflectance**

Surface Waves Reflectance, Scattering, and the Sea State Bias: We expect surface waves to have dominant effects on the ICESat2 returns from the open ocean.

Reflectance: Surface waves and wind speed have a critical effect on reflectance. Menzies et al. [Menzies et al., 1998] indicate reflectance is given by:

$$R = W R_f + (1-W) R_s + (1-W R_f) R_u \quad (1)$$

where  $R$  is the total backscatter or retro-reflectance,  $W$  is the fraction of the ocean covered by foam (up to 0[1] for winds above about 7 m/s)),  $R_f$  is the reflectance of foam,

$R_s$  is reflectance due to specular reflection from the wave roughened surface, and  $R_u$  is the apparent reflectance due to light that penetrates and comes back up through the surface anywhere it is not reflected downward by surface foam.

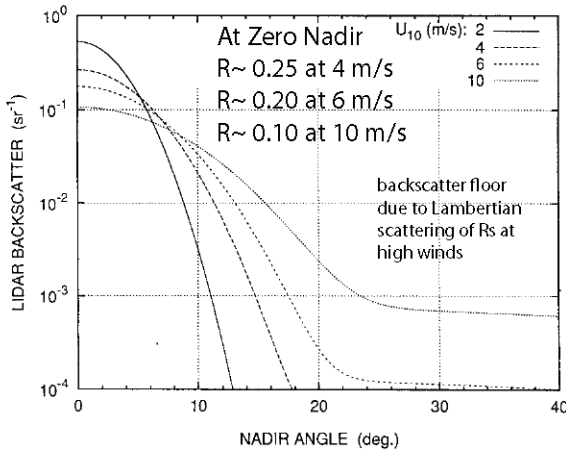


Figure 3. Reflectance as modeled by *Menzies et al.* [1998] as a function of wind speed and nadir angle.

$R_f$  is considered diffuse Lambertian scattering independent of incidence angle. As we would expect,  $R_s$  is highly dependent on incidence angle and is the dominant form of backscatter.  $R_u$  is Lambertian but it is usually small, about 0.0075 maximum. Menzies et al, model the reflectance owing to  $R_s$  and  $R_f$ . The main part is an inverse relation between  $R_s$  and the variance in surface slope,  $R_s \sim 1 / \langle S^2 \rangle$ , due to wind generated surface waves. They use a relation between wind speed,  $U_{10}$ , and  $\langle S^2 \rangle$  by Wu [Wu, 1972] based on results of Cox and Munk [Cox and Munk, 1954];  $\langle S^2 \rangle$  goes up as the log of wind speed. The model

results are given in Figure 3, wherein the strong dependence on nadir angle is apparent. The exception is at high wind speeds where the backscatter from foam starts to become important, flattening the  $R$  curves for nadir angles greater than  $30^\circ$ . Other results in [Menzies et al., 1998] show good agreement between the model and data from the Lidar In-

Table 1

Case	Description	Water Reflectance, Lambertian, Green	Water Reflectance, Lambertian, IR
10a	Conical Scan, low wind	0.28	
10b	Conical Scan, medium wind	0.12	
10c	Conical Scan, high wind	0.07	

Modeled Reflectance for Zero Nadir Angle from Figure 4, *Menzies et al.* [1998] Figure 1

Case	Description	Water Reflectance, Green
10a	Wind = 4 m/s	0.25
10b	Wind = 6 m/s	0.20
10c	Wind = 10 m/s	0.1

space Technology Experiment (LITE) shuttle lidar mission of September 1994. The modeled reflectance essentially agrees with the values for reflectance used in the design

performance study for ATLAS (Table 1). However, most important with respect to this ATBD, the dependence of sea surface directional reflectance on surface wind stress suggests a method for deriving surface wind speed from ICESat2 measurements of sea surface backscatter. Working solely with ICESat2 observations, we can conceivably estimate  $U_{10}$  from reflectance. As we discuss below this estimate of  $U_{10}$  may be used with SWH, estimated from the variance of the photon height distributions, to calculate the Sea State Bias in ICESat2 SSH measurements.

### 2.2.2 Waves and Sea State Bias

Sea state bias is a critical issue that has been found to relate to the amplitude of waves and to wind forcing. The SSB problem is fundamental and has received considerable attention with respect to radar altimetry [Elfouhaily et al., 2000; Gaspar et al., 1994]. Improved corrections for SSB in the TOPEX altimeters have been developed [Chambers et al., 2003] relating SSB to wind speed,  $U_{10}$ , and significant wave height (SWH, the trough-to-crest height of the highest third of ocean waves) measured with the radar altimeter. Studies using both laser and radar instruments find a fair degree of commonality [Chapron et al., 2000; Vandemark et al., 2005]. Urban and Schutz [Urban and Schutz, 2005] compare ICESat-derived SSH with TOPEX/Poseidon SSH and find a negative 10 cm bias in ICESat relative to the radar altimeters. They indicate that the bias is unknown, but that it may be

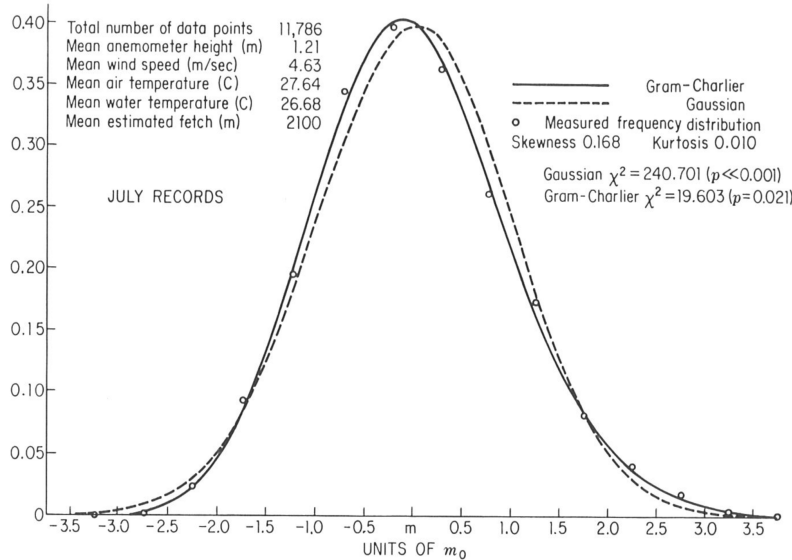


Figure 4. Typical Gram-Charlier distribution sea surface height in a wave environment. The positive skewness and excess kurtosis (Gaussian skewness and excess kurtosis = 0) is due to truncation at low heights and a long tail at high heights. Fig. 7.4-1 of Kinsman [1965].

related in part to sea state, and they recognize that the radar altimeter is corrected for SSB using a relation with SWH. Unfortunately, a SWH parameter was not provided with the ICESat GLAS data, a shortcoming we cannot repeat with ICESat2.

The ICESat ATBD document made the assumption that sea surface heights are Gaussian distributed, so that with a Gaussian transmission pulse, the reflected pulse received by ICESat could be assumed to be Gaussian also. In fact, the ocean surface is not Gaussian and this affects the reflection of either radar or light from the surface. The

distribution of surface height in a wave-covered ocean (Fig. 4) is typically given by the Gram-Charlier distribution [Kinsman, 1965]. For this the third and fourth moments of the distribution expressed as skewness and kurtosis (or excess kurtosis = kurtosis-3) are important and indicate truncation of the distribution at low heights with a long tail at high heights. This reflects the shape of surface waves.

In general, surface waves have trochoidal shape, with narrow, steep sided peaks and relatively broad flat troughs (Fig. 5). This applies particularly to the short-wavelength

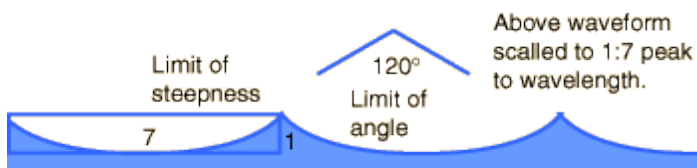


Figure 5. Trochoidal shape of surface waves at the limit of steepness, wavelength equal to seven times height. The sharply peaked trochoidal shape is common to all surface waves longer than capillary waves, which have an inverted trochoidal shape. At the steepness limit the waves begin to break. (Figure from <http://hyperphysics.phy-astr.gsu.edu/hbase/waves/watwav2.html>)

surface is composed of swell and wind waves. Swell is the manifestation of large long-wavelength waves that are mature and forced elsewhere. The wavelengths are long enough that in spite of significant amplitude, the slopes are small and the waves are linear and well represented by sine waves. The wind waves, forced by local wind, are shorter (down to capillary wavelengths) and steeper with trochoidal shape. In the extreme, when they reach the limit of steepness (Figure 5), they break and form white caps. As such, these waves can by their shape affect sea state bias in altimetry returns, but their direct bias is small because their amplitudes are small. However, several studies including one done for the development of this ATBD, suggest the character of the short waves varies with position on the larger linear waves and thus can contribute to large SSB.

We have performed a study of the effect of long waves on short waves and their implications for ICESat-2 sea state bias. We have sought a model sea surface suitable for driving the NASA GSFC numerical ATLAS simulator. With this we will be able to test the performance ATLAS over the open ocean and evaluate such things as the sea state bias in mean sea surface height measurements. There are two elements to our artificial sea surface. The first is a realistic representation of the height and surface slope due to waves with wavelengths greater than the 10-m footprint of an ATLAS laser pulse. This captures the bulk of the energy in the wave field. Because the waves are long, a linear model of them can be used. The second component is a measure of the distribution of surface slopes due

waves proximally forced by wind. Photons striking the upper portions of these wave are less likely to be returned to ICESat2 than photons striking the lower portions of wave surfaces; peaks are undersampled relative to troughs resulting in a sea state bias (SSB) in estimates of SSH based on the mean of an ICESat2 photon height distribution or, in the case of ICESat, mean arrival time of a return pulse.

However, commonly the sea

to the waves with wavelengths less than 10-m laser pulse footprint of ATLAS. The distribution of surface slopes, shifted by the instantaneous slope of the long wave component determines the probability of ATLAS finding a specular return resulting from a photon laser pulse. Knowing this as a function of surface height and slope due to the long-wave will allow us to predict SSB in the ICESat2 measurements.

We have taken advantage of a code simulating long-wave surface height based on a long-wave spectrum developed by Donelan et al. (1985) to model the long wave component of our ATLAS ocean surface model (AOSM).

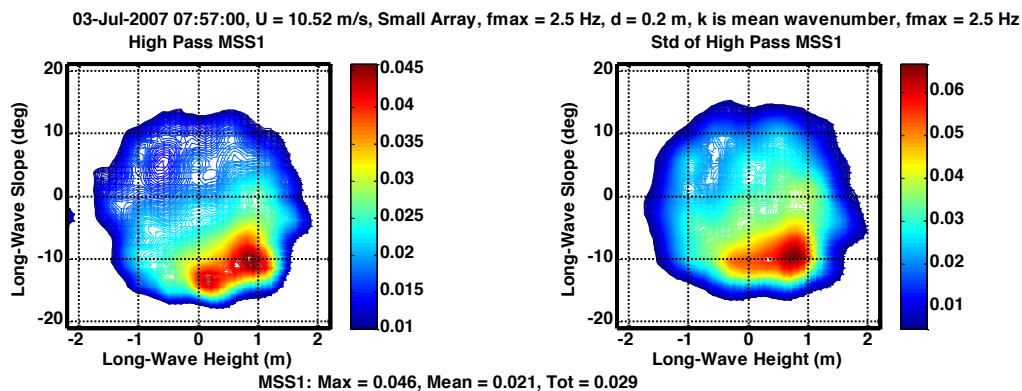


Figure 6. Left – Short wave MSS as a function of long-wave height and slope. Right – the standard deviation of short wave MSS as a function of the same variables.

Our main challenge has been determining the mean square slope (MSS) representing short-wave roughness and its dependence on long-wave height and slope. We had thought that wave wire or some other type of field observation would have been analyzed or at least readily available to determine this relationship, but surprisingly we found no such analysis in the literature. Instead we have analyzed original data from a four-wire wave-gauge array on the University of Miami’s ASIS buoy [Will Drennan, personal communication]. The work is described in detail by W. Plant.[*Plant, 2015a; b*] but we provide a brief synopsis here. The ASIS Buoy data were collected in the Deep Ocean Gas Exchange Experiment in the Atlantic Ocean on July 3, 2007 at a wind speed between 10 and 11 m/s. The wave-gauges measure surface heights at orthogonal positions 20 cm apart, so in principle any two gauges measure slope directly down to  $\sim 2$  Hz or wavelength  $\sim 0.8$  m in this case. A single gauge yields a time series of height, and with the dispersion relation, the spectrum of height can be converted to a spectrum of surface slope. The single gauge approach is complicated by the need for the dispersion relation for the short waves to be modified to account for the orbital velocities of the long waves. We have compared the two approaches and found the two-gauge approach yields results inconsistent with the known gauge spacing. However, we can account for the complications to the dispersion relation and produce consistent estimates of the short-wave slope spectra. Spectra for higher

frequencies (wave numbers) than 2 Hz are extrapolated using the observed frequency<sup>-1</sup> spectral slope at 2 Hz. The MSS is obtained by integrating the spectrum out to a maximum frequency (100 Hz), above which increases in MSS are negligible.

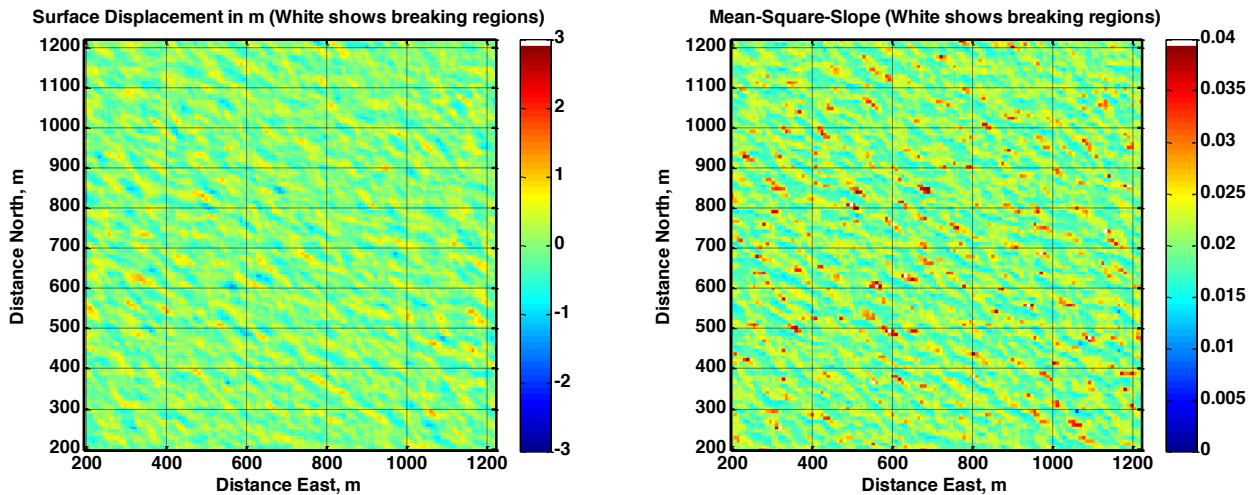


Figure 7. From *Plant* [2015b]. Left – Simulated 2D surface displacement , Right – 2D variation of short-wave mean MSS values that were calculated up to 2 Hz. Downwind direction is from upper right to lower left.

The preliminary result of this analysis has been the dependence of observed short-wave MSS on the slope and height of the long-waves (Fig. 6). MSS is greatest for high heights and

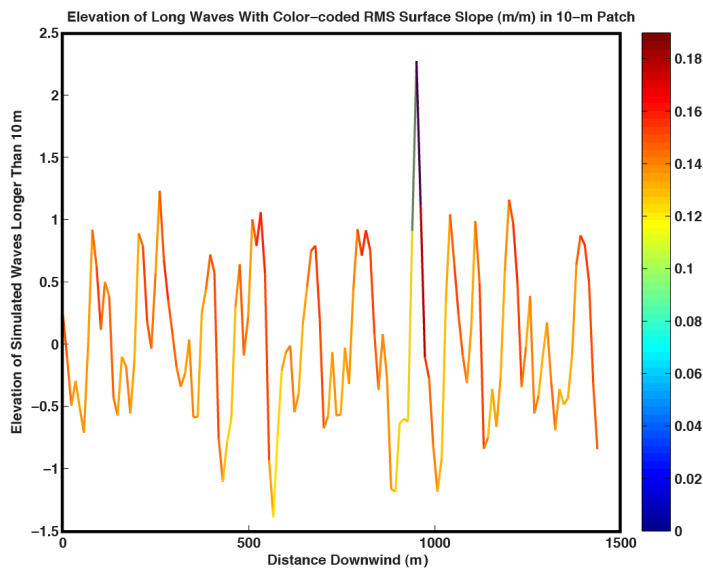


Figure 8. Height due to long-waves versus distance downstream (from upper right corner to lower left in Figure A-left) with color-coded corresponding MSS from Figure A-right.

negative slopes, i.e., on the upper part of the downwind face of the long-waves. The correlation maps of Figure 6 have been used as a table to specify MSS in a 10-m spot corresponding to the 2D model of long-wave slope and displacement derived from the Donelan spectrum. A realization of long wave height and slope and the corresponding 10-m spot MSS is shown in Figure 7 [*Plant*, 2015a&b].

A 1-D slice in the downwind direction (Figure 8) through the combined data from Figure 7 illustrates how MSS slope tends to increase on the upper parts of the downwind face of

waves. It also illustrates in a much-simplified way how the interplay of the short-wave MSS and long-wave amplitude and slope can affect the probability of specular reflection and consequent sea state bias. For each point along the slice, we assume the surface is normally distributed with a mean equal to the local long-wave slope and a variance equal to the MSS corresponding (Fig. 6) to the long-wave height and slope. The probability of any one photon striking the spot finding a specular point is estimated as the integral of the idealized slope distribution between plus and minus  $10^{-5}$  radians (Fig. 9).

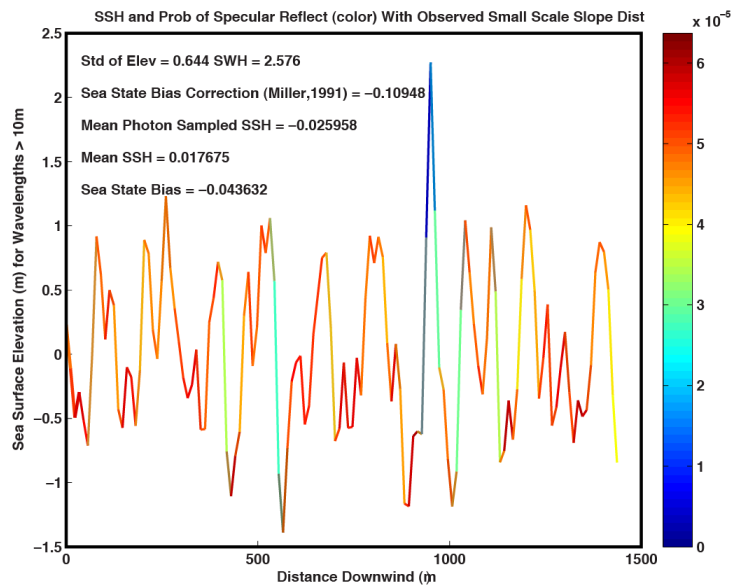


Figure 9. Height due to long-waves versus distance downstream (from upper right corner to lower left in Figure 6-left) with color-coded probability of specular reflection.

on the long-waves. The simulation uses a linear spectrum-based representation of the long waves; there are no trochoidal long waves. When we repeat the probability weighted mean calculation assuming the MSS is uniformly equal to the cut-wise mean MSS, the mean height is only biased -0.7 cm.

There are improvements to be made to this wave analysis, including drawing the MSS values as random values from distributions conditioned on long-wave slope and height and doing the analysis for data at other wind speeds. However, this limited sample suggests that that the systematic distribution of small-scale surface roughness towards the upper parts of the waves produces a negative sea state bias because the wave troughs provide more specular returns than the wave crests. This type of bias is likely compounded by shape-induced biases due to any nonlinearity in the long-waves. As a result is that the SSH observations by ICESat-2 will be non-Gaussian and exhibit sea state bias.

The probability of finding a specular point is highest in the troughs and at the peaks, likely because the mean slope is zero. However, the increased MSS in the upper parts of the waves tends to decrease the probability of specular points for higher heights. We know the true mean height along the slice is 1.8 cm. Weighting the samples of height by the probability of a specular point yields a photon sampled mean height of -2.6 cm, a -4.4 cm bias. Interestingly this is about twice the typical sea state bias for radar altimeters for the 10-m wind speed at the time of these ASIS Buoy observations. The bias is not due to nonlinearities

However, further analysis of the wave gauge data taking into account both the Doppler shifting of the small scale wave by long wave orbital velocity of the long waves and the effects of convergence by long-wave orbital velocity on short wave amplitude results in almost the opposite dependence of short wave slope on long wave height and slope and suggests a positive sea state bias. {SEE BILL'S LATEST WRITEUP}, Consequently, lacking further data about the dependence of short wave characteristics on long wave position, we seek a method whereby the SSB can be determined from ICESat-2 data themselves.

### **2.2.3 ICESat2 Height Statistics and Sea State Bias**

Sea State Bias (SSB) is the error in average sea surface height measured by an altimeter due to the dependence of altimeter returns over different parts of waves. The SSB for radar altimeters is negative because the troughs of waves reflect more radar energy than the crests of waves. This effect is averaged over many surface waves encompassed by the typical radar footprint (e.g. 17 km for CryoSat2). Improved corrections for SSB in the TOPEX altimeters have been developed [*Chambers et al., 2003*] relating SSB to wind speed,  $U_{10}$ , and significant wave height (SWH, the trough-to-crest height of the highest third of ocean waves) measured with the radar altimeter. All these studies have measured the SSB empirically by comparing SSH measured by various means or comparing repeat measurements at the same location by a given satellite for different sea states and wind speeds [*Hausman and Zlotnicki, 2010*].

Studies using both laser and radar instruments find a fair degree of commonality [*Chapron et al., 2000; Vandemark et al., 2005*]. Urban and Schutz [*Urban and Schutz, 2005*] compare ICESat-derived SSH with TOPEX/Poseidon SSH and find a negative 10 cm bias in ICESat relative to the radar altimeters. They indicate that the bias is unknown, but that it may be related in part to sea state, and they recognize that the radar altimeter is corrected for SSB using a relation with SWH. Unfortunately, a SWH parameter was not provided with the ICESat GLAS data, a shortcoming we cannot repeat with ICESat2.

#### ***A Priori* Estimation of SSB Using Only Altimeter Data**

The small footprint of ICESat2 (17 m for  $4\sigma$  diameter Gaussian intensity), short distance between pulse/footprint centers (0.7 m) and the essential point sampling at random positions within the footprint of the photon counting lidar, may present an opportunity to capture the shape of the long wave length, energy containing surface waves. If this is true it will be possible to estimate ICESat2 sea state bias solely on the basis of contemporaneous ICESat2 returns without resorting to outside data or even comparison with past ICESat2 returns. The key is evaluating the rate of surface photon returns as a function of surface height. A simple example of this considers an ocean surface with sea surface height,  $H_{ss}$ , disturbed by a long sinusoidal surface wave with amplitude  $A$ , plus random normally distributed perturbations,  $N$ :

$$Y = H_{SS} + A \sin \frac{2\pi}{L} x + N(0, \sigma) \quad 2$$

If ICESat-2 samples this surface at a constant rate,  $\bar{r}$  surface returns per meter, the surface will be uniformly sampled, and there will be no sea state bias. If there is a variation in sample rate,  $r$ , that is correlated with variations in sea surface height such that:

$$r = \bar{r} + \alpha A \sin \frac{2\pi}{L} x, \quad (3)$$

where  $\alpha$  is the covariance between  $r$  and  $y$  normalized by the variance in  $y$ :

$$\alpha = \frac{\text{cov}(ry)}{\sigma_y^2}. \quad (4)$$

The surface height estimate,  $y_e$ , over a large distance,  $X$ , is the average of the true height weighted by the sample rate:

$$\begin{aligned} y_e &= \frac{1}{X\bar{r}} \int_0^X Yr dx = \frac{1}{X\bar{r}} \int_0^X (H_{SS} + A \sin \frac{2\pi}{L} x + N)r dx \\ &= \frac{1}{X\bar{r}} \int_0^X (H_{SS} + A \sin \frac{2\pi}{L} x + N)(\bar{r} + \alpha A \sin \frac{2\pi}{L} x) dx \end{aligned} \quad (5)$$

$$\begin{aligned} &= \frac{1}{X\bar{r}} \int_0^X H_{SS}(\bar{r} + \alpha A \sin \frac{2\pi}{L} x) dx \rightarrow \frac{1}{X\bar{r}} \int_0^X H_{SS}\bar{r} dx \\ &+ \frac{1}{X\bar{r}} \int_0^X (A \sin \frac{2\pi}{L} x)(\bar{r} + \alpha A \sin \frac{2\pi}{L} x) dx \rightarrow \frac{1}{X\bar{r}} \int_0^X (A \sin \frac{2\pi}{L} x)(\alpha A \sin \frac{2\pi}{L} x) dx \\ &+ \frac{1}{X\bar{r}} \int_0^X N(\bar{r} + \alpha A \sin \frac{2\pi}{L} x) dx \rightarrow 0 \end{aligned} \quad (6)$$

For  $X$  equal to an integral number of wavelengths or very long compared to many wavelengths:

$$y_e = \frac{1}{X\bar{r}} \left[ H_{SS} X\bar{r} + \frac{X}{2} \alpha A^2 \right] = H_{SS} + \frac{\alpha A^2}{2\bar{r}} \quad (7)$$

So sea state bias,  $SSB = y_e - H_{SS}$ , is:

$$SSB = y_e - H_{SS} = \frac{\alpha A^2}{2\bar{r}} \quad (8)$$

Similarly, Arnold et al. [Arnold et al., 1995] in evaluating Ku-band SSB measured with a combination of radar altimeters and capacitive wave wires mounted on an oil platform in

the Gulf of Mexico, calculate electromagnetic bias,  $\varepsilon$ , due to the variation of backscatter coefficient with surface waves as

$$\varepsilon = \frac{\sum_{i=1}^N b_i^0 \eta_i}{\sum_{i=1}^N b_i^0} \quad (9)$$

where  $\eta_i$  is the measured surfaced displacement corresponding  $A \sin(2\pi x/L)$  in our idealized example and  $\sigma_i^0$  is the measured backscatter coefficient proportional to the rate of photon returns,  $r$ . Our  $\alpha$  expressed in the terms of Arnold et al. [1995] is:

$$\alpha = \frac{\frac{1}{N} \sum_{i=1}^N b_i^0 \eta_i}{\frac{1}{N} \sum_{i=1}^N \eta_i^2}, \quad (10)$$

so their expression for electromagnetic bias is the same as the SSB for the sine wave example:

$$\varepsilon = \frac{\sum_{i=1}^N b_i^0 \eta_i}{\sum_{i=1}^N b_i^0} = \frac{\frac{\alpha}{N} \sum_{i=1}^N \eta_i^2}{\frac{1}{N} \sum_{i=1}^N b_i^0} = \frac{\alpha A^2}{2\bar{r}} = SSB \quad (11)$$

Appendix B gives a more detailed derivation of (9) in terms of rate of photon return for a photon counting lidar in place of cross-section. It also describes the corresponding EM or sea state bias in the higher moments of the surface distribution (Equation B20 in Appendix B).

### Example of SSB Determination for the Uneven Data Distribution of a Photon Detecting Pulsed Lidar Altimeter

Application of 8 is straightforward, and is accurate in cases such as that of *Arnold et al.* [1995], in which the spacing of the data is uniform and the energy of the return is measured and is the metric weighting the sampled surface height. In that application, each radar pulse was powerful and the range and footprint size were small so that every pulse returned a surface height. The energy returned with each pulse and its correlation with height could be expected to aggregate into the SSB over the much larger footprint of satellite radar altimeter.

This is not totally true in the case of the pulsed photon-counting altimeter such as MABEL or ICESat2; the return rate of the height samples is not uniform and the average sea surface height is derived from the histogram of photon heights. The correlation between

the rate of surface returns and surface height is only one of several components in the histogram skewness. Other contributors to skewness include the true distribution to surface height and subsurface returns. However, the dominant surface waves typically have long wavelengths and are nearly linear so they can be approximated as sine waves. With this in mind, we experimented with fitting multiple sine waves to the raw history of unevenly spaced photon surface heights and calculating the correlation of observed rate of surface returns with the sine wave fit to yield an estimate of SSB using equation 7. However, in testing the method on Greenland Sea MABEL data and Airborne Topographic Mapper (ATM) over the Pacific, we found the method was sensitive to finding the correct wavenumbers for the spectral decomposition of the ocean surface. A more robust method is to average both the raw photon heights from the surface finding step and the rate of photon returns in evenly spaced bins of along track distance. The covariance of these averages is then used to evaluate equation 7 for the sea state bias. This method is easier to

automate and accounts for more of the energy in the wave field than does the harmonic method.

MABEL data from the Greenland Sea in April 19, 2012 illustrates the application of equation 7. In this example, a 9-km length of MABEL track is broken into 3-km segments. Each 3-km segment is divided into 300 10-m along track bins. Once surface finding selects the surface photon heights, these are edited with two passes of a 3-standard deviation editor, and detrended with along track distance.

The rate of photon returns is computed from the along-track record of sample intervals. The record of sample intervals is given by the difference between successive surface photon along-track locations. For the MABEL data shown here, the sample spacings vary significantly but average a little over one meter. To align the data, the surface height and sample position are interpolated to the center of the sample interval by computing the

Aggregate SSB Determination for three 3-km MABEL Greenland Sea Segements 4/25/2012

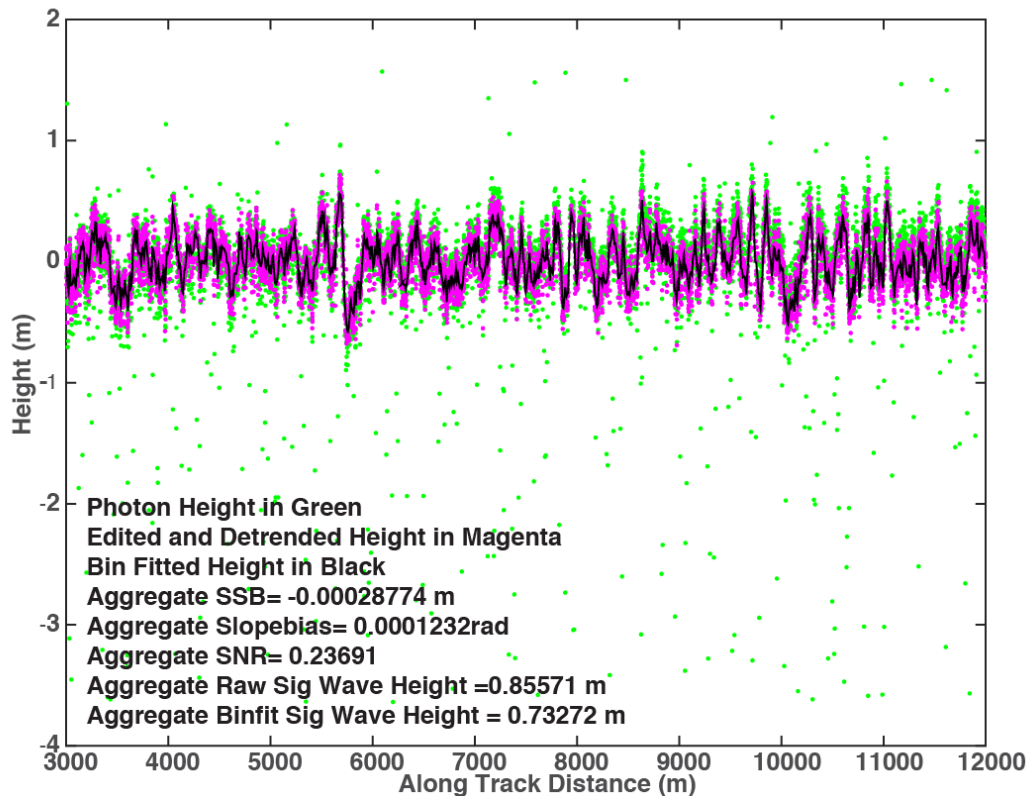


Figure 10. Surface return heights in green from MABEL transit over the Greenland Sea versus distance along track. Three-sigma edited and detrended heights are plotted in green and a 10-m bin averages are plotted in black. The bin averages and a priori SSB estimates were computed in three 3000-m segments and aggregated to yield SSB=-0.00029 m.

average of pairs of successive sample heights and position. The resulting records of sample rate are then accumulated in 10-m along track bins and averaged. The bin averaged sample intervals are then inverted to yield the bin averaged sample rate. Interpolating height to the center of the sample interval and bin-averaging sample interval before inverting avoids an apparent increase in average sample rate in adjacent sample intervals.

The bin averaged sample rates and heights are then used to compute the height rate covariance and the average sample rates used in X8 to determine SSB.

The method is illustrated in Figure 10 with MABEL data gathered April 25, 2012 over the Greenland Sea. Aggregated over three 3000-m intervals, the correlation of photon return rate and height is very low on average, and results in a sea state bias of 0.3 mm, a result that is not surprising given the low energy of the surface waves with a significant wave height (4 x Std of height) of less than a meter for the raw photon returns and the bin-averaged heights.





### **3.0 OPEN OCEAN PRODUCTS**

#### **3.1 Open Ocean Surface Height (ATL12/L3A)**

The ATL12 product contains sea surface heights over the ice-free oceans for each of 3 ATLAS strong beams. It provides the most basic data from ICESat-2: the sea surface height at a given point on the open ocean surface at a given time plus parameters needed to assess the quality of the surface height estimates and to interpret and aggregate the estimates over greater distances. These heights can be used in comparisons of ICESat-2 data with other geodetic data and as inputs to higher-level ICESat-2 products, particularly ATL19.

Heights over the sea surface are defined for ocean segments with variable length at variable intervals along the ground track; this is necessary to adapt to the reduced photon counts from the low but variable reflectance of the open ocean surfaces. It also is consistent with surface finding routine used for sea ice covered ocean (ATL07/L3A). Based on initial data ATLAS gets on the order of one surface reflected photon per laser pulse or 0.7 m of track, so 100 photon retrievals in the adaptive surface detection algorithm would result in segment lengths of about 70 m. Given the 17-m footprint of the ICESat2 beams, this is equivalent to 4 independent (non-overlapping) spatial samples of the sea surface.

In future developments, heights in marginal ice zones or coastal zones may be defined for shorter variable length segments sampled at variable intervals along the ground track to adapt to the patches of water between sea ice in the first instance or near land in the second instance. These overlap regions are those that are classified as both sea ice and ocean (marginal ice zone) or land and ocean (coastal zone). The methods of distinguishing open ocean from sea ice and land and setting the ocean segment lengths in these mixed regions are TBD.

In purely ocean regions, only strong beams will be active, but in the marginal ice zone and coastal zone overlap regions, the three weak beams will also be active and should be processed identically to the strong beams and output in addition to the strong beam results as part of the ATL 12 ocean product. This is to facilitate a rational merging of the open ocean products (ATL12) and sea ice products (ATL07) and coastal products (ATL??) related to sea surface height.

However, the presence of ocean surface waves in the open ocean far from marginal ice zone and coastal regions, present challenges and an opportunity. The non-Gaussian character of ocean surface waves and the scattering and effective reflectance of the ICESat2 photons likely cause a negative sea state bias (SSB). We anticipate that the higher order moments of the photon height statistics will allow us to better estimate SSB. We will estimate for each ATL12 variable segment at minimum the mean, standard deviation, skewness and kurtosis of the height distribution. These four moments can be determined from the means and standard deviations of a 2-component Gaussian mixture, which will also provide a mixing ratio for the two components. These higher moments make it possible to characterize not only the mean sea surface height, but also the sea state and

likely sea state bias of the height estimate.

However, it is necessary to accumulate large number of surface reflected photons to make meaningful estimates of the higher moments of the height distribution. Given the low number of returns from open water (e.g., 0[1 photon / pulse]), and considering that ocean waves can have wavelengths of hundreds of meters, to get meaningful statistics over open water with significant wave activity requires accumulating data over several kilometers. The atmospheric cloud flag (***layer\_flag*** in ATL03) is used in part in setting the ocean segment length required to achieve a minimum number of photons. It and other geophysical data such as the background photon rate from ATL09 and the geoid are reported every 400 pulses (25 Hz) or 14 geo-bins. Consequently, over the open ocean, we will seek a minimum photon count of 8,000 photons equivalent to about 5.6 km or 280 20-m geo-bins for meaningful higher order statistics.

### **3.1.1 Height Segment Parameters**

#### **3.1.1.1 Geolocation/Time**

The location is the mean location of designated signal photons used as input to the surface finding procedure. The time is the mean time of designated signal photons used as input to the surface finding procedure.

#### **3.1.1.2 Height**

This is the mean height estimate from the surface detection algorithm. Quality metrics include: Confidence level in the surface height estimate based on the number of photons, the background noise rate, and the analysis from the detection algorithm.

#### **3.1.1.3 Subsurface-scattering corrections**

Subsurface-scattering corrections are yet to be determined. They are expected to be minimal for the deep open ocean where the water is clear, but may be significant in near coastal regions where more scattering elements are to be expected in the water. These conditions will be most likely to be apparent as positive skewness in the return height distributions especially as correlated with outside measures of surface color or scattering. Guided by the treatment of subsurface scattering for the Inland Water ATBD and as we are able to develop relations between photon height distribution skewness and other evidence of scattering, we will derive an appropriate correction for subsurface scattering where applicable and provide it as an output of ATL12.

#### **3.1.1.4 First-photon-bias corrections**

Pending further analysis, given the low apparent reflectance of the ocean surface first-photon-bias corrections will likely not be needed for the ocean products.

#### **3.1.1.5 Height Statistics**

The photon statistics describe the distribution of the population used in the surface-tracking algorithm. These parameters include the: number of photons, histogram of the population, and, at minimum the mean, variance, and skewness, and kurtosis.

#### **3.1.1.6 Initial Sea State Bias Correction and Surface Wave Properties**

As discussed in 2.2.3, ICESat-2 gives us a unique opportunity to make an a priori estimate of sea state bias using only the heights from the surface finding system. The approach is to use the surface photon heights to estimate the surface height and the rate of photon returns in 10-m along-track segments. The correlation of height and return rate normalized by the average photon return rate is the EM or sea state bias. This will be estimated from the surface photon height record before separation of the impulse response in the height histogram and made available as output. The standard deviation of photon heights over the whole segment will be provided as a measure of SWH (=4xStd.) that can be compared with reanalysis products. The standard deviation about the 10-m bin averages will also be provided as an estimate of the energy of short waves that arguably has an important effect on reflectance and sea state bias.

#### **3.1.1.7 Solar Background**

The solar background photon rate, *backgr\_r\_200*, is estimated as an average over 50 laser pulses in ATL03. It is based on the photons included in the altimetric histogram less the photons deemed signal (surface or cloud reflected) photons by ATL03. This is converted to a rate in photons per second by dividing by the total time window reduced by the duration of the window containing signal photons.

For ATL12 we will use the average of the estimated solar background. We will not use the predicted solar background rate based on the solar zenith angle, the solar flux in the receiver etalon's pass band, and the effective aperture of the detectors.

#### **3.1.1.8 Apparent Reflectance**

This is based on the comparison of expected photon counts over a sea surface with SWH estimated from photon statistics and photon counts from the actual surface (see 2.2.1.4 and Fig. 2).

### **3.1.2 Input from IS-2 Products**

#### **3.1.2.1 Classified photons (Level 2)**

Photons classified as to whether the height is signal, noise, or extended signal. These have a confidence as to type.

#### **3.1.2.2 Atmosphere (Level 3)**

Relative/calibrated backscatter, background rates, cloud statistics at 25 Hz.

### **3.1.3 Corrections to height (based on external inputs)**

In anticipation of higher level processing, the standard height products will include a number of corrections applied to the raw height estimates. For example to reduce aliasing problems, corrections for high-frequency and fine spatial scale variations in SSH (e.g., tides and other high frequency ocean circulation changes) that may be inadequately sampled by ICESat2 should be applied before averaging. Estimates of these corrections will be given here. All corrections will be given in terms of height so that to apply a correction, users will add it to the height estimate, and to remove it they will subtract it. Additional corrections that some users may decide to apply will be provided with the product.

#### **3.1.3.1 Geoid adjustment (Static)**

Heights are adjusted for local geoid height using mean tide EGM2008 model being reported by ATL03 as taken from the mean-tide EGM2008 model.

#### **3.1.3.2 Atmospheric delay corrections**

Heights will be corrected based on an atmospheric model, giving corrections for total delay correction that accounts for wet and dry wet troposphere.

Corrections will be available for the forward-scattering bias, based on available atmospheric-scattering data and an estimate of the attenuation calculated from the apparent surface reflectance.

#### **3.1.3.3 Dynamic Atmospheric Correction and the Inverse Barometer Effect (IBE, time-varying)**

Heights are corrected for the inverse barometer effect due to the direct application of atmospheric pressure to the sea surface and the dynamic changes forced by wind. ICESat-2 has adopted the utilization of global, empirical, 6-h, AVISO MOG2D,  $1/4^\circ \times 1/4^\circ$  grids to be used as a near-real time Inverted Barometer (IB) and Dynamic Atmospheric Correction (DAC)[*Carrère and Lyard, 2003*]. These grids are forced by the European Center for Medium-Range Weather Forecasting (ECMWF) model for the surface pressure and 10-m

wind fields. This combined correction typically has amplitude on the order of  $\pm 50$  cm [Markus *et al.*, 2016].

#### **3.1.3.4 Tidal corrections (time-varying)**

Heights are corrected for:

Solid earth tides (*tide\_earth*): Solid earth tides are derived using IERS (2010) conventions are  $\pm 30$  cm max (details in ATL03 ATBD section 6.3.3)

Ocean load tides (*tide\_load*): The local displacement due to ocean loading (-6 to 0 cm) derived from ocean tide model GOT4.8. Details in ATL03 ATBD, section 6.3.1

Pole tide (*tide\_pole*): Pole tides include both solid earth and ocean pole tides. These each are computed via IERS (2010) conventions. Details are found in ATL03 ATBD sections 6.3.5 and 6.3.6, respectively.

Ocean pole tide (*tide\_oc\_pole*): Ocean Pole Tide -Loading due to centrifugal effect of polar motion on the oceans (2 mm, max), subsumed in Pole tide (*tide\_pole*)

Ocean tides (*tide\_ocean*): Ocean Tides including diurnal and semi-diurnal (harmonic analysis), and longer period tides (dynamic and self-consistent equilibrium) ( $\pm 4$  m) are from the GOT4.8. Details in ATL03 ATBD, section 6.3.1.

Equilibrium tides (*tide\_equilibrium*): Equilibrium long-period tide computed using a subroutine attached to GOT4.8 called LPEQMT.F by Richard Ray. It is a Fortran routine in which fifteen tidal spectral lines from the Cartwright-Tayler-Edden tables are summed. (See section 6.3.1 of the ATL03 ATBD.)

#### **3.1.3.5 Wind and SWH Estimates**

Surface winds and significant wave height for forecast/reanalysis products will be taken from an appropriate source such as the ECMWF and with the ATL12 product for comparison for comparison with ICESat-2 derivations of SWH as part of the sea state bias calculation.

## **3.2 Gridded Sea Surface Height - Open Ocean (ATL19/ L3B)**

This product, based entirely on Product ATL12/L3A with no external dependence, contains gridded monthly estimates of sea surface from all IS-2 tracks from the beginning to the end of each month. Below 60°N and above 60°S, the data are mapped on the curvilinear grid of the TOPEX/Poseidon with spacing equivalent to 0.25° of longitude. Above 60°N and below 60°S the grid data are mapped onto a planimetric grid using the SSM/I Polar Stereographic Projection equations at a grid spacing of about 24 km. The exact spacing of the Polar Stereographic grid should be adjusted to match the longitudinal spacing of the TOPEX/Poseidon grid at 60°S and 60°N, and the latitudinal spacing adjust to have an integer number of grid cells between 60°N (S) and the North (South) Pole.

### **3.2.1 Grid Parameters**

#### **3.2.1.1 Sea surface height estimate**

With only ATL12 needed as input, this derived product contains the statistical description of the sea surface (mean; standard deviation, skewness, kurtosis) within grid cell. These will be computed in two ways, using aggregation of segment histograms discussed in this section, and aggregation of segment moments discussed in Section 3.2.1.2. The gridding scheme will take as input from ATL12, the histograms of DOT accumulated in segments lying within each grid cell these will be combined by adding the photon counts from each segment in each height bin of each segment in the grid cell.

The average geoid height from each segment will also be averaged, weighted by the number of signal photons in each segment. Similarly, the weighted average a priori sea state bias will be computed.

The four moments of the aggregate histogram will be computed using the 2-Gaussian Maximum Likelihood approach. The sea state bias will be subtracted from the first moment to yield the mean grid cell DOT. The mean SSH can be calculated as the mean DOT plus the weighted average geoid height.

#### **3.2.1.2 Sea surface statistics histogram within grid**

We will perform a weighted average of the first through fourth moments of heights in the length segments that go into the grid cell in a given month. Being mindful that each segment going into a grid average may have a different underlying distribution, we will essentially compute the moments of the segment moments. Thus, the moments for the individual segments will be weighted by the number of surface photons in their segments relative to the total number of photons going into the grid cell and then added to yield estimates of the average moments in the grid cell. Where enough segments are included in a grid cell (e.g., more than 20), histograms of the moments going into the grid cell can be included as output.

### **3.2.1.3 Wave statistics within grid**

Estimates of SWH, short wave energy and SSB from the *a priori* estimation of sea state bias will also be grid-averaged with appropriate normalization for the number of surface photons in each segment.

### **3.2.1.4 Sea surface segments (Input)**

Sea surface height in surface height segments as described above with the time/location/quality of the sea surface height in the segment.





## **4.0 ALGORITHM THEORY**

In this section, we discuss the following topics:

1. Finding the collection of photon heights representing reflection from the sea surface.
2. Separating the surface wave generated variation in photon heights from other sources of variance.
3. Determining SWH and higher order measures of sea state
4. Formulating the best sea state bias correction

### **4.1 Introduction**

The main purpose of the algorithms developed here is the determination of Sea Surface Height (SSH). There are two main steps to determining sea surface height (SSH) from ICESat-2 photon heights (ATL-03) over the ocean. These are identifying photon heights that likely represent reflection from the sea surface, loosely termed surface finding (Sec. 4.2), and determining the correct statistics of the sea surface height distribution (Sec 4.3). Most importantly we seek the SSH equal to the mean of the height distribution. Because of the motion of the sea surface, surface finding over open water is inherently a search for a distribution of heights representative of the sea surface. Our main product will be the mean of this distribution over time, length and space scales to be determined as part of testing and analysis. In addition other properties of the distribution are useful for assessing the surface wave environment and biases in the SSH determination. Though we focus here on obtaining meaningful statistical distributions of sea surface heights, we have found it possible in tests with MABEL data to create meaningful moving 21-photon means of the heights from the photons designated signal photons by the surface finding routines. This gives a relatively high-resolution time- (or space-) series trace of the sea surface in fair agreement with the analysis using the high-resolution sea ice analysis. This may be used in experimental analyses for surface waves. Figure 11 shows the block diagram for the ATL12 processing to go from ATL03 photon data to along-track histograms and statistics of dynamic ocean topography. Figure 13 illustrates the gridding procedure to go from ATL12 products to ATL19 gridded DOT and SSH.

### **4.2 ATL12: Finding the surface-reflected photon heights in the photon cloud**

Surface finding over the open ocean rests on our limited experience with MABEL data over open water. With few surface returns per pulse and significant wave heights much less than the range of samples, the majority of the of the bins will contain only noise photons so that the median will equal the number of noise photons per bin. Thus the fundamental idea for surface finding is to identify as surface height bins, those bins with counts exceeding the median number of counts. In extreme cases where ICESat-2 encounters significant wave heights approaching the 30-m downlink range of bins, we may have to adopt a slightly different threshold such as the count value equal to or exceeding 20% of the bin population.

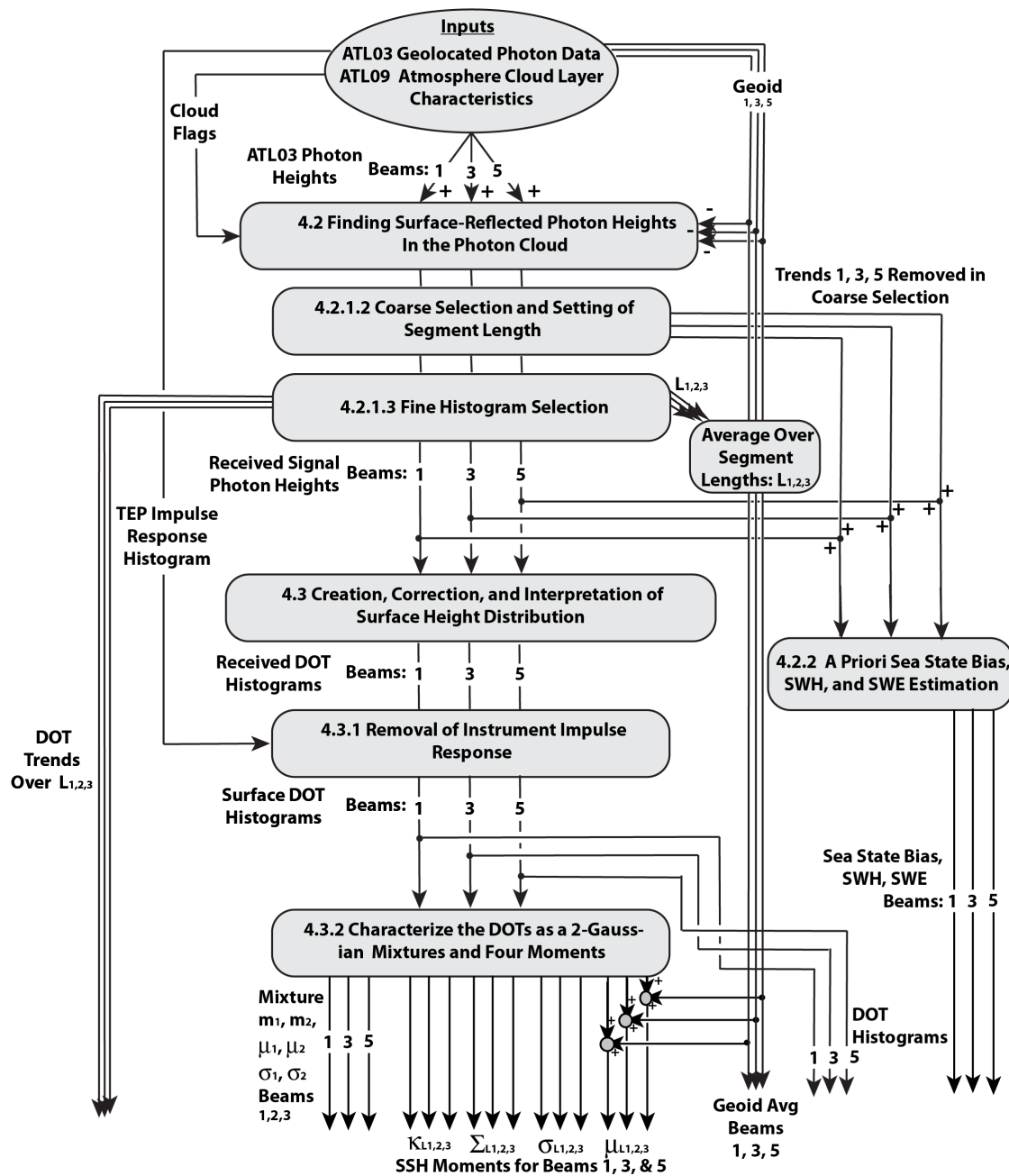


Figure 11. ATL 12 processing block diagram as discussed in Section 3 and 4.  $\mu$ ,  $\sigma$ ,  $\Sigma$ , and  $K$  denote mean, standard deviation, skewness, and kurtosis respectively.

We anticipate a large number of surface reflected photons may be needed to adequately resolve the higher moments of the sea surface height distribution. Also, fine spatial resolution is probably not required in most open ocean settings. Therefore, we will use a semi-adaptive scheme to accumulate segments long enough to capture up to 10,000 candidate surface photons. This will involve a coarse median-based selection and segment-length setting process (4.2.1.2). This will be followed by a finer scale histogram construction that includes median-based selection of surface photons, a detrending process, and repeat selection (4.2.1.3)

#### **4.2.1 Selection of Signal Photon Heights**

##### **4.2.1.1 Input to Selection of Photons:**

ATL12 will require ATL03 photon heights for each pulse in the ocean  $\pm 15$ -m downlink band and associated time geolocation, geophysical corrections (geoid, tides, dynamic atmospheric correction), and confidence level information, plus the cloud flag, *layer\_flag*, every 400 pulses from ATL09. Based on early discussions, this ATBD and the developmental software developed from it assumed that ICESat-2 over the ocean would downlink photon heights within  $\pm 15$  m of the EGM2008 geoid. Also aside from the  $\pm 15$ -m band about the geoid, no classification as to surface/non-surface photons is made for the ATL03 ocean results. As configured in December 2018, the Flight Science Receiver Algorithms (FSRA) downlinks photon heights in  $\pm 15$ -m band about heights chosen by signal finding procedure described in text in "ATLAS Flight Science Receiver Algorithms Version 3.7c". This identifies center heights over 200-shot major frames as those where the most photon heights relative to noise are found in adjacent bins of a coarse altimetry band. When operating in local daylight and in the presence of even thin clouds, and perhaps over parts of the ocean with reduced reflectance, for example wave slopes, the most popular height bin can shift to chance concentrations of noise photons up to 200 to 300 m above or below the geoid.

The resulting 30-m erroneous downlink bands of photon heights appear in 200-pulse major frames and one or two height bands supposedly bracketed by heights topping at (using the example of ground track 2 right) `gt2r/bckgrd_atlas/tlm_top_band1` and `gt2r/bckgrd_atlas/tlm_top_band2`, with heights given as `gt2r/bckgrd_atlas/tlm_height_band1` and `gt2r/bckgrd_atlas/tlm_height_band2`.

The most concerning problem is that when the downlink band is pulled away from the true surface we can arguably lose true surface reflected photons, biasing sea surface heights in some unknown direction and violating the assumptions of the ATL12 sea state bias determination. Unless the FSRA is changed to simply downlink all photon heights within  $\pm 15$  m of the geoid when over the ocean, the photons from major frames for which

the center of the downlink band is more than 2 or 3-m from the true sea surface should be eliminated from ATL03.

We will use heights referenced to the EGM2008 geoid and corrected for ocean tides, and dynamic atmospheric correction provided in ATL03.

We will use the signal confidence product in ATL03 to edit out the erroneous downlink bands. This grades each photon height return as to likelihood that it is a surface return by examining height bins at 50-pulse rate for signal to noise ratio in the context of noise level. Early ICESat-2 ocean data suggests that photon heights with high, medium, and low (4, 3, 2) confidence levels very seldom appear in the erroneous downlink bands. Further, the confidence level software assigns a fill-in confidence level of 1 to what would be zero confidence heights in order to fill a  $\pm 10$ -m (to be changed to  $\pm 15$ -m) bin about the high confidence heights. Therefore, in practice confidence level 1 or essentially covers the geoid  $\pm 15$ -m band and can be used to edit out the erroneous downlink bands.

Because we are using this ground-based editing, in the future we will have to investigate the effect on the sea surface height and SSB calculation of missing true surface photons not downlinked in the presence of erroneous downlink bands, probably by comparing daytime and nighttime data over the same region.

#### **4.2.1.2 Coarse Selection and Setting of Segment Length**

The process is basically to first establish a variable length (e.g., up to 7 km) ocean segment with enough (e.g.) photon heights to yield a histogram with reasonable moments up to 4<sup>th</sup> order.

1. Examine ocean depth and cloud parameters against control parameters to test for suitability for ocean processing.
  - Ignore data collected over land or too close to land. If ocean depth, *depth\_ocn*, is less than a depth, *depth\_shore*, specifying the effective shoreline of water for which ocean processing is appropriate, then proceed to next 14 geo-bin (400-pulse) segment. The default value for control parameter *depth\_shore* will be 10 m.
  - Similarly, if control parameter *layer\_swch* is equal to 1 and *layer\_flag* is equal to 1, then proceed to next 14 geo-bin (400-pulse) segment. When *layer\_swch* equals the default value, 0, the software will ignore the cloud cover in accepting data during coarse surface finding.
2. Correct for photon heights for short period and long period ocean tides (*gtxx/geophys\_corr/tide\_ocean and tide\_equilibrium*), the inverse barometer effect and the modeled dynamic response to the atmosphere (dynamic atmospheric correction, *gtxx/geophys\_corr/dac*),
3. Select only photon heights for which the signal confidence (*gtxx/signal\_conf\_ph*) is greater than or equal to 1. This will select photons in the likely surface  $\pm 15$ -m buffer window. Also delete any photon heights outside the band defined by geoid plus or minus half the height of the ocean downlink window (presently geoid  $\pm 15$ -m, to

become geoid  $\pm 20$ -m). (Is the height of the downlink band reported in ATL03 perhaps at the geoseg rate and if so, what is the variable name? The height is listed at the major frame rate. But it would be handier if it was at the geoseg rate)

4. Subtract the EGM2008 geoid from photon heights to reference all heights to the geoid. Note that EGM2008 includes a correction for the permanent or mean tide.
5. Establish an initial coarse histogram array,  $H_c$ , spanning  $\pm 15$  m with bin size  $B_1$  (TBD, e.g., 0.01 m) and a data array,  $A_{coarse}$ , for up to 10,000 photon heights and associated information (index, geolocation, time) plus noise photon counts. This will be populated with data for the coarse selection of signal photons.
6. Aggregate photon heights over 14 geo-bins (400-pulses) and construct a temporary 14 geo-bin (400-pulse) height histogram spanning  $\pm 15$  m with bin size  $B_i$  (e.g., 0.01 m). This is used to estimate a running total number of signal and noise photons. We suggest a bin size of 0.01 for consistency with later steps in the processing. The 14 geo-bin (400-pulse) segment should be aligned so that the once per 14 geo-bin (400-pulse, approximately 280 m along track distance) cloudiness flag, *layer\_flag* in ATL09, represents the aggregate effect of cloudiness and background radiation derived from solar zenith, *cloud\_flag\_ASR*, *cloud\_flag\_atm*, and *bsnow\_con*, during the 280-m segment.
7. Photons in the 14 geo-bin (400-pulse) histogram bins with greater than the  $Th_{Nc\_c}$  times the median number of photons,  $N_{median}$ , are candidate signal photons and photons in the bins with the median number of samples or less are considered noise photons. We have been using  $Th_{Nc\_c} = 1$  in our tests with early ICESat-2 data. Note that with few surface returns per pulse and significant wave heights much less than 30 m, the majority of the of the bins will contain only noise photons so that the median will equal the number of noise photons per bin. In extreme cases where ICESat-2 encounters significant wave heights approaching 30 m, we may have to adopt a slightly different threshold such as the count value equal to or exceeding 20% of the bin population.
8. Add the signal and noise photons from this 14 geo-bin (400-pulse) segment to the running total of candidate signal photons and noise photons, and add all the photons to the coarse histogram,  $H_c$ .
9. If the total number of candidate signal photons is greater than or equal to a minimum number,  $Th_{Ps}$  (e.g., 8,000), of photons or  $S_{egmax}$  (e.g., 25) 14 geo-bin (400-pulse) segments have been collected this defines an ocean segment, and we go on to Fine Selection (Sec 4.2.1.3) with the populated coarse histogram,  $H_c$ ,  $\pm 15$  m with bin size  $B_1$  (TBD, e.g., 0.01 m), and the data array,  $A_{coarse}$ . If the total number of signal photons is less than  $Th_{Ps}$ , repeat steps 4.2.1.2-2 to 4.2.1.2-5 above and intake another 14 geo-bin (400-pulse) segment until the ocean segment reaches a length of 7 km maximum. If the 7-km length is reached and there are less than a threshold number of photons (e.g. *photon\_min* = 4000), ignore that ocean segment and repeat 4.2.1.2-2 to 4.2.1.2-6. For photon counts above this in the 7-km segment, proceed to 4.2.1.3 and fine histogram based signal finding.

### 4.2.1.3 Fine Histogram Selection

1. Considering the coarse histogram array,  $H_c$ , perform a  $N_{bmv} = 20\text{-cm/B1}$  bin (e.g., 21 bins over 20-cm) moving bin arithmetic average incremented by 1 bin. Pad the ends of the smoothed histogram with  $N_{bmv}/2$  bins (equal the smoothed first and last values) to match the length of the original histogram.
2. The ASAS 5.1 finds the bin limits of the fine histogram as all the coarse histogram bins on either side of the maximum in the 20-cm smoothed histogram, from the  $J_{low}$  bin position to the  $J_{high}$  bin, where the smoothed histogram bin photon count is greater than the median of the smoothed histogram photon count. In practice with preliminary ATLAS data the median has usually been zero. Essentially, we have moved out from the middle of the histogram until the histogram levels fall to zero.

As of 6/4/2019, the developmental code finds preliminary the bin limits of the fine histogram as all the coarse histogram bins on either side of the maximum in the 20-cm smoothed histogram, from the preliminary  $J_{low}$  bin position to the preliminary  $J_{high}$  bin, where the coarse bin photon count is greater than the coarse histogram median. Then the average counts in the bins above the preliminary  $J_{high}$  are calculated and set equal to  $tailnoisehigh$  and the average counts in the bins below the preliminary  $J_{low}$  are calculated and set equal to  $tailnoiselow$ . Then we find the bin limits of the fine histogram as all the coarse histogram bins on either side of the maximum in the 20-cm smoothed histogram, from the final  $J_{low}$  bin position to the final  $J_{high}$  bin, where the final  $J_{low}$  bin position is that below which the smoothed histogram bin photon count is less than  $Th_{Nc\_f}$  times  $tailnoiselow$ , and the final  $J_{high}$  bin position is that above which the smoothed histogram bin photon count is less than  $Th_{Nc\_f}$  times  $tailnoisehigh$ . This procedure is better able to differentially remove subsurface noise returns and above surface returns.

3. Consider the time series of all the heights stored in  $A_{coarse}$  that lie between

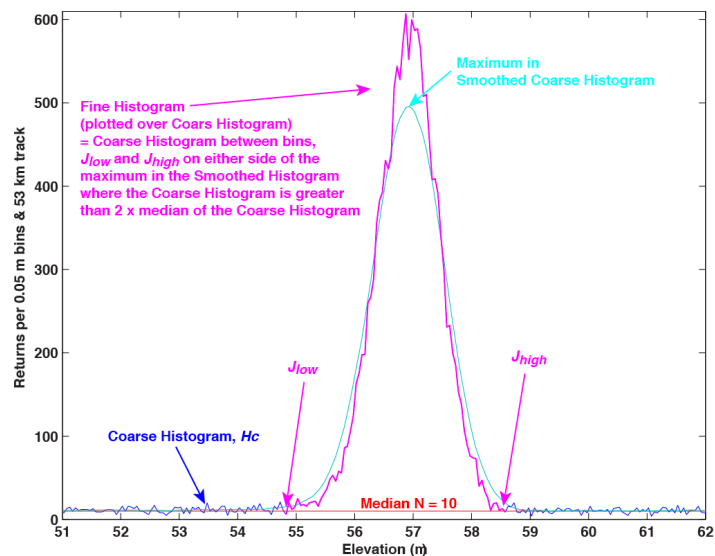


Figure 12. Illustrative coarse, smoothed, and fine histograms from steps 1 and 2 of 4.2.1.3 as applied to 10 minutes of April 2012 MABEL data over Chesapeake Bay. The corresponding figure for detrended data in the second iteration (steps 4-6) are similar.

heights corresponding the  $J_{low}$  and the  $J_{high}$  bin positions. This array of heights and times represents the first iteration on surface height statistics, but the higher moments are elevated by variations of the mean with time (or distance). Therefore, calculate the least squares linear fit to these versus time (or distance). Store the constant and first order coefficients,  $P0$  and  $P1$ , of the linear fit used for detrending **as output variables for the segment** and subtract them from the data of  $A_{coarse}$  to yield array  $A_{fine}$  of detrended photon heights and associated geolocation data.

4. From the heights of  $A_{fine}$ , create the detrended coarse histogram,  $H_d$ ,  $\pm 15$  m with bin size  $B_1$  (TBD, e.g., 0.01 m). Then repeat steps 1 and 2 substituting  $H_d$  for  $H_c$ :
5. Considering the detrended coarse histogram array,  $H_d$ , perform a  $N_{bmv} = 20$ -cm/ $B_1$  bin (e.g., 21 bins) moving bin arithmetic average incremented by 1 bin. Pad the ends of the smoothed histogram with  $N_{bmv}/2$  bins (equal the smoothed first and last values) to match the length of the original histogram.
6. The ASAS 5.1 finds the bin limits of the fine histogram as all the coarse histogram bins on either side of the maximum in the 20-cm smoothed histogram, from the  $J_{low}$  bin position to the  $J_{high}$  bin, where the smoothed histogram bin photon count is greater than the median of the smoothed histogram photon count. In practice with preliminary ATLAS data the median has usually been zero. Essentially, we have moved out from the middle of the histogram until the histogram levels fall to zero.

As of 6/4/2019, the developmental code finds preliminary the bin limits of the fine histogram as all the coarse histogram bins on either side of the maximum in the 20-cm smoothed histogram, from the preliminary  $J_{low}$  bin position to the preliminary  $J_{high}$  bin, where the coarse bin photon count is greater than the coarse histogram median. Then the average counts in the bins above the preliminary  $J_{high}$  are calculated and set equal to  $tailnoisehigh$  and the average counts in the bins below the preliminary  $J_{low}$  are calculated and set equal to  $tailnoiselow$ . Then we find the bin limits of the fine histogram as all the coarse histogram bins on either side of the maximum in the 20-cm smoothed histogram, from the final  $J_{low}$  bin position to the final  $J_{high}$  bin, where the final  $J_{low}$  bin position is that below which the smoothed histogram bin photon count is less than  $Th\_Nc\_f$  times  $tailnoiselow$ , and the final  $J_{high}$  bin position is that above which the smoothed histogram bin photon count is less than  $Th\_Nc\_f$  times  $tailnoisehigh$ . This procedure is better able to differentially remove subsurface noise returns and above surface returns. We have used  $Th\_Nc\_f = 1.5$  in practice with Release 001 ATLAS data and this has resulted in greatly improved rejection of subsurface returns.

7. The resulting  $H_R$  is the fine histogram of received surface heights to be used in further analysis. The time series of all the heights stored in  $A_{fine}$  that lie between heights corresponding the second iteration  $J_{low}$  and the  $J_{high}$  bin positions will be saved for wave and sea state bias analysis (Section 4.2.2).

#### 4.2.2 A Priori Sea State Bias Estimation and Significant Wave Height

As a side calculation, we will use the spatial record of signal photon heights derived

through the process described in Sections 4.2.1.1-4.2.1.3 as an approximation to the true surface height. This height record has been detrended during surface finding and the mean of this fit (linear fit coefficients  $P0$  and  $P1$  in 4.2.1.3) over the positions of the surface detected points must be added back to the surface heights to include all SSB in the record. With this height record, we resolve the structure of surface waves versus along track distance and the variation in photon return rate to estimate sea state bias. The inherently high spatial resolution of ICESat-2 will allow us to measure the variation in surface height over the large energy containing surface waves that lead to sea state bias. We will also know the photon return rate along the waves. Over the ocean segments (equivalent to 8,000 candidate signal photons or 7 km whichever is less), we will determine surface height variation and photon return rate in 10—m along-track bins. To calculate the photon return rate per meter it will be necessary to sort the photon height record in ascending order of along-track distance. From the height and photon rate records we will compute the covariance of surface height and photon return rate. Combined with the average photon return rate, the covariance of height and return rate is the sea state bias according to equation (11). We can approximate the significant wave height (SWH) as four times the standard deviation of the bin-averaged heights.

### 4.3 ATL12: Correction and Interpretation of the Surface Height Distribution

There are two main issues in deriving surface statistics from the apparent heights of surface-reflected photons identified in the surface detection phase and manifest in the fine histogram,  $H_R$ , of Section 4.2. These are correcting the heights for the instrument impulse response and deriving higher order moments of the corrected surface height distribution.

#### 4.3.1 Separating the Uncertainty due to Instrument impulse response

The received heights of surface reflected photons are the sum of a true height of the surface plus an uncertainty due to the instrument impulse response. The latter is the total of all instrument uncertainty, but it is dominated by uncertainty in the time the individual photons are transmitted. The ATLAS uncertainty in height due to instrument impulse response will have a standard deviation of 15-22 cm. Because the instrument impulse response uncertainty and the true height variation are additive, the received surface photon distribution,  $H_R$ , is equal to the convolution of the instrument impulse response height error distribution,  $H_T$ , and the true height distribution,  $H_Y$ :

$$H_R = H_T * H_Y \quad (12)$$

where  $*$  denotes convolution. Consequently, if we want to know the statistics of the surface from ICESat-2 returns, we must deconvolve  $H_T$  from  $H_R$  to get  $H_Y$ .

If we know that  $H_Y$  is a Gaussian distribution, we only need concern ourselves computing the mean and standard deviation of the distribution. However, we expect received ocean surface heights to depart from a Gaussian distribution because of a combination the shape

of surface waves and the non-uniform sampling due wave-induced variations of specular reflection. In addition to the mean and standard deviation, the third and second moments (skewness, and kurtosis) are also important. If we knew the true sample heights, we could calculate these moments as sample moments, e.g., the  $n^{\text{th}}$  sample moment for  $Y_i$  from the time series of heights:

$$M_n(Y) = \frac{1}{m} \sum_{i=1}^m (Y_i - \bar{Y})^n \quad (13)$$

or as the discrete form of the integral over the probability density function,

$$\int_{-\infty}^{\infty} (Y - M_1)^n H(Y) dY, \text{ if we knew } H(Y).$$

However, the instrument impulse response delay,  $T$ , and the received height,  $R$ , are independent and additive ( $R=T+Y$ ), so in principle it is possible to calculate sample moments for  $Y$  from the sample moments of  $T$  and  $R$ :

$$M_1(Y) = M_1(R) - M_1(T) \approx \frac{1}{m} \sum_{i=1}^m R_i - \frac{1}{m} \sum_{i=1}^m T_i \quad (14)$$

$$M_2(Y) = M_2(R) - M_2(T) \approx \frac{1}{m} \sum_{i=1}^m (R_i - \bar{R})^2 - \frac{1}{m} \sum_{i=1}^m (T_i - \bar{T})^2 \quad (15)$$

$$M_3(Y) = M_3(R) - M_3(T) \approx \frac{1}{m} \sum_{i=1}^m (R_i - \bar{R})^3 - \frac{1}{m} \sum_{i=1}^m (T_i - \bar{T})^3 \quad (16)$$

$$\begin{aligned} M_4(Y) &= M_4(R) - M_4(T) - M_2(Y)M_2(T) \\ &\approx \frac{1}{m} \sum_{i=1}^m (R_i - \bar{R})^4 - \frac{1}{m} \sum_{i=1}^m (T_i - \bar{T})^4 - M_2(Y)M_2(T) \end{aligned} \quad (17)$$

These sample moments will be calculated for the ICESat-2 heights as a check on more exact methods. However, pending further study, it is TBD whether they will be included in the ATL12 data output. The uncertainty in sample moments is significant [Percival, personal communication] and this uncertainty is compounded with combinations such as (14)-(16). These problems are liable to be particularly important when looking for small variation in skewness,  $M_3/M_2^{3/2}$ , and excess kurtosis,  $M_4/M_2^2 - 3$ . Optimized approaches for determining the moments of the height distribution require that we separate the effect of instrument impulse response from the received heights to give us the distribution of surface height,  $H_Y$ . To do this we must deconvolve  $H_T$  from  $H_R$ .

Deconvolution can be done in several ways. The Inland Water ATBD (ATL-13) expresses the convolution of (12) for the received histogram as the multiplication of a matrix representing the instrument impulse response histogram times a vector representing the surface height histogram. This matrix is inverted and multiplied times the received histogram to yield the surface histogram. The technique is reportedly sensitive to proper binning to produce a matrix that can be inverted.

Deconvolution can also be done by taking the Fourier transform of (12) and noting that the Fourier transform,  $\mathcal{F}(\cdot)$ , of the convolution of two variables,  $H_R(k)=\mathcal{F}(H_R)=\mathcal{F}(H_T*H_Y)$  is equal to the product of the Fourier transform of the two variables,

$$H_R(k)=\mathcal{F}(H_R)=\mathcal{F}(H_T*H_Y)=\mathcal{F}(H_T)\mathcal{F}(H_Y) \quad (18)$$

where  $k$  is the wavenumber in units of  $m^{-1}$ , the Fourier space counterpart to height in meters, the histogram independent variable. From (18), we can compute  $H_Y$  as an inverse Fourier transform,  $\mathcal{F}^{-1}(\cdot)$  of the ratio of  $\mathcal{F}(H_R)$  and  $\mathcal{F}(H_T)$ ,

$$H_Y=\mathcal{F}^{-1}(\mathcal{F}(H_R)/\mathcal{F}(H_T)) \quad (19)$$

The problem with this approach is that there is invariably noise in the received signal histogram,  $H_R$  that produces significant values in  $\mathcal{F}(H_R)$  at wavenumbers where  $\mathcal{F}(H_T)$  has small values or zeros. This may have something in common with problem of conditioning of the matrix in the matrix inversion technique. In any event, these unrealistic combinations make the inverse Fourier transform unstable. To account for the noise in  $H_R$ , we consider Wiener deconvolution, in which it is assumed the received histogram is contaminated with noise,  $N$ , and (12) and (18) become

$$H_R = H_T * H_Y + N \quad (20)$$

and where  $H_T(k)=\mathcal{F}(H_T)$ ,  $H_Y(k)=\mathcal{F}(H_Y)$ ,  $H_R(k)=\mathcal{F}(H_R)$ , and  $N(k)=\mathcal{F}(N)$ ,

$$H_R(k) = H_T(k)H_Y(k) + N(k) \quad (21)$$

An estimate  $H_Y(k)$  for  $H_{Yest}(k)$  of the form

$$H_{Yest}(k)=W(k)H_R(k)/H_T(k) \quad (22)$$

is sought such the expected value of  $(H_Y(k)-H_{Yest}(k))^2$  is a minimum. This is found for

$$W(k)=\mathcal{F}(H_T)^2/[\mathcal{F}(H_T)^2+\mathcal{F}(Noise)^2/\mathcal{F}(H_Y)^2] \sim \mathcal{F}(H_T)^2/[\mathcal{F}(H_T)^2+\mathcal{F}(Noise)^2/\mathcal{F}(H_R)^2] \quad (23)$$

and

$$H_{Yest}=\mathcal{F}^{-1}(H_{Yest}(k))=\mathcal{F}^{-1}(W(k)\mathcal{F}(H_R)/\mathcal{F}(H_T)) \quad (24)$$

For wave numbers where the inverse signal to noise ratio,  $\mathcal{F}(Noise)^2/\mathcal{F}(H_R)^2$ , is low relative to  $H_T(k)$ ,  $W(k)$  goes to one and equation (24) reverts to (19). Where the inverse signal to

noise ratio is high (high noise),  $W(k)$  goes to zero and the noise is filtered out of the resulting  $H_{Yest}(k)$ .

### 4.3.2 Characterizing the Random Sea Surface

The best method for determining sample moments is the method of maximum likelihood (ML). For a distribution of known type  $f(x \setminus \mu_{1,2,3,4})$ , the optimum choice of parameters,  $\mu_{1,2,3,4}$ , for data values  $x_1, x_2, x_3, \dots, x_m$ , are those which maximize the likelihood,  $L$ ,

$$L(\mu_{1,2,3,4} \setminus x_1, x_2, x_3, \dots, x_m) = \prod_{i=1}^m f(x_i \setminus \mu_{1,2,3,4}) \quad (25)$$

For ICESat-2 sea surface height, we are not sure of the form of the probability density function but commonly the ocean surface has been characterized by the Gram-Charlier distribution for which the first 4 moments are important. Such a distribution can be represented it by mixture of two Gaussian distributions,  $N_a$  and  $N_b$

$$\begin{aligned} f(x_i \setminus \mu_{1,2,3,4}) &= m_a N_a(x_i \setminus \mu_{a1,2}) + m_b N_b(x_i \setminus \mu_{b1,2}) \\ m_a + m_b &= 1 \end{aligned} \quad (26)$$

and the two moments of each distribution plus the mixing ratio,  $m_a/m_b$ . Given the surface height histogram, the parameters of the two normal distributions and the mixing ratio can be determined by maximum likelihood.

The aggregate moments of the Gaussian mixture  $X$  with  $n$  component Gaussian distributions are functions of the component means,  $\mu_{\square}$ , and variances,  $\sigma_i^2$ , and the mixing ratio,  $m_i$ ,

$$E[(X - \mu_{mix})^j] = \sum_{i=1}^2 \sum_{k=0}^j \frac{j!}{k!(j-k)!} (\mu_i - \mu_{mix})^{j-k} m_i E[(X_i - \mu_i)^k] \quad (27)$$

For example, the aggregate mixture mean is:

$$\mu_{mix} = m_1 \mu_1 + m_2 \mu_2 \quad (28)$$

and the aggregate variance is:

$$\sigma_{mix}^2 = m_1 \left( (\mu_1 - \mu_{mix})^2 + \sigma_1^2 \right) + m_2 \left( (\mu_2 - \mu_{mix})^2 + \sigma_2^2 \right) \quad (29)$$

### 4.3.3 Maximum Likelihood Versus Expectation Maximization

In the Matlab code used for development of the ATL12 software, an Expectation Maximization (EM) code (gmdistributin.fit) was used to derive a 2-component Gaussian Mixture fit to the derived surface distribution. The mean and variance of the two Gaussian distributions along with the mixing ratio allows of the two Gaussians allows the accurate determination of the most likely first four moments of the distribution of surface height. In discussion of the developmental code results and examples in Section 5, we will refer to Expectation Maximization, but Instead of Expectation Maximization, the ASAS Fortran code developed for ATL12 uses the Maximum Likelihood approach of ATL07 Appendix E (shown in Appendix C of this ATBD) to do the 2-Gaussian Mixture fit. For synthetic test data the Fortran Maximum Likelihood produced equivalent result to the Matlab Expectation Maximization approach, and for consistency with ATL07, ASAS ATL12 will use Maximum Likelihood.

## 4.4 Calculation of Uncertainty

We have found the wave environment, rather than instrumental factors, is probably the biggest contributor to uncertainty in estimates of the mean SSH. This is illustrated by our analysis of multiple ocean segments in the southern part of the central North Pacific. These segments show variability in their mean sea surface heights of approximately  $\pm 0.12$ , much greater than we'd expect from instrumental factors. The standard error,  $\sigma_L$ , in the estimates of the mean are given by

where  $\sigma_i$  is the standard deviation of the population and  $N_{df}$  is the number of degrees of freedom. If every one of the  $\sim 8,000$  photon heights were independent, even with a SWH = 2.5 m ( $\sigma_i = .625$  m), the uncertainty in estimates of the mean would be less than 1 cm. The problem is that owing presence of long large waves, successive photon heights are far from independent. The fact that the underlying wave signal is periodic makes the estimate of the effective degrees of freedom in terms of correlation length scale more problematic. As a worst case if we set  $N_{df}$  equal to the number of wave periods in the ocean segment, 15 in the case of long waves crossed at an acute angle, the uncertainty,  $\sigma_L$ , in the estimate of the mean equals 0.16 m, close to the mean SSH we see over many similar ocean segments. This problem is not instrumental; it is just made apparent by the ability of ICESat-2 to resolve waves. To lower this uncertainty, we are

exploring using harmonic analysis of surface height over each ocean segment and use of the zero wave-number amplitude to represent SSH (D. Percival, personal communication, 2019) as a way of removing large periodic variations in height as a cause of uncertainty. A further advantage of this approach will be that it will add a measure of wave spectral properties to ATL 12. In any event, we will have to derive measures of the effective number of degrees of freedom as an ATL12 output for each ocean segment in order to properly account for uncertainties in the ATL19 gridded SSH product.

#### 4.5 ATL19: Gridding the DOT and SSH

This product, based entirely on Product ATL12/L3A with no external dependence, contains gridded monthly estimates of sea surface from all IS-2 tracks from the beginning to the end of each month. Below 60°N and above 60°S, the data are mapped on the curvilinear grid of the TOPEX/Poseidon with spacing equivalent to 0.25° of longitude. Above 60°N and below 60°S the grid data are mapped onto a planimetric grid using the SSM/I Polar Stereographic Projection equations at a grid spacing of about 24 km. The exact spacing of the Polar Stereographic grid should be adjusted to match the longitudinal spacing of the TOPEX/Poseidon grid at 60°S and 60°N, and the latitudinal spacing adjust to have an integer number of grid cells between 60°N (S) and the North (South) Pole.

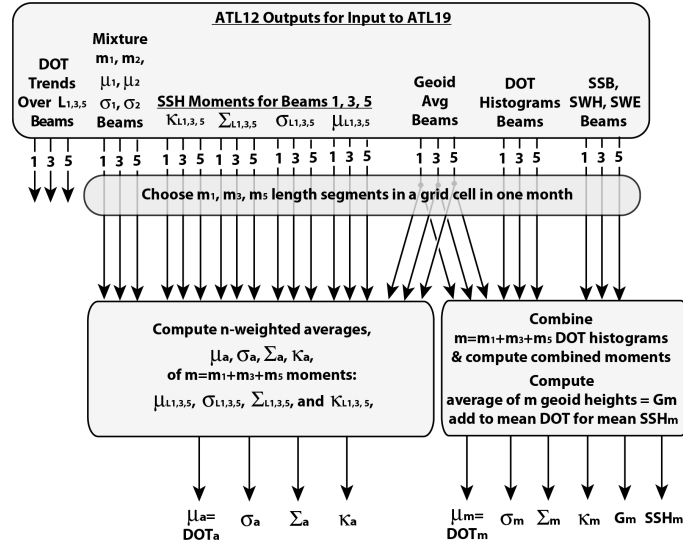


Figure 13. Block diagram for the ATL19 gridding procedure taking ATL12 ocean products as input.  $\mu$ ,  $\sigma$ ,  $\Sigma$ , and  $K$  denote mean, standard deviation, skewness, and kurtosis respectively.

## 5.0 ALGORITHM IMPLEMENTATION

This section describes the specific implementation of the algorithm for program development.

### 5.1 Outline of Procedure

- 1) Finding the surface-reflected photon heights in the photon cloud
  - a) Coarse Selection and Setting of Segment Length:  
Use a median-based selection criterion to accumulate a large number of surface-reflected photons.
  - b) Fine Histogram Selection:  
Use a median-based selection criterion to derive a preliminary surface height histogram, compute the mean and trend in surface height, remove this trend from all heights, and repeat the median-based selection criterion to derive a final surface height histogram
- 2) Using the along track signal photon heights from the fine histogram selection step and signal photon return rate to estimate sea state bias and surface wave properties.
- 3) Correction and Interpretation of the Surface Height Distribution
  - a) Separating the Uncertainty due to Instrument impulse response  
Use Wiener deconvolution to derive the surface height histogram with the uncertainty due to the instrument impulse response removed.
  - b) Characterizing the Random Sea Surface  
Characterize the surface height histogram as a mixture of two normal distributions and calculate up to 4<sup>th</sup> moment of the mixture.
  - c) Compute the mean, variance, skewness, and kurtosis for the aggregate Gaussian mixture using Equation 17; the final determination of SSH for ATL12 is the mean of the aggregate mixture distribution computed using (28) and the SSH variance is given by (29).

### 5.2 Input Parameters

#### 5.2.1 Parameters Required from ICESat-2 Data

See Tables 2 and 3. For ATL12, the primary inputs will be photon heights in the downlink band and associated time, geolocation, the geoid (*geoid*), ocean tides (*tide\_ocean*, *tide\_equilibrium*), and dynamic atmospheric correction (*dac*) information from ATL03, plus the cloud flag (*layer\_flag* in ATL09) every 400 laser pulses from ATL09 and ocean depth, *depth\_ocn*, from interpolated from GEBCO-2014 gridded ocean bathymetry. Normally over the open ocean (or sea ice) regions not overlapping with terrestrial or ice sheet regions, the downlink band will be  $\pm 15$  m centered about the signal area identified by the ATLAS on-board flight software. In the ocean regions overlapping with land and ice sheet regions, the downlink band will expand to match the band for those regions. Also for ATLAS special operations such as ocean scans and Transmitter Echo Pulse data collection

the telemetry band is expanded. For the purposes of ATL12, the EGM2008 geoid supplied with ATL03 (/gtx/geophys\_corr/ posted at the 20m along-track rate for each beam in ATL\_03) will be used to establish the narrower  $\pm 15$ -m band within the expanded downlink band of the overlap and special operations regions. Aside from the  $\pm 15$ -m band about the geoid, no prior classification as to surface/non-surface photons is considered from the ATL03 ocean results. The 14 geo-bin (400-pulse) ocean segment should be aligned so that the once per 14 geo-bin (400-pulse) cloud flag (***layer\_flag*** in ATL09) represents the cloud conditions during the ocean segment.

**Table 2 Input parameters (Source: ATL03)**

Label	Description	Symbol
<i>delta_time</i>	Elapsed seconds since first data point in granule	<b><i>time_initial</i></b>
<i>h_lat</i>	latitude of each received photon	<b><i>lat_initial</i></b> ,
<i>h_lon</i>	longitude of each received photon	<b><i>lon_initial</i></b>
<i>h_ph</i>	height of each received photon	<b><i>ht_initial</i></b>
<i>dist_ph_along</i>	Along track distance	
<i>sigma_along</i>	Uncertainty in along-tack distance	
<i>dist_ph_across</i>	Across-track distance	
<i>sigma_across</i>	Uncertainty in across-track distance	
<i>segment_ID</i>	Geo-bin ID	<b><i>lat_initial</i></b> ,
<i>segment_length</i>	Segment length of each geo-bin	<b><i>lat_initial</i></b> ,
<i>signal_conf_ph</i>	Confidence level associated with each photon event selected as signal. Zero equals noise. One means added to allow for $\pm 15$ -m buffer around high confidence, but algorithm classifies as background. Two equals low confidence. Three equals medium. Four equals high.	<b><i>signal_conf_ph</i></b>
<i>beam_azimuth</i>	The direction, eastwards from north, of the laser beam vector as seen by an observer at the laser ground spot viewing toward the spacecraft (i.e., the vector from the ground to the spacecraft). When the spacecraft is precisely at the geodetic zenith, the value will be 99999 degrees. 40 Hz.	
<i>beam_coelv</i>	Co-elevation (CE) is direction from vertical of the laser beam as seen by an observer located at the laser ground spot.	
<i>solar_azimuth</i>	The direction, eastwards from north, of the sun vector as seen by an observer at the laser ground spot.	
<i>solar_elevation</i>	Solar Angle above or below the plane tangent to the ellipsoid surface at the laser spot. Positive values mean the sun is above the horizon, while negative values mean it is below the horizon. The effect of atmospheric refraction is not included. This is a low precision value.	
<i>bckgrd_rate</i>	Background count rate ( <i>bckgrd_atlas/bckgrd_rate</i> ), simply averaged over the segment	
<i>track_type_flag</i>	Flag describing if the track is in normal ice sheet, terrian, ocean scan, target or other non-normal pointing control	

<i>fpb_parm(n)</i>	parameter needed to compute first-photon bias correction to a mean height	TBD
<i>gd_ht</i>	The height of the geoid above the ellipsoid	
<i>dac</i>	Dnamic atmospheric correction (DAC) includes inverted barometer (IB) effect ( $\pm 20$ cm)	
<i>tide_earth</i>	Solid Earth Tides ( $\pm 30$ cm, max)	
<i>tide_equilibrium</i>	Equilibrium long-period tide	
<i>tide_load</i>	Load Tide - Local displacement due to Ocean Loading (-6 to 0 cm)	
<i>tide_oc_pole</i>	Ocean Pole Tide -Loading due to centrifugal effect of polar motion on the oceans ( 2 mm, max)	
<i>tide_ocean</i>	Ocean Tides including diurnal and semi-diurnal (harmonic analysis), and longer period tides (dynamic and self-consistent equilibrium) ( $\pm 4$ m)	
<i>tide_pole</i>	Pole Tide -Rotational deformation due to polar motion (-1.5 to 1.5 cm)	
<i>tot_geo</i>	total of the geophysical range corrections applied to compute height.	
<i>tropo_dry</i>	Dry Troposphere range correction	
<i>tropo_wet</i>	Wet Troposphere range correction	
<i>surf_type</i>	Five-element array in the geolocation group indicating the surface masks that apply to that segment	

**Table 3 Input parameters (Source: ATL09)**

Label	Description	Symbol
<i>delta_time</i>	Elapsed GPS seconds since start of the granule. Use the metadata attribute granule_start_seconds to compute full gpstime.	
<i>latitude</i>	Latitude, WGS84, North=+, Lat of segment center	
<i>longitude</i>	Longitude, WGS84, East=+,Lon of segment center	
<i>cloud_asr_prob</i>	Cloud probability based on Apparent Surface Reflectivity	
<i>cloud_flg</i>	Cloud present flag	<i>Pc</i>
<i>cloud_flg_conf</i>	cloud probability $p=(1-asr/t)*100$ flag_values: 0 = clear_with_high_confidence 1 = clear_with_medium_confidence 2 = clear_with_low_confidence 3 = cloudy_with_low_confidence 4 = cloudy_with_medium_confidence 5 = cloudy_with_high_confidence	
<i>erd_flg</i>	Flag that indictes probable atmosphere induced range delay	
<i>asr</i>	Apparent Surface Reflectivity (25Hz)	<i>asr_25</i>
<i>asr_q</i>	ASR Quality Flag	<i>asr_b_25</i>
<i>bgr</i>	Background count rate, averaged over the segment	<i>bgr_25</i>

<i>cab</i>	Calibrated Attenuated Backscatter (CAB) profiles for the RT strong beam or and a sum of the 3 beams covering (nominally) 13 to -1 km at 25 Hz	
<i>cloud_prob</i>	Cloud Probability based on Apparent Surface Reflectivity	

### 5.2.2 Parameters Required from Other Sources

Bathymetry – Because the ocean mask extends into non-ocean areas we need a way to determine which parts of the ocean data are over water for which our analysis procedure is appropriate. For this we will take the ocean depth, ***depth\_ocn***, from the General Bathymetric Chart of the Oceans (GEBCO) 2014 gridded data set ([https://www.gebco.net/data\\_and\\_products/gridded\\_bathymetry\\_data/](https://www.gebco.net/data_and_products/gridded_bathymetry_data/)) evaluated at the geo-segment ***latitude*** and ***longitude***.

### 5.2.3 Control Parameters for ATL12 Processing

Bathymetry – The coarse surface finding described in 5.3.1 will ignore data collected in ocean waters with a depth, ***depth\_ocn***, less than a depth, ***depth\_shore***, defining the effective shoreline of water for which our analysis procedure is appropriate. The default value for ***depth\_shore***, will be 10 m.

Cloud cover – In the coarse surface finding described in 5.3.1 we may need to ignore data collected in ocean waters where and when the cloud cover is heavy as indicated by ***layer\_flag***, equal to 1. The control parameter ***layer\_swth*** will specify if the cloudiness test is to be applied. If control parameter ***layer\_swth*** is equal to 1 and ***layer\_flag*** is equal to 1, photon heights will not be included in the ATL12 processing. When ***layer\_swth*** equals the default value, 0, the software will ignore the cloud cover in accepting data during coarse surface finding.

## 5.3 Processing Procedure

### 5.3.1 Coarse Surface Finding and Setting of Segment Length

The process is basically to first establish a variable length (e.g., up to 7 km) ocean segment with enough (e.g.) photon heights that will yield a histogram with reasonable moments up to 4<sup>th</sup> order. We start with 14 geo-bin (400-pulse) segments of ATL03 photon heights (see 5.2.1)

#### (A) Ocean Data Selection and Basic Geophysical Corrections

-----

- 1) Stepping through 14-geobin segments, examine ocean depth and cloud parameters against control parameters to test for suitability for ocean processing. If ocean depth,

$depth_{ocn}$ , is less than a depth,  $depth_{shore}$ , specifying the effective shoreline of water for which ocean processing is appropriate, then proceed to next 14 geo-bin (400-pulse) segment. The default value for control parameter  $depth_{shore}$  will be 10 m.

Similarly, if control parameter  $layer_{swtch}$  is equal to 1 and  $layer_{flag}$  is equal to 1, then proceed to next 14 geo-bin (400-pulse) segment. When  $layer_{swtch}$  equals the default value, 0, the software will

- ignore the cloud cover in accepting data during coarse surface finding.
- 2) Correct for photon heights for short period and long period ocean tides

**Table 4 Control parameters – Coarse surface finding**

Parameter	Description	Value
$B_c$	Bin size of coarse histogram	5 cm
$Th_{Nc_c}$	Number of photons times median required to classify as surface bin	1 typical
$Th_{Ps}$	Minimum number of candidate surface photons per segment	8,000
$Segmax$	Max number of 400-pulse segments in a surface finding segment	25
$layer_{swtch}$	Flag determining if $layer_{flag}$ will ( $layer_{swtch}=1$ ) or won't ( $layer_{swtch}=0$ ) be editing photon heights.	Default = 0
$depth_{shore}$	Prescribed depth defining ( $depth_{ocn}>depth_{shore}$ ) boundary of ocean processing	Default= 10 m

( $gtxx/geophys\_corr/tide\_ocean$  and  $tide\_equilibrium$ ), the inverse barometer effect and the modeled dynamic response to the atmosphere (dynamic atmospheric correction,  $gtxx/geophys\_corr/dac$ ),

- 3) Select only photon heights for which the signal confidence ( $gtxx/signal\_conf\_ph$ ) is greater than or equal to 1. This will select photons in the likely surface  $\pm 15$ -m buffer window. Also delete any photon heights outside the band defined by geoid plus or minus half the height of the ocean downlink window (presently geoid  $\pm 15$ -m, to become geoid  $\pm 20$ -m). **(Is the height of the downlink band reported in ATL03 and if so, what is the variable name?)**
- 4) To narrow the range of variability, subtract the EGM2008 geoid height ( $gtxx/geophys\_corr/geoid$ ), varying over meters to tens of meters, from the photon heights so that we are dealing dynamic ocean topography varying over centimeters to 10s of centimeters. from photon heights to reference all heights to the geoid. Note that EGM2008 includes a correction for the permanent or mean tide.

(B) Establish a Working Histogram Array

Establish an initial coarse histogram array,  $H_c$ , spanning  $\pm 15$  m with bin size  $B_1$  (TBD, e.g., 0.01 m) and a data array,  $A_{coarse}$ , for up to 10,000 photon heights and associated

information (index, geolocation, time) plus noise photon counts. This will be populated with data as we step through 14-geobin segments searching for an adequate number of surface photon candidates.

(C) Step Through 14-Geo-bin Segments

-----  
Aggregate photon heights over 14 geo-bins (400-pulses) and construct a temporary 14 geo-bin (400-pulse) height histogram spanning  $\pm 15$  m with bin size  $B_1$  (e.g., 0.01 m). This is used to estimate a running total number of signal and noise photons. We suggest a bin size of 0.01 for consistency with later steps in the processing. The 14 geo-bin (400-pulse) segment should be aligned so that the once per 14 geo-bin (400-pulse, approximately 280 m along track distance) cloudiness flag, *layer\_flag* in ATL09, represents the aggregate effect of cloudiness and background radiation derived from solar zenith, *cloud\_flag\_ASR*, *cloud\_flag\_atm*, and *bsnow\_con*, during the 280-m segment.

(D) Test for Surface Photons

-----  
Photons in the 14 geo-bin (400-pulse) histogram bins with greater than the  $Th\_Nc\_c$  times the median number of photons,  $N_{median}$ , are candidate signal photons and photons in the bins with the median number of samples or less are considered noise photons.  $Th\_Nc\_c$  is TBD, but we have been using  $Th\_Nc\_c = 1$  in our tests with early ICESat-2 data. Note that with few surface returns per pulse and significant wave heights much less than 30 m, the majority of the of the bins will contain only noise photons so that the median will equal the number of noise photons per bin. In extreme cases where ICESat-2 encounters significant wave heights approaching 30 m, we may have to adopt a slightly different threshold such as the count value equal to or exceeding 20% of the bin population.

(E) Increase the Count of Surface Photons

-----  
Add the number of surface reflected photons to  $N_{good}$ , the running total of candidate surface photons and noise photons.

(F) Add All Photons to Data Array

-----  
Add the all the photons, signal and noise, and their associated geolocation and time information from this 14 geo-bin (400-pulse) segment to the data array *HTin*.

(G) Test Counter for Sufficient Surface Photons

-----  
If the total number of candidate signal photons is greater than or equal to a **minimum number**,  $Th\_Ps$  (8,000), of photons or if the number,  $N_{seg400}$ , of 14 geo-bin (400-pulse)

segments collected reaches  $S_{egmax}$  (e.g., 25 equivalent to ~7 km)), go on to 5.3.2 Processing Procedure for Classifying Ocean Surface Photons, Detrending, and Generating a Refined Histogram of Sea Surface Heights with the data array, **HTin**. The total number of pulses for the segment,  $n_{pls\_seg}$ , equals  $400 \times N_{seg400}$ . If the total number of candidate surface reflected photons is less than  $Th\_Ps$ , intake another 14 geo-bin (400-pulse) segment and repeat steps 5.3.1 A-G above.

### 5.3.2 Processing Procedure for Classifying Ocean Surface Photons, Detrending, and Generating a Refined Histogram of Sea Surface Heights

The procedure based on development of Matlab Program:  
ATBDDraftMABEL\_reader\_PhotonClassifyX2Channel6B\_noprint.m.

We start with the array of photon height data in **HTin** from 5.2.4. These are candidate heights accumulated over a segment of sufficient length to provide an adequate number of signal photons. In view of the low reflectance of the ocean surface this may require as many as 10,000 laser pulses. Following the developmental code used on MABEL we break **HTin**

**Table 5 Control parameters – Fine surface finding and analysis**

$B_f$	Bin size of fine histogram	5 cm, MABEL 1 cm, ICESat-2
$Th\_Nc\_f$	Surface qualified= smooth hist > $Th\_Nc\_f$ * tail noise	1.5, ICESat-2
$pts2bin$	Bins in boxcar smoother	21, ICESat-2

into a vector of initial photon heights, **ht\_initial**, a vector of initial times, **time\_initial**, and vectors of initial location, **lat\_initial** and **lon\_initial**. For ATLAS we would also add a vector of along track distance, **trackdist\_initial**.

#### (A) Establish or Summon the Bin Edge Vector

-----

Set up for the surface finding histogram, **N**, by establishing the vector, **Edges**, (with a length one greater than **N**) of histogram bin edges with bins **Bf** wide between -15 m to +15 m. Also establish the vector, **Ctrpnt**, of bin center points (with length equal to **N**; for our tests **Ctrpnt** values equal **Edges** values plus **Bf/2**, deleting the last and largest value). Also establish a vector array, **BinB**, as long as **ht\_initial** for bin assignments.

#### (B) Compute Initial Histogram and Keep Track of Bin Assignment for Each Photon Height

-----

Populate the histogram array **N** such that each element equals the number of values from **ht\_initial** that are in the corresponding bin boundaries of **Edges**. Also, for each value in

**ht\_initial**, populate the vector **BinB** with the bin number to which **ht\_initial** is assigned from one to the length, **LN**, of **N** (in Matlab, [N,BinB]=histc(ht\_initial,Edges).

(C) Find Median of Initial Histogram  
-----

Find the median, **medianN**, of **N**.

(D) Smooth Initial Histogram with Boxcar Smoother  
-----

- Create a smoothed version, **smoothN**, of the histogram, **N**, with a boxcar smoother incremented in one-bin steps over **pts2bin** where **pts2bin** is a control parameter in Table 5. It should equal **nbin** + 1 where **nbin** is an even number. We have chosen **nbins**=20 and **pts2bin** set at 21 based on success with the developmental code. In this ATBD with 1-cm bin size, we refer to this nominally as the “20-cm smoother” although it actually smooths over 21 bins. (In the ASAS 5.1 code used for ICESat-2 Rel. 001, **nbin** equals 100 corresponding to **pts2bin** = 101 and a 100-cm smoother).

- If needed, pad the ends of the smoothed histogram to match length of **N**. For example, a smoother that starts **nbin/2+1** points in from the beginning of the original array and stops at an equal number of points before the end, will be **nbin** points shorter than the original array. In this case add **nbin/2** points equal to the first smoothed value to the beginning of the array and add **nbin/2** points equal to the last smoothed value to the end of the array.

(E) Find Limits of Valid Histogram  
-----

The ASAS 5.1 finds the limits of the histogram above (**jlow**) and below (**jhigh**) for which, searching from the index of the maximum in the 20-cm smoothed histogram **smoothN**, the value in **smoothN** is greater than median of **smoothN**.

- First find the index, **imax**, where **smoothN(imax)** equals the maximum in **smoothN**.
- Increment the index, **i**, downward from **imax** until **smoothN(i)** is less than the median of **smoothN**. At this point **jlow** = **i+1**.
- Increment the index, **i**, upward from **imax** until **smoothN(i)** is greater than the median of **smoothN**. At this point **jhigh** = **i-1**.

As of 6/4/2019, the developmental code finds the limits of the histogram above a preliminary **jlow** and below a preliminary **jhigh** for which, searching from the index of the maximum in the 20-cm smoothed histogram **smoothN**, the value in **N** is greater than median of **N**.

- First find the index, **imax**, where **smoothN(imax)** equals the maximum in **smoothN**.

- Increment the index,  $i$ , downward from  $imax$  until  $N(i)$  is less than the median of  $N$ . At this point preliminary  $jlow = i+1$ .
- Increment the index,  $i$ , upward from  $imax$  until  $N(i)$  is greater than the median of  $N$ . At this point preliminary  $jhigh = i-1$ .
- Then the average counts in all the bins above the preliminary  $J_{high}$  are calculated and set equal to  $tailnoisehigh$  and
- The average counts in all the bins below the preliminary  $J_{low}$  are calculated and set equal to  $tailnoiselow$ .
- Increment the index,  $i$ , downward from  $imax$  until  $smoothN(i)$  is less than the  $Th_{Nc} * tailnoiselow$ . At this point  $jlow = i+1$ .
- Increment the index,  $i$ , upward from  $imax$  until  $smoothN(i)$  is greater than  $Th_{Nc}_f * tailnoisehigh$ . At this point  $jhigh = i-1$ .

(F) Choose First Cut Signal Photons

-----

The first-cut signal or surface photons are those in the bins of histogram  $N$  between  $jlow$  and  $jhigh$ . The noise photons are those from bins below the  $jlow$  bin and above the  $jhigh$  bin. The vector  $BinB$  lists the bin assignment for each photon elevation. Therefore, the indices  $ii$  for which  $BinB(ii)$  is less than or equal to  $jhigh$  and greater than or equal to  $jlow$ , are the indices of the surface reflected photon heights in  $ht\_initial$ .

- Populate the vector of surface photon heights,  $ht\_initial\_surf$ , with the heights at indices  $ii$  in  $ht\_initial$  (in Matlab these surface heights would be  $ht\_initial\_surf=ht\_initial(ii)$ ; where  $ii$  is the vector of surface photon indices).
- Identify the corresponding track distances,  $trackdist\_initial\_surf$ , in  $trackdist\_initial$  at the indices in  $ii$ .

(G) Do a Linear Fit of Height Versus Track Distance

-----

We need to do a linear fit to surface heights versus track distance because the trend in surface height contributes substantial variance to the histogram, which can cloud the surface finding algorithm. Therefore, perform a least squares linear fit of the form  $P1 \times trackdist\_initial\_surf + P0$  to  $ht\_initial\_surf$ .

(H) Subtract Surface Trend

We make a new vector array of detrended heights,  $ht\_initial2$ , by subtracting the linear surface trend derived above at step 5.2.4 (G) from  $ht\_initial$ ,

i.e.,  
 $ht\_initial2 = ht\_initial - P1 \times trackdist\_initial + P0$ .

REPEAT SURFACE FINDING AFTER REMOVING TREND

(I) Repeat Steps (B) Through (F) Acting on the Detrended Elevations Starting With: Compute Initial Histogram and Keep Track of Bin Assignment for Each Photon Height

Populate the histogram array  $N$  such that each element equals the number of values from  $ht\_initial2$  that are in the corresponding bin boundaries of  $Edges$ . Also, for each value in  $ht\_initial2$ , populate the vector  $BinB$  with the bin number to which  $ht\_initial2$  is assigned from one to the length,  $LN$ , of  $N$  [in Matlab,  $[N, BinB] = histc(ht\_initial2, Edges)$ ].

(J) Find Median of Initial Histogram

Find the median,  $medianN$ , of  $N$ .

(K) Smooth the Initial Histogram with Boxcar Smoother

Create a smoothed version,  $smoothN$ , of the histogram,  $N$ , with a boxcar smoother incremented in one-bin steps over  $pts2bin$  where  $pts2bin$  is a control parameter in Table 5. It should equal  $nbin + 1$  where  $nbin$  is an even number. We have chosen  $nbins = 20$  and

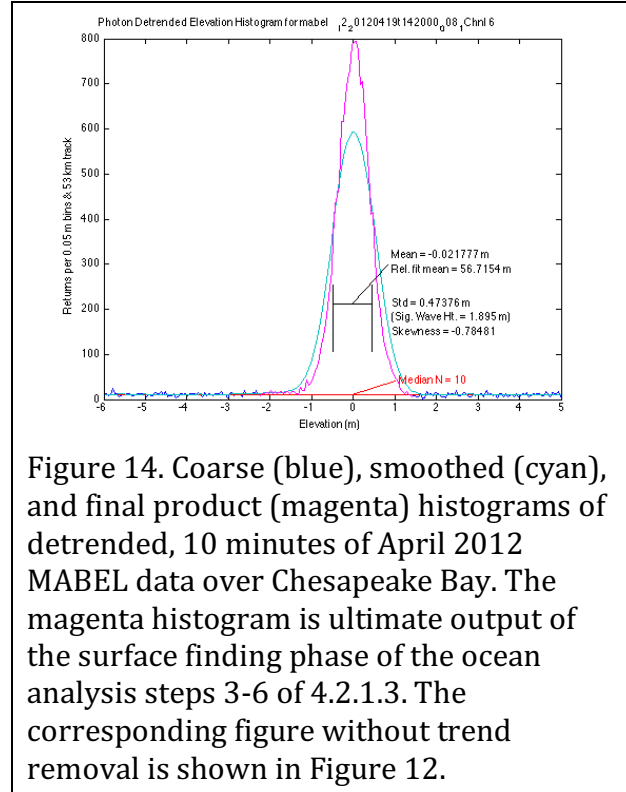


Figure 14. Coarse (blue), smoothed (cyan), and final product (magenta) histograms of detrended, 10 minutes of April 2012 MABEL data over Chesapeake Bay. The magenta histogram is ultimate output of the surface finding phase of the ocean analysis steps 3-6 of 4.2.1.3. The corresponding figure without trend removal is shown in Figure 12.

**pts2bin** set at 21 based on success with the developmental code. In this ATBD with 1-cm bin size, we refer to this nominally as the “20-cm smoother” although it actually smooths over 21 bins. (In the ASAS 5.1 code used for ICESat-2 Rel. 001, **nbin** equals 100 corresponding to **pts2bin** = 101 and a 100-cm smoother).

- If needed, pad the ends of the smoothed histogram to match length of  $N$ . For example, a smoother that starts  $nbin/2+1$  points in from the beginning of the original array and stops at an equal number of points before the end, will be  $nbin$  points shorter than the original array. In this case add  $nbin/2$  points equal to the first smoothed value to the beginning of the array and add  $nbin/2$  points equal to the last smoothed value to the end of the array.

(L) Find Limits of Valid Histogram

-----

The ASAS 5.1 finds the limits of the histogram above (**jlow**) and below (**jhigh**) for which, searching from the index of the maximum in the 20-cm smoothed histogram **smoothN**, the value in **smoothN** is greater than median of **smoothN**.

- First find the index, **imax**, where **smoothN(imax)** equals the maximum in **smoothN**.
- Increment the index, **i**, downward from **imax** until **smoothN(i)** is less than the median of **smoothN**.. At this point **jlow** = **i+1**.
- Increment the index, **i**, upward from **imax** until **smoothN(i)** is greater than the median of **smoothN**. At this point **jhigh** = **i-1**.

As of 6/4/2019, the developmental code finds the limits of the histogram above a preliminary **jlow** and below a preliminary **jhigh** for which, searching from the index of the maximum in the 20-cm smoothed histogram **smoothN**, the value in **N** is greater than median of **N**.

- First find the index, **imax**, where **smoothN(imax)** equals the maximum in **smoothN**.
- Increment the index, **i**, downward from **imax** until **N(i)** is less than the median of **N**.. At this point preliminary **jlow** = **i+1**.
- Increment the index, **i**, upward from **imax** until **N(i)** is greater than the median of **N**. At this point preliminary **jhigh** = **i-1**.
- Then the average counts in all the bins above the preliminary **J<sub>high</sub>** are calculated and set equal to **tailnoisehigh** and
- The average counts in all the bins below the preliminary **J<sub>low</sub>** are calculated and set equal to **tailnoiselow**.
- Increment the index, **i**, downward from **imax** until **smoothN(i)** is less than the **Th\_Nc\_f** \* **tailnoiselow**. At this point **jlow** = **i+1**.
- Increment the index, **i**, upward from **imax** until **smoothN(i)** is less than **Th\_Nc\_f** \* **tailnoisehigh**. At this point **jhigh** = **i-1**.

(M) Choose Second-Cut Signal Photons

-----  
 The second-cut signal or surface photons are those in the bins of histogram  $N$  between  $jlow$  and  $jhigh$ . The noise photons are those from bins below the  $jlow$  bin and above the  $jhigh$  bin. The vector  $BinB$  lists the bin assignment for each photon elevation. Therefore, the indices  $ii$  for which  $BinB(ii)$  is less than or equal to  $jhigh$  and greater than or equal to  $jlow$ , are the indices of the surface reflected photon heights in  $ht\_initial2$ .

- Populate the vector of surface photon heights,  $ht\_initial2\_surf$ , with the heights at indices  $ii$  in  $ht\_initial2$  (in Matlab these surface heights would be  $ht\_initial2\_surf=ht\_initial2(ii)$ ; where  $ii$  is the vector of surface photon indices).
- Identify the corresponding track distances,  $trackdist\_initial\_surf$ , in  $trackdist\_initial$  at the indices in  $ii$ , [i.e., in Matlab code  $trackdist\_initial\_surf=trackdist\_initial(ii)$ ].

$ht\_initial2\_surf$  is the main product of the surface finding routine. In addition, the second-pass surface indices in  $ii$  are the indices for the time, geolocation, track distance and all other data corresponding to  $ht\_initial\_surf$ . An example of the second pass and the histogram of surface heights for MABEL data are shown in Figure 14.

(N) Calculate Number of Photons, Mean Time, and Geolocation for Segment

-----  
 The number of surface reflected photons in the segment,  $n\_photons$ , is the length of the index vector  $ii$ . The time, geolocation, and track distance of the surface reflected photons are equal to the values in the vectors  $time\_initial$ ,  $lat\_initial$ ,  $lon\_initial$ , and  $trackdist\_initial$  at the index positions given by  $ii$  (e.g.,  $time\_initial(ii)$ ). Compute the segment time,  $t\_seg$ , as the mean of  $time\_initial(ii)$ , and the duration of the segment,  $delt\_seg$ , as the last value of  $time\_initial$  - the first value of  $time\_initial$ . Compute the segment latitude,  $lat\_seg$ , and segment longitude,  $lon\_seg$ , as the means of  $lat\_initial(ii)$  and  $lon\_initial(ii)$ , and the segment length,  $length\_seg$ , as the last value of  $trackdist\_initial(ii)$  - the first value of  $trackdist\_initial(ii)$ .

The total number of photons,  $n\_ttl\_photon$ , equals the length of  $time\_initial$ , and as above, the number of photons reflected from the surface equals  $n\_photons$  equal to the length of  $ii$ . The surface reflected photon rate,  $r_{surf}$ , is equal to  $n\_photons$  divided by  $delt\_seg$ , and the noise photon rate,  $r_{noise}$ , is equal to the difference of  $n\_ttl\_photon$  minus  $n\_photons$  divided by  $delt\_seg$ .

### 5.3.3 Processing to Characterize Long Wavelength Waves, Dependence of Sample Rate on Long Wave Displacement, and A Priori Sea State Bias Estimate

G) Processing Steps to Estimate Sea State Bias

---

In this part we compute the Sea State Bias proportional to the covariance of photo return rate and surface height in 10-m along-track bins. This constitutes what is commonly referred to as the Electro-Magnetic or EM bias that is expected to dominate ICESat2 SSB. The steps are:

1. Add *meanoffit2* to *ht\_initial2\_surf*.
2. Convert *trackdist\_initial\_surf* to meters if necessary
3. Over ocean segments and sort height data in ascending order of along track distance, *trackdist\_initial\_surf*, to allow calculation of photon return rate per meter
4. Define *x* as the sorted *trackdist\_initial\_surf* and the associated heights from *ht\_initial2\_surf*, as *hty*.
5. Compute data spacing, *xs*, as difference in successive *x* values.
6. If *xs* is negative, correct to the mean of nearest neighbor data spacing values. If the negative data spacing, *xs*, is the first or last value in the ocean segment (~8000 photons or 7-km) simply replace it with the nearest neighbor value.
7. Average between adjacent *hty* elements to correspond to *xs*. The length of *hty* will be reduced by one to match the length of *xs*.
8. Do the following analysis for each 10-m bin in the ocean segment (~8000 photons or 7-km) ocean segment:
  - a) Set *xbin* to middle of 10-m bin.
  - b) Set *htybin* to mean of *hty* in each 10-m bin.
  - c) Average data spacing, *xs* and set to *xsbind*.
  - d) Compute the photon data rate per meter, *xrbind*, by inverting 10-m bin average data spacing, *xsbind*. If *xsbind* is zero, set *xrbind* equal to NaN.
  - e) Establish *slopebinfit* :
    - I. = NaN if only one photon in a 10-m bin
    - II. = change in *hty* over change in *x* if only two photons in a 10-m bin
    - III. = linear fit if three or more photons in a 10-m bin
9. Delete data from 10-m bins if there are no photons in the bin or if the data rate, *xrbind* is NaN
10. Compute covariance of bin averaged height and data rate, *binCOVHtXr*, as the average over all 10-m bins of the product of the detrended binned heights, *htybin*, and the detrended binned data rate, *xrbind*.
11. Compute, *binAVG\_Xr*, the average of binned data rate, *xrbind*.
12. Compute the sea state bias, *binSSBias*, as *binCOVHtXr* divided by *binAVG\_Xr*.
13. If there are more than one 10-m in a 2800-m segment with a valid *slopebinfit*:
  - a) Compute *slopeXreturn* as the product of the detrended slope, *slopebinfit*, and the detrended binned data rate, *xrbind*.
  - b) Compute the covariance of the photon rate and the slope, *binCOVslope\_Xr*, as the sum of the *slopeXreturn* divided by the number of 10-m bins with a valid *slopebinfit*.

- c) Compute the sea state slope bias, **binSlopeBias**, as the covariance of the inverted data rate and the slope, **binCOVslope\_Xr**, divided by the mean of the inverted data rate.

14. Save vector arrays **xbin**, **htybin**, and **xrbin** for segment output .

Since the rationale for some of these steps may not be obvious, we provide the following explanations for the steps:

To determine the SSB using Eq. 11 requires that we know the covariance of the surface return rate and the height anomaly associated with the dominant surface waves. To do this we must establish the height variations and photon return rate in evenly spaced 10-m bins along each ocean segment found during the coarse signal finding step. Section 5.3.1.

#### Estimating sea state bias over ocean segments

At this point, if not earlier, because we want to estimate the properties of waves typically hundreds of meters long, it will be necessary to aggregate **ht\_initial2\_surf** and **trackdist\_initial\_surf** along each ocean segment found during the coarse signal finding step. Section 5.3.1

#### Add mean from detrending used after first cut surface finding

The means from the first cut of surface finding are computed from photon heights over surface waves and are therefore contaminated by the correlation of photon return rate with height of the surface over surface waves. If these are not added back into the height record, that contamination by SSB will be lost. Therefore, we add **meanoffit2**, the mean of  $P0 + P1 \times \text{trackdist\_initial\_surf}$  (the along-track position of 2<sup>nd</sup> iteration surface photons), back into the photon height record, **hty = ht\_initial2\_surf + meanoffit2**

#### Calculate data spacing

Defining **x** equal to **trackdist\_initial\_surf over the 2800-m segment**, compute the along-track spacing successive positions in **x**,  $x_i - x_{i-1}$  or in the parlance of Matlab, yield an array of spacings: **xs = x (2:end) - x (1:end-1)**. Average over negative spacings where  $(X_i - X_{i-1}) < 0$ . In our experience with MABEL and ATM data if there is a negative value **xs**, it can be replaced by the average of the previous and succeeding values. If the negative data spacing, **xs**, is the first or last value in the 2800-m segment simply replace it with the nearest neighbor value.

#### Align along-track distance and height with sample spacing.

The data rates in units of meter<sup>-1</sup> are the inverses of the sample interval  $xs_i = (x_i - x_{i-1})^{-1}$ . However, if spacing varies significantly and one tries to interpolate between or average two rates together, the result will be biased away from the true average (i.e.  $2/(x_{i+1} - x_{i-1})^{-1}$ ) toward the higher rate. When many individual rates are averaged in this way the result is greater than the number of photon surface returns divided by the total distance. The problem is eliminated by averaging sample intervals and by interpolating heights and

positions to the midpoint between samples rather than interpolating spacing or sample rate back to sample position. Consequently, we next interpolate height and along-track distance to the middle of each sample interval corresponding to the position of **xs** by averaging between adjacent **hty** elements and averaging between adjacent **x** elements. The lengths of **hty** and **x** will then be reduced by one to match the length of **xs**.

Quantify surface height and slope and return rate in 10-m along-track bins.

First divide the ocean segment into  $N_{bin10}$  10-m bins. Assign each sample interval (*ii*) to one of these bins with a bin index *ibin* where  $ibin(ii) = \text{round-up}((x(ii) - \min(x))/10)$  and cumulatively add the **hty**(*ii*) to **htybin**(*ibin*(*ii*)), cumulatively add the **xs**(*ii*) to **xsbind**(*ibin*(*ii*)), and increment a bin counter, **nbinc**(*ibin*(*ii*)), by one for each added sample.

Find averages, photon return rate and straight-line fits in each 10-m bin

For *ibin* equal to 1 through  $N_{bin10}$  compute bin averages:

Compute the bin averages of height and data spacing:

$htybin(ibin) = htybin(ibin) / nbinc(ibin)$  and

$xsbind(ibin) = xsbind(ibin) / nbinc(ibin)$ .

Set the bin along-track position, **xbin**, to middle of 10-m bin.

The bin-average sample rate is taken equal to the inverse of the bin averaged sample interval:

$xrbind(ibin) = (xsbind(ibin))^{-1}$ , but if **xsbind** is zero, set **xrbind** equal to NaN.

Also compute fits of surface height slope, **slopebinfit**, in each bin

- In the cases with only 1 point in a bin, **slopebinfit** will be set to NaN (not a number).

- In the case of two points in a bin, **slopebinfit** will be equal to the change in **hty** over change in **x**

- If the number of points in a bin is greater than or equal to 3, **slopebinfit** will equal the slope of a linear fit with distance over the points.

Compute interval quantities for the ocean segment

First, delete from consideration any bins with no points at all (i.e. bins for which **nbinc**=0 or if the data rate, **xrbind** is NaN). The remaining bins will be termed viable bins.

Compute Sea State Bias using all viable bins.

Compute covariance of bin averaged height and data rate, **binCOVHtXr**, as the average over all 10-m bins of the product of the detrended binned heights, **htybin**, and the detrended binned data rate, **xrbind**, i.e., the sum over viable bins, *iii*, from 1 to  $N_{bin10}$  of  $(\text{detrended}(htybin(iii)) * \text{detrended}(xrbind(iii))) / N_{bin10}$ .

Similarly, compute **binAVG\_Xr**, the average of binned data rate, **xrbind**, i.e., the average of **xrbind**(*iii*) from *iii*=1 to  $N_{bin10}$ .

Compute the bin average sea state bias estimate according to Equation X7,:  
**binSSBias** equals **binCOVhtXr** divided by **binAVG\_Xr**.

Compute Significant Wave Height, SWH  
 Compute significant wave height (**SWH**) equal to four times the standard deviation of the bin-averaged surface heights in all the 10-m along-track bins in the segment.

Compute photon rate slope correlation.

The bin average slope bias estimate is an experimental parameter that indicates if photons are being preferentially returned from the backsides or front faces of waves.

If there are more than one 10-m in a 2800-m segment with a valid **slopebinfit**, compute **slopeXreturn** as the product of the detrended slope, **slopebinfit**, and the detrended binned data rate, **xrbind**.

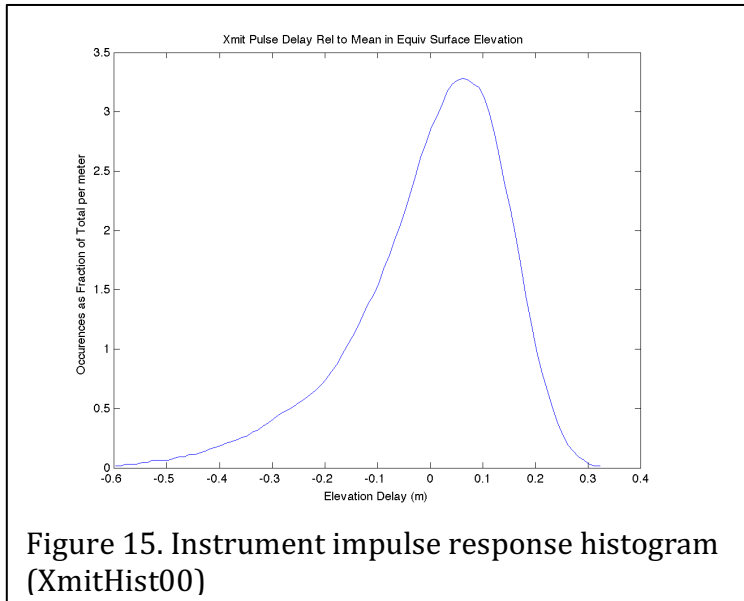


Figure 15. Instrument impulse response histogram (XmitHist00)

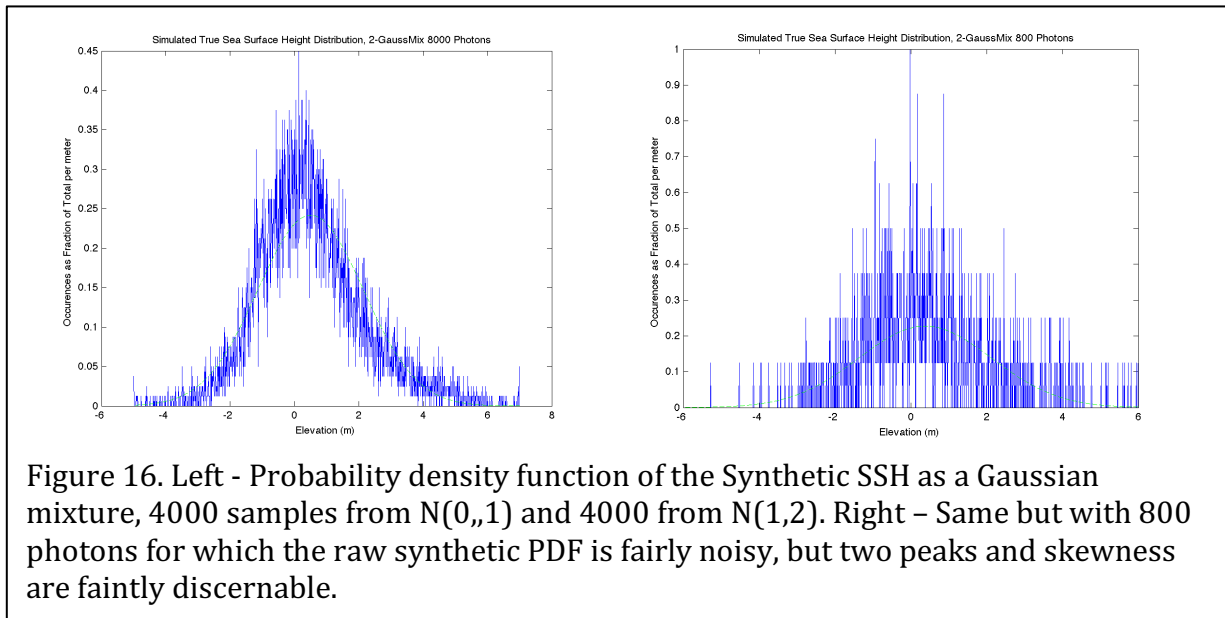
Then compute the covariance of the photon rate and the slope, **binCOVslope\_Xr**, as the sum of the **slopeXreturn** divided by the number of 10-m bins with a valid **slopebinfit**.

Save vector arrays **xbin**, **htybin**, and **xrbin** for segment output .

**5.3.4 Processing Procedure for Correction and Interpretation of the Surface Height Distribution**

This section, 5.3.4, describes processing steps that analyzes the histogram of received surface photon heights, *N* from Section 5.3.2. The procedure has been tested in a developmental Matlab code (WienerTest\_GaussMixandNoise2.m). Matlab executable lines have been replaced by detailed text descriptions.

As described in Section 5.6, to illustrate and validate the program steps in the developmental code we convolved a real impulse response distribution taken from MABEL data (Fig. 15) with a synthetic sea surface height, 2-Gaussian mixture distribution with a specified statistical properties (Fig. 16). A representative amount of noise was then added to this to yield received signal photon height distribution (Fig. 17) with a known true parent surface distribution.



Here parts (A) through (G) go through the analysis process described in part 4.3.1 to determine the true surface distribution, namely Wiener deconvolution to remove the instrument impulse response distribution. This is where the processing of ATL03 histograms begins. Part (H) in 5.2.5 (Characterizing the Random Sea Surface) breaks the processed histogram into a Gaussian Mixture and computes the aggregate distribution statistics for ATL12 using equation 17.

#### 5.3.4.1 Separating the Uncertainty due to Instrument impulse response

Parts

- (A) Starting with histogram of received photon heights from the previous section, compute a constant signal to noise ratio (SNRc)
- (B) Impulse Response Distribution
- (C) Fourier transform of the received histogram
- (D) Fourier transform of the instrument impulse response histogram
- (E) Compute the Wiener filter
- (F) Apply Wiener Deconvolution to Yield the Fourier Transform of the Surface Distribution
- (G) Compute the Surface Height Distribution

## Code Steps

### (A) Noise Ratio Determination

---

- Start with the histogram of surface reflected photons heights,  $N$ , from section (5.3.2 (M)) versus the sea surface height vector,  $sshx$ , with height bin size equal to  $Bf$  (e.g.,  $Bf= 0.01$  m). Convert the histogram to a vector array of probability density function (pdf) values,  $rechist$ . The dimensions of  $rechist$  and  $sshx$  are the same.
- Smooth the received pdf with a 12<sup>th</sup> order, low-pass Butterworth filter with cutoff wavenumber corresponding to  $0.1/binsize$ . Run the filter forward and backward over  $rechist$  to yield the smoothed histogram,  $smoothrechist$ . Figure 17 shows  $rechist$  in blue and  $smoothrechist$  in red for an 8000 photon sample (left) and 800 photon sample (right)

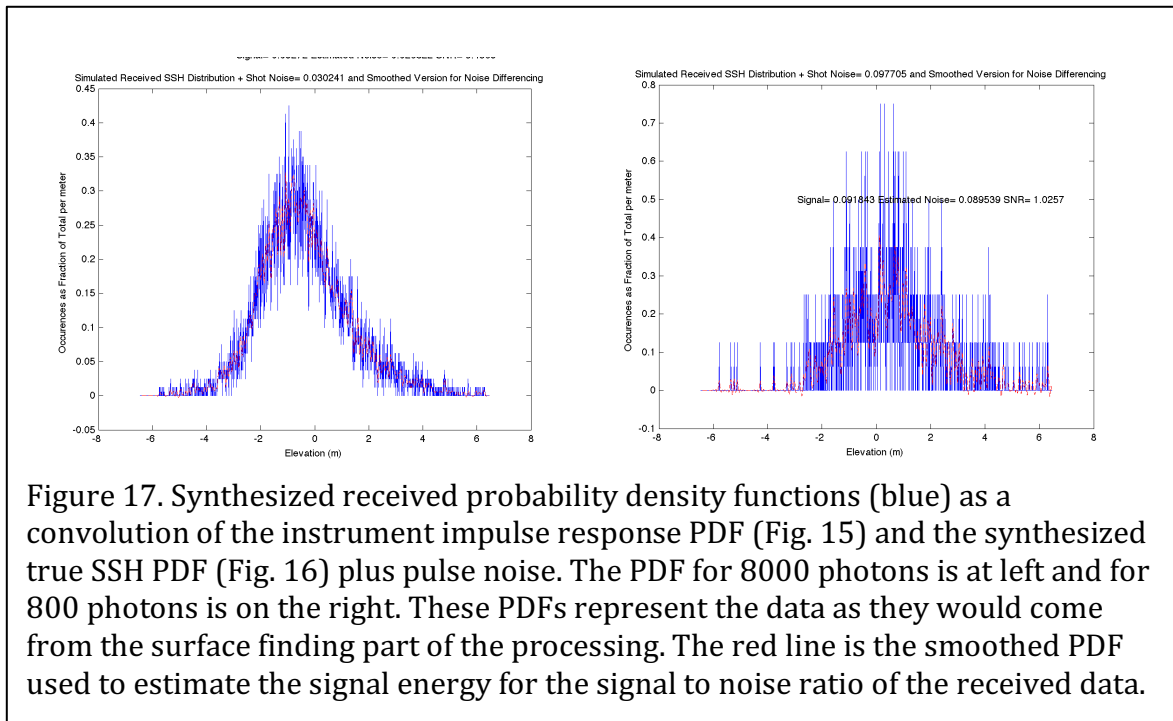


Figure 17. Synthesized received probability density functions (blue) as a convolution of the instrument impulse response PDF (Fig. 15) and the synthesized true SSH PDF (Fig. 16) plus pulse noise. The PDF for 8000 photons is at left and for 800 photons is on the right. These PDFs represent the data as they would come from the surface finding part of the processing. The red line is the smoothed PDF used to estimate the signal energy for the signal to noise ratio of the received data.

- Compute a signal to noise ratio ( $SNRc$ ) equal to the standard deviation (std) of  $smoothrechist$  divided by the standard deviation of the difference between the received histogram and the smoothed histogram,  $SNRc= \text{std}(smoothrechist)/\text{std}((rechist-smoothrechist))$ .
- 

### (B) Impulse Response Distribution

---

Obtain the current best estimate for the instrument response distribution,  $XmitHist000$ , a vector array of probability density function values for the impulse response.

The instrument impulse response distribution is calculated from the most recent transmit echo pulse (TEP) passed from ATL03 in **/atlas\_impulse\_response/pce1\_spot1 or /pce2\_spot3**.

#### *The Transmit Echo Pulse*

The TEP are derived from photons detected via the transmitter echo path (TEP, see Section 7.2.2 of the ATL03 ATBD). These photons are picked off from the transmitted laser pulse, and routed into the ATLAS receiver, for ATLAS strong beams 1 and 3. These data monitor the internal timing bias of ATLAS, as well as the instrument impulse response for the beam. We will assign TEP 1 or TEP 3 to each beam we process, mainly 1, 3, and 5, according to the recommendations in ***tep\_valid\_spot***, a 6x1 array indicating which TEP to use for each spot. Order of the array is by ground track (gt1l; gt1r; gt2l; gt2r; gt3l; gt3r), from ATL03. (Note also, that when the spacecraft is flying forward beam 1 with a TEP is covering spot gt1r and beam 3 with a TEP is covering spot gt2r. When the spacecraft is flying backward beam 1 with a TEP is covering spot gt3l and beam 3 with a TEP is covering spot gt2l.) According to ATL03, the parameters are generated as often as sufficient TEP data exists in the granule, typically about every five granules (granules each span about 1/14<sup>th</sup> of an orbit.). Otherwise data from the prior granule is retained in the current granule. The TEP photon event arrival times are provided in a histogram, ***tep\_hist\_times***.

The TEP photon events are downlinked when the TEP photon events happen to occur within the telemetry band approximately twice per orbit, for about three hundred seconds. The number of TEP photons per shot for a particular beam varies. However, the ratio of the number of TEP photons between beams 1 and 3 appears stable with a value of 0.7, with beam 1 being the stronger of the two. Averaging across a range of instrument configurations, beam 1 generates approximately 0.09 TEP photons per laser pulse, and beam 3 generates approximately 0.07 TEP photons per laser pulse. Assuming one TEP photon event per twenty pulses as the lower limit for the TEP strength, downlinking TEP photons for approximately three hundred seconds should yield about 150,000 TEP photons. TEP photon events are captured any time there are more than thirty seconds of contiguous possible TEP photon events identified in ATL02 (e.g., 15,000 TEP photons), and there are at least 2000 possible TEP photons in the set. All available TEP photons within a given set are used; there is no upper limit on the duration or number of TEP photons. The set is ended when the TEP photons are no longer present in the telemetry band, or five seconds have passed with no additional TEP photons. With a sufficient number of possible TEP photon events identified, these will either be background photon events, misclassified signal photon events, or TEP photon events. The time of day of the start of the TEP data used in subsequent analyses is reported on ATL03 as ***tep\_tod***, while the duration of TEP data is reported as ***tep\_duration***.

The histogram of these possible TEP photon events is formed using 50 picoseconds bin widths. There is more than a single mean arrival time of TEP photons; with two bands with the primary band being at ~ 20 nanoseconds and the secondary band being at 46

nanoseconds. The actual time band limits for each TEP will be indicated by the ATL03 variable ***tep\_range\_prim***. Additional noise photons are also present. The mean background photon rate is determined by excluding the bins between 17 and 24 ns (the region of the primary return) and the region between 43 and 50 ns (the region of the secondary return) and calculating the mean of the remaining bins. This value is reported on the ATL03 output product as ***tep\_bckgrd***, and is subtracted from all bin counts. The number of counts in the remaining histogram is reported as ***tep\_hist\_sum***. The number of counts in each bin is normalized by ***tep\_hist\_sum*** and reported for each bin as ***tep\_hist***. Time is measured relative to the centroid transmit pulse, and on average for the TEP represents the travel time back and forth through the ATLAS optical path. The time of the histogram bin centers (the mean of the times of the leading and trailing edges of the bins) is recorded as ***tep\_hist\_time***. The parameter ***tep\_tod*** indicates when the TEP data on a given ATL03 granule was generated. The parameters derived from TEP data are part of the ATL03 data product in the groups /atlas\_impulse\_response/pce1\_spot1/ and /atlas\_impulse\_response/pce2\_spot3/.

*Turning the TEP histogram into the Instrument Impulse Response*

We convert from ***tep\_hist*** expressed as normalized counts in *tepbinsize*=50 picosecond wide bins to an impulse response expressed as the probability density function with ***binsize*** wide bins of surface height. For the purpose of calculating the length of the derived surface distribution it is conceptually useful to interpolate to values in ***XmitHist000*** so that there are an odd number of bins with the origin bin at zero delay (or elevation) and the same bin size (***binsize***) as is used for the received elevation histogram. The process of deriving this impulse response from a TEP first requires identifying the appropriate TEP to use for a particular beam specified by ***tep\_valid\_spot***, isolating the primary band of times specified by ***tep\_range\_prim***, trimming the TEP to primary histogram levels above the background noise rate, converting from travel time to surface photon height offset, converting to ***binsize*** wide bins starting from negative offsets, and normalizing to a probability density function by dividing by the sum of the histogram levels multiplied by ***binsize***. For the purpose of calculating the length of the derived surface distribution it is conceptually useful to interpolate values in ***XmitHist000*** so that there are an odd number of bins with the origin bin at zero delay (or elevation) and the same bin size (***binsize***) as is used for the received elevation histogram.

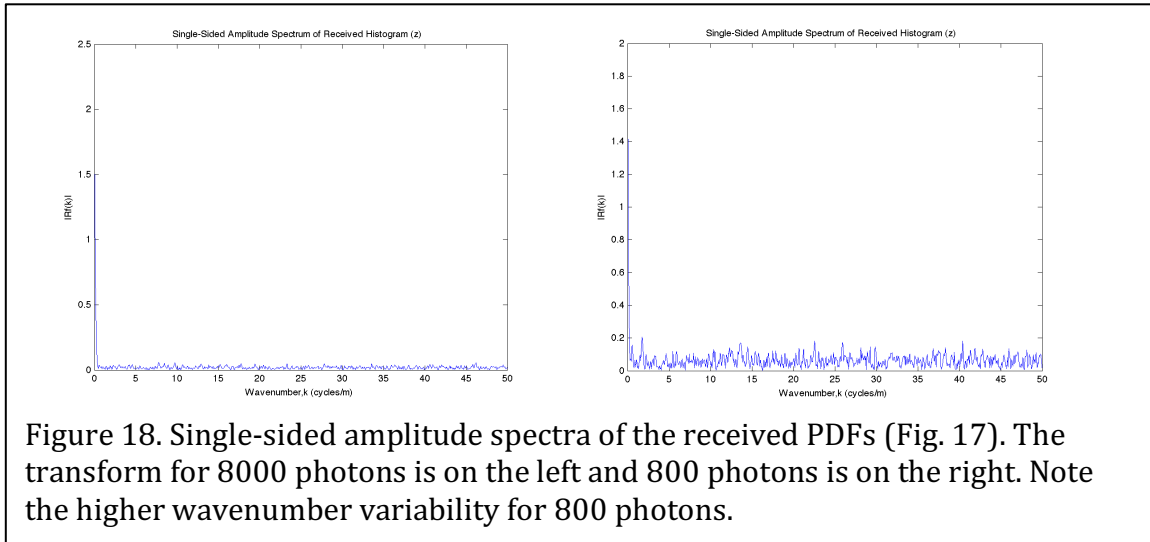
In part this pseudo code comes from the Matlab program BinconvertWF\_JM3.m.

- The appropriate TEP histogram, ***tep\_hist***, as specified by ***tep\_valid\_spot*** for a particular beam includes both the primary and secondary arrivals. Choose the primary TEP arrivals in bins between ***tep\_range\_prim***(1) and ***tep\_range\_prim***(2) (typically around 17 and 24 ns) for use in ATL12 processing. e.g., (iprimary=find(tepT>= ***tep\_range\_prim***(1) & tepT<= ***tep\_range\_prim***(2); tepT=tepT(jprimary); tepP=tepP(jprimary);
- Because ***tep\_bckgrd*** is subtracted from the TEP histogram, the tails of the TEP will include bins with negative values. We trim off these tails where negative values appear indicating the TEP is below the noise floor. Working from time of TEP maximum

out, set the TEP value to zero at the first bins where TEP is less than zero, and delete all bins beyond those points.

- Convert from travel time to surface height coordinate for the histogram by multiplying it times minus half the speed of light.
- Reverse the order of the histogram and its distance axis so that the array starts at negative height offsets.
- Center the TEP histogram so that it has height offset equals zero at the centroid of the distribution.
- Confirm the TEP bin size, *bin\_TEP*, as the distance between bin centers 50 picoseconds/ (2 x speed of light).
- Convert TEP bin centers to bin boundaries in meters
- Establish an array of impulse response histogram bin boundaries with an odd number of bins, a bin size equal to *binsize*, interior bin centered on zero, and all within the range of the TEP bin boundaries.
- Compute the cumulative histogram of the TEP versus the TEP bin boundaries and interpolate to the impulse response histogram bin boundaries.
- Differentiate the resulting cumulative impulse response histogram and form a corresponding array of bin centers to produce the instrument impulse response histogram.
- Divide the impulse response histogram by the product of *binsize* and the sum of values in the histogram to yield the impulse response probability density function.

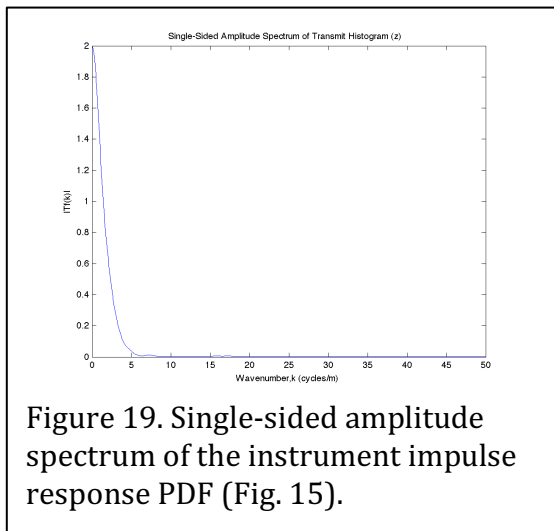
At this point, we have described the averaged pulse shape characteristics from the threshold crossing times posted at the nominal ~20 meters along-track segment rate. We also have described the TEP photon events and have formed a histogram and related parameters based on TEP events. Since the times of these respective groups are known, it is possible to examine how the SPD-based statistics vary during the period spanned by the TEP data. However, combining these two groups quantitatively is complicated by two aspects. First, the SPD-based data and the TEP-based data have unique paths through the instrument and so the reported times of these data will be substantially different. While these differences are characterized with pre-launch data, we have little insight into how the temporal bias between these data will evolve through time. Secondly, the SPD-based data is derived from the reported times when a filtered version of the transmitted laser pulse crosses a particular amplitude threshold (measured in volts). The TEP-based data on the other hand is a histogram of counts of a massively attenuated version of the transmitted laser pulse. As such a quantitative correspondence between voltages and counts is problematic. A relationship could possibly be made between the standard deviation of the threshold crossing times and the apparent width of the TEP-based histogram at several points along the profile. This may allow a user to better predict how the transmitted pulse is changing between realizations of the TEP.



(C) Fourier Transform of Received Height Distribution

---

- Find length of record ( $NFFT$ ) equal to the next power of two greater than the length of  $rcvhist$ . This should cover the longest of the impulse response distribution,  $XmitHist000$ , and  $rcvhist$ .
- Pad the end of  $rcvhist$  with zeros to extend it to length  $NFFT$
- Compute the fast Fourier transform,  $Rf$ , of the received height distribution,  $rcvhist$



- Ensure consistent scaling so that energy is preserved (e.g., with Matlab FFT, we multiply the result by the binsize to reflect integration in the space domain
- The highest wavenumber (cycles per meter) is the Nyquist wavenumber equal to half the sampling wavenumber,  $wvns$ , which equals the inverse of  $binsize$  ( $wvns=1/binsize$ ). Using this, we compute the wavenumber vector ( $wvn$ ) corresponding to the Fourier transform of the received histogram. Examples of  $Rf$  plotted versus  $wvn$  are shown in Figure 18.

(D) Fourier Transform of Instrument Impulse Response

---

- Pad the end of  $XmitHist000$  with zeros to extend it to the length  $NFFT$

- Compute the fast Fourier transform,  $Tf$ , of the impulse response distribution,  $XmitHist000$
- Ensure consistent scaling so that energy is preserved (e.g., with Matlab FFT, we multiply the result by the *binsize* to reflect integration in the space domain)
- Examples of  $Tf$  plotted versus  $wvn$  are shown in Figure 19.

(E) Compute the Wiener Filter

- 
- Compute the Wiener filter,  $WienerF$ , equal to  $Tf \times Tf_{cc} / (Tf \times Tf_{cc} + SNRc^2)$ , where subscript cc denotes complex conjugate.
  - Note that ultimately, we may compute the Wiener filter with a signal to noise variation,  $SNRf$ , that varies with wavenumber wavenumber, e.g.,  $SNRf$  equal the absolute value of the Fourier transform of the received distribution ( $Rf$ ) divided by the perceived noise ( $NoiseRec$ ), but tests so far using the constant  $SNRc$  have worked well.
  - Examples of  $WienerF$  plotted versus  $wvn$  are shown in Figure 20.

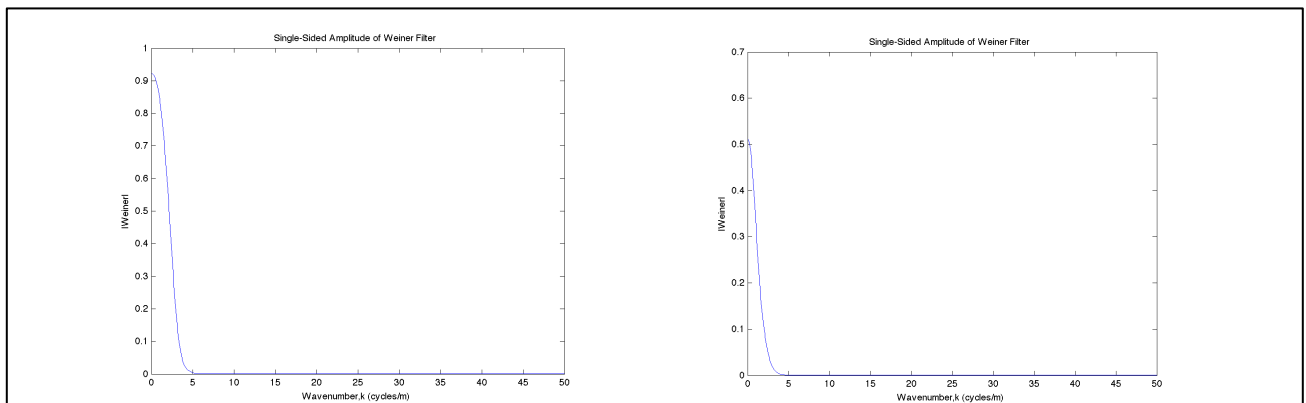
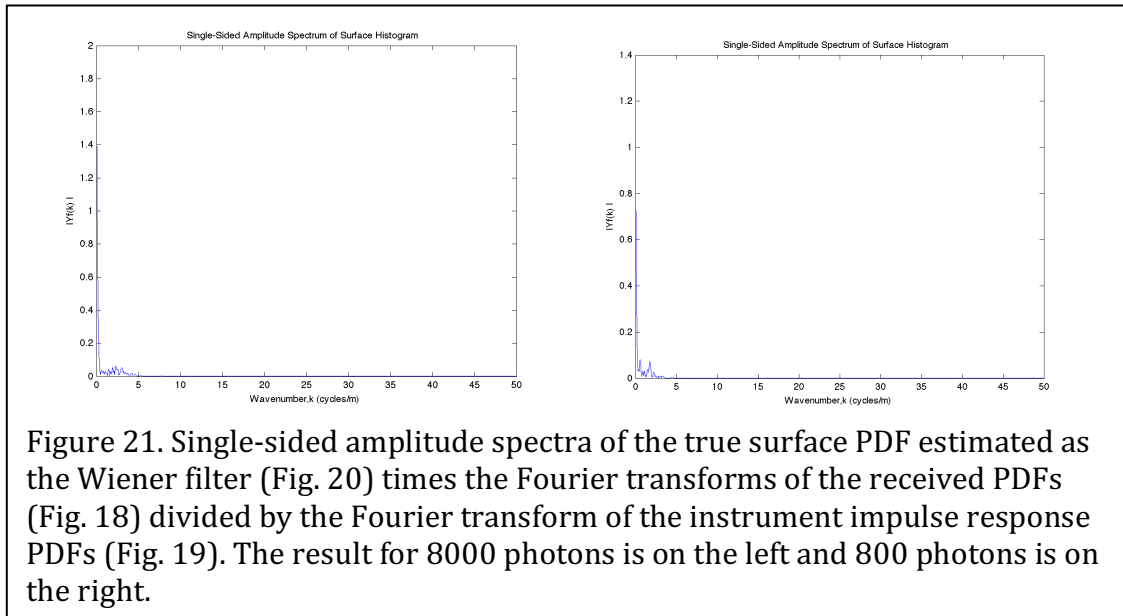


Figure 20. Single-sided amplitude spectra of the Wiener filters computed from the Fourier transform of the instrument impulse response PDFs (Fig. 19) and the signal to noise ratio estimated from the received height PDFs and smoothed versions of them (Fig. 17). Owing to a lower signal to noise ratio, the Wiener filter for 800 photons (right) has a narrower low frequency pass band than the 8000 photon filter (left).

(F) Apply Wiener Deconvolution to Yield the Fourier Transform of the Surface Distribution

- 
- Compute the Fourier transform of the surface distribution,  $Yf$ , as the Wiener deconvolution of the instrument impulse response distribution and the received height distribution. In Fourier (wavenumber) space this is the Wiener filter,  $WienerF$ , multiplied times the ratio of the transform of the received distribution,  $Rf$ , and the transform of the impulse response,  $Tf$ , i.e.,  $Yf = WienerF \times Rf / Tf$ .

- Examples of  $Yf$  plotted versus  $wvn$  are shown in Figure 21.



### G) Compute the Surface Height Distribution

In this part, we compute the distribution of surface height as a probability density function (PDF) starting with the Fourier transform of that PDF output by the Weiner deconvolution. The steps are:

1. Compute  $Yfi$ , as the inverse Fourier Transform of  $Yf$  divided by  $binsize$
2. Determine the x-axis,  $derivedsshx$ , for the surface histogram
  - a) Set  $derivedsshx$  equal to the x-axis for the received histogram,  $xrechist$ .
  - b) Find  $zbin$ , the cell number where  $xmithist$  equals zero.
  - c) Remove the following number of values from the end of  $derivedsshx$ :  
length( $xmithist$ ) minus  $zbin + 1$
  - d) Remove the following number of values from the front end of  $derivedsshx$ :  $zbin$  minus 1. The length of  $derivedsshx$  should now be equal to the length of  $Y$ .
3. Compute  $derivedlsshhist$  equal to length of the received surface histogram ( $xrechist$ ) minus length of impulse response ( $lmithist$ ) plus 1.
4. Compute  $Y$ , by truncating  $Yfi$ , to the first  $derivedlsshhist$  values.
5. Normalize  $Y$ , by dividing  $Y$  by the sum of the product of  $Yfi$  and  $binsize$ .
6. Compute the mean or centroid of  $Y$ ,  $meanY$ , by summing the product of  $Y$  and  $derivedsshx$  and dividing that sum by the sum of  $Y$ .
7. Compute the standard deviation of  $Y$ ,  $stdY$ :
  - a) square  $derivedsshx$  minus  $meanY$
  - b) Multiply a) by  $Y$
  - c) Take sum of b)

- d) Divide c) by sum of  $Y$
- e) Take square root of d)
- 8. Compute the skewness of  $Y$ , **skewness $Y$** :
  - a) Cube **derivedsshx** minus **mean $Y$**
  - b) Multiply a) by  $Y$
  - c) Take sum of b)
  - d) Divide c) by sum of  $Y$
  - e) Divide d) by the cube **std $Y$** .
- 9. Compute the kurtosis of  $Y$ :
  - a) Compute **derivedsshx** minus **mean $Y$**  to the fourth power
  - b) Multiply a) by  $Y$
  - c) Take sum of b)
  - d) Divide c) by sum of  $Y$
  - e) Divide d) by the **std $Y$**  to the fourth power
  - f) Subtract three from e)

Since the rationale for some of these steps may not be obvious, and the steps may have to be modified depending on the differences between the Matlab (used in the developmental code) and Fortran (used in the ASAS code), we provide the following explanations for the steps:

- Compute **Yfi**, equal to the inverse Fourier transform of the output of the Wiener filtering process, **Yf**. Ensure that the result is normalized to conserve energy and dimensional consistency. For example, the output of the Matlab inverse Fourier transform (ifft.m) must be divided by **binsize** for dimensional consistency.

Compute x-axis derived from **xrechist** and characteristics of instrument impulse response. Convolution of one finite series of length  $N$  with another of length  $M$  results in a series of length  $N+M-1$ . We know further that if the instrument impulse response histogram has zero mean with the zero bin at index position **zbin** this will dictate where the points are added to the true height histogram to lengthen the received height histogram. If the impulse response distribution were symmetric, equal points would be added to each end, but this is not generally true. In fact, assuming the length of the impulse response histogram is **lxmithist**, and the zero point is at index, **zbin**, **zbin-1** points will be added to the beginning of the true surface height histogram and **lxmithist-zbin** points will be added to the end of the surface height histogram to produce the convolved received histogram.

- In processing, we reverse this to trim the length of the vector x-axis of the received height histogram, **xrechist**, to the appropriate x-axis for the underlying surface height histogram, by deleting the first **zbin-1** points and the last **lxmithist-zbin** points from **xrechist** to yield the vector of x-axis of the surface histogram, **derivedsshx**, with length, **derivedlsshhist** equal to  $\text{length}(\text{xrechist}) - (\text{lxmithist} - 1)$ .

Trimming the vector of surface histogram values is complicated by the necessity of padding received histogram with zeros to a length equal to a power of two for computation of its fast

Fourier transform. As a result, at least in the prototype Matlab code, the inverse Fourier transform of the output of the Wiener deconvolution process,  $Y_{fi}$ , also has a length equal to this same power of two and should be truncated to the appropriate length.

- Consequently, truncate  $Y_{fi}$  keeping only the first number of points in the original received histogram less  $(l_{xmithist}-1)$ , i.e., set  $derivedlsshx$  equal to  $length(xrechist)-(l_{xmithist}-1)$ . This yields the surface histogram,  $Y$ , defined over  $derivedsshx$ , that will have the number of points consistent with deconvolving the impulse response from the received histogram.
- To give the surface height probability density function,  $Y$ , normalize the  $Y_{fi}$  to make up for energy lost in the Wiener filter application. The integral of  $Y$  should equal unity, so take  $Y$  equal to  $Y_{fi}$  divided by the integral of  $Y_{fi}$ , i.e.,  $Y = Y_{fi} / (\text{sum of } Y_{fi} \times \text{binsize})$ .
- As a check on the deconvolution computation, the centroid of  $rechist$  and  $Y$  should both be near zero on account of the detrending of the surface heights and the assumed zero mean of the instrument impulse response computation
- Examples of  $Y$  and the difference between  $Y$  and the synthetic surface examples that we started

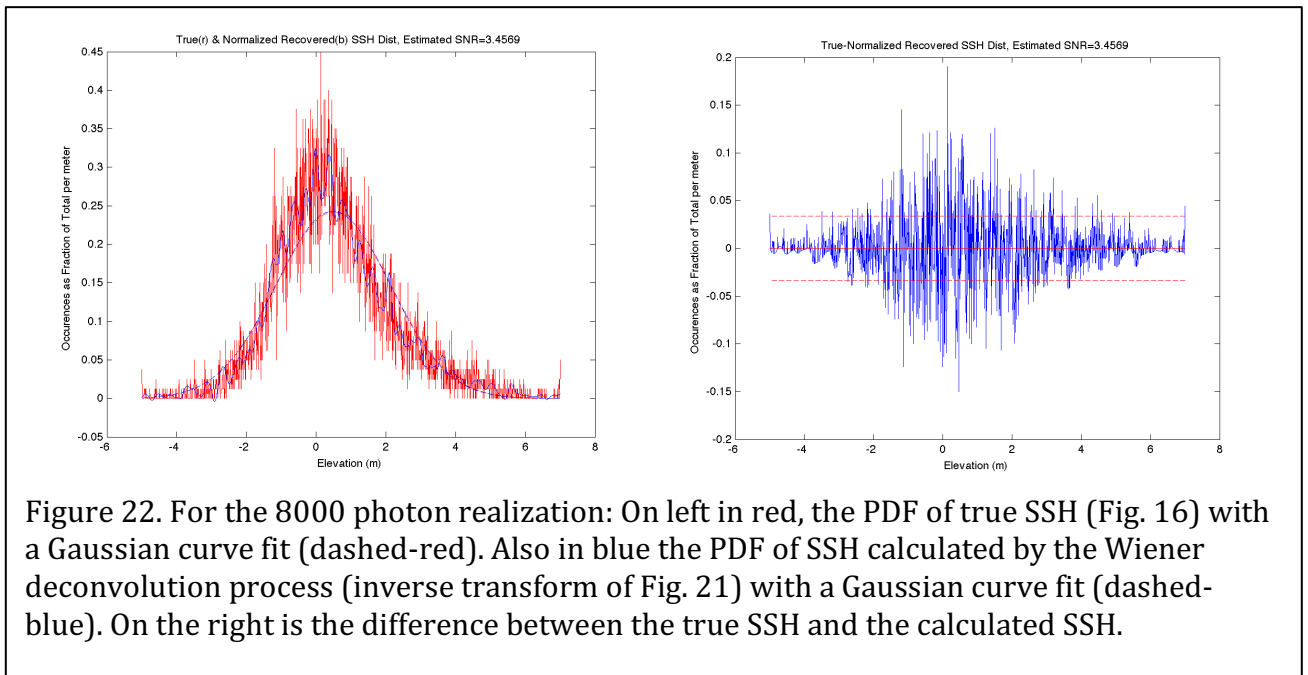


Figure 22. For the 8000 photon realization: On left in red, the PDF of true SSH (Fig. 16) with a Gaussian curve fit (dashed-red). Also in blue the PDF of SSH calculated by the Wiener deconvolution process (inverse transform of Fig. 21) with a Gaussian curve fit (dashed-blue). On the right is the difference between the true SSH and the calculated SSH.

with are given in Figure 22 for 8000 photons and Figure 23 for 800 photons.

- For subsequent use in the derivation of the ATL19 gridded product, the surface pdf,  $Y$ , will also be output for each segment along with the total number of surface photons,  $N$ , and bin size,  $binsize$ .
- $Y$  is defined over a vector of bin centers,  $sshx$ , but  $Y$  will be output as a 1001 element vector for every segment with the 501<sup>st</sup> center bin being for height zero, bin  $501 - Y_{lowX}/binsize$  being the lowest bin with nonzero  $Y$  and bin  $501 + Y_{lowX}/binsize$  being the highest bin with nonzero  $Y$ .

- As a simple check on the optimum Gaussian Mixture determination of the higher moment of the sea surface distribution we will compute and output the mean, variance, skewness, and excess kurtosis (***Ymean***, ***Yvar***, ***Yskew***, ***Ykurt***) related to the higher moments of ***Y*** directly.

$$Ymean = \mu_Y = \left( \sum_{Y_i > 0} X_i Y_i \right) / \left( \sum_{Y_i > 0} Y_i \right) \quad (30)$$

$$Yvar = \left( \sum_{Y_i > 0} (X_i - \mu_Y)^2 Y_i \right) / \left( \sum_{Y_i > 0} Y_i \right) \quad (31)$$

$$Yskew = \left[ \left( \sum_{Y_i > 0} (X_i - \mu_Y)^3 Y_i \right) / \left( \sum_{Y_i > 0} Y_i \right) \right] / Yvar^{3/2} \quad (32)$$

$$Ykurt = \left[ \left( \sum_{Y_i > 0} (X_i - \mu_Y)^4 Y_i \right) / \left( \sum_{Y_i > 0} Y_i \right) \right] / Yvar^2 - 3 \quad (33)$$

### 5.3.4.2 Characterizing the Random Sea Surface

This part goes through the analysis process described in part 4.3.2 to determine the true surface distribution, namely: Maximum likelihood analysis to determine the means, variance, and mixing ratio of the two parent normal distributions.

(H) Compute the 2-component Gaussian mixture Equivalent of the Surface Distribution

- At this point we have the probability density function, ***Y***, of detrended DOT over height bins with centers at ***sshx***. The detrending process used in surface finding removed an average, ***meanoffit2***, from the original heights. Once we have determined the mean and higher moments of ***Y***, we could add ***meanoffit2*** to the mean of ***Y*** to learn the mean DOT over the ocean segment. However, preliminary analysis suggests if we add ***meanoffit2*** back into the distribution before the optimal Gaussian Mixture determination, the resulting higher moments are less noisy over many ocean segments. This can be done by shifting ***sshx*** by adding ***meanoffit2*** to each value in ***sshx***. Then the true average DOT will be derived as the aggregate mean of the optimally derived Gaussian mixture. For the developmental Matlab code a slightly different but equivalent approach was used.
- While the Matlab development code used a maximum likelihood approach (Matlab function `gmdistribution.fit`) to compute the 2-component Gaussian mixture corresponding to the observed surface height distribution, ***Y***. The ASAS code will use an iterative Maximum Expectation approach from ATBD ATL07 Appendix E.

- For the development code using the Matlab `gmfitdistribution.fit` routine, we first created a sea surface height spatial series with the height distribution  $Y$ . This is accomplished by first multiplying  $Y$  by 10,000, rounding and deleting zeros to produce an integer distribution,  $YI$ . A series,  $XY$ , is assembled by concatenating for each value of  $YI(i)$  for index  $i$  corresponding to height  $sshx(i)$ ,  $YI(i)$  values equal to  $sshx(i)$ . The shift to heights including *meanoffit2* was accomplished in this case by adding *meanoffit2* to each value in  $XY$ . Although it is not strictly necessary, the values of  $XY$  are randomly permuted to produce a realistic distribution of heights with the probability density function  $Y$  on

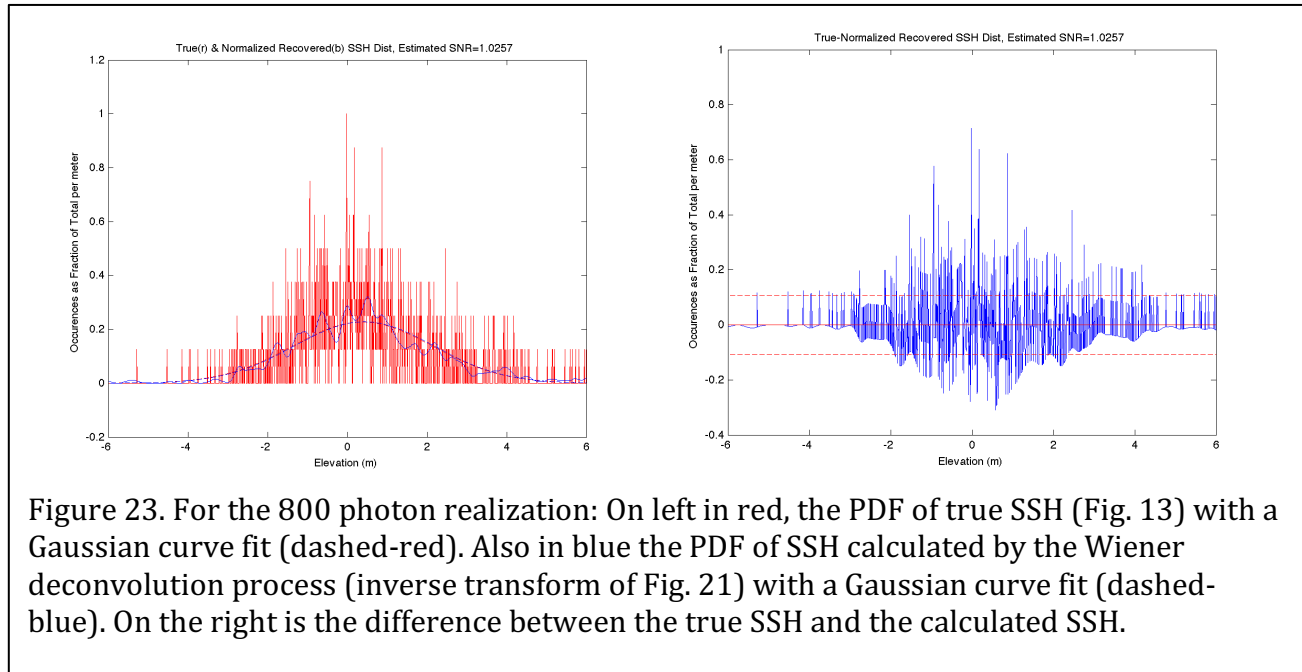


Figure 23. For the 800 photon realization: On left in red, the PDF of true SSH (Fig. 13) with a Gaussian curve fit (dashed-red). Also in blue the PDF of SSH calculated by the Wiener deconvolution process (inverse transform of Fig. 21) with a Gaussian curve fit (dashed-blue). On the right is the difference between the true SSH and the calculated SSH.

heights given in *sshx* shifted by adding *meanoffit2*.

- We then compute the 2-component Gaussian mixture variables, of the two-Gaussian mixture using `GMfit=gmfitdistribution.fit(XY',2)`.
- The result is Gaussian mixture distribution with 2 components:

- With example output for 8000 photons  
Gaussian mixture distribution with 2 components in 1 dimensions

Component 1:

Mixing proportion,  $m1 = 0.457026$

Mean,  $\mu1 = 1.0488$

Standard Deviation,  $\text{Sig1} = 2.0062$

Component 2:

Mixing proportion,  $m2 = 0.542974$

Mean,  $\mu2 = 0.0081$

Standard Deviation,  $\text{Sig2} = 1.0533$

- For the 800 photon case the results are:

Gaussian mixture distribution with 2 components in 1 dimensions

Component 1:

Mixing proportion, **m1** = 0.533033

Mean, **mu1** = 0.8430

Standard Deviation, **Sig1** = 2.0559

Component 2:

Mixing proportion, **m2** = 0.466967

Mean, **mu2** = -0.0553

Standard Deviation, **Sig2** = 1.0533

(I) Compute the Aggregate Mean, Variance, Skewness and Kurtosis of Sea Surface Height

-----

– Use the five parameters of the 2-Gaussian mixture to compute the aggregate moments, first through fourth of the aggregate mixture. From (27), for a mixture of two Gaussians with a fraction **m1** ( $m_1$ ) from the first Gaussian with mean **mu1** ( $\mu_1$ ) and standard deviation **sig1** ( $\sigma_1$ ) and a fraction **m2** ( $m_2$ ) (note:  $m_1+m_2=1$ ) from the second Gaussian with mean **mu2** ( $\mu_2$ ) and standard deviation **sig2** ( $\sigma_2$ ) the  $j^{\text{th}}$  moment of the mixture is calculated according to:

$$E\left[(X - \mu_{mix})^j\right] = \sum_{i=1}^2 \sum_{k=0}^j \frac{j!}{k!(j-k)!} (\mu_i - \mu_{mix})^{j-k} m_i E\left[(X_i - \mu_i)^k\right] \quad (34)$$

$$E\left[(X - \mu_{mix})^j\right] = \sum_{i=1}^L \sum_{k=0}^j \frac{j!}{k!(j-k)!} (\mu_i - \mu_{mix})^{j-k} m_i E\left[(X_i - \mu_i)^k\right]$$

Note that in computing the moments (34), the histogram data the expectation operation ( $E[ ]$ ) is not actual executed, because obviously we do not have the sample populations of the mixture components. The expectation operator appears in (34) to indicate the mixture moments and the mixture component moments coming from Section 5.2.5.2 (H) above. These are applied sequentially using only first and second moments of the mixture components and the mixing proportions to get up to the fourth moment of the mixture.

- The first moment or mean of the mixture,  $\mu_{mix} = m_1\mu_1 + m_2\mu_2$  (28) is the mean of the detrended surface photon heights relative to the geoid with the mean of the detrending process, **meanoffit2** (equal to the mean of **P0+P1\*trackdist\_initial\_surf**), added back in prior to the Gaussian mixture determination. Thus it represents the mean DOT uncorrected for sea state bias, along the ocean segment. Therefore, the mean sea surface height, **SSH**, for the segment to be output in ATL12 is equal to the mean of the mixture,  $\mu_{mix}$ , plus **meangdht** equal to the mean of geoid height, **gd\_ht**, over the segment:

$$SSH = \mu_{mix} + meangdht = m_1\mu_1 + m_2\mu_2 + meangdht \quad (35)$$

- The second moment of the mixture is the sea surface height variance, **SSHvar**, for the segment to be output in ATL12 and used to estimate significant wave height. Here we don't include the variance due to the segment trend in sea surface height due to underlying trends in the DOT or geoid height. From (29), the second moment, or squared standard deviation,  $\sigma_{mix}^2$ , of the mixture is:

$$SSHvar = \sigma_{mix}^2 = m_1\left((\mu_1 - \mu_{mix})^2 + \sigma_1^2\right) + m_2\left((\mu_2 - \mu_{mix})^2 + \sigma_2^2\right) \quad (36)$$

- Using (34), compute third and fourth moments, we obtain the sea surface height skewness, **SSHskew**, and excess kurtosis **SSHkurt**,

$$SSHskew = E\left[(Y - \mu_{mix})^3\right] / \sigma_{mix}^3 \quad (37)$$

$$SSHkurt = E\left[(Y - \mu_{mix})^4\right] / \sigma_{mix}^4 - 3 \quad (38)$$

and output these as part of ATL12 to better characterize the sea surface. Here we don't include the skewness and kurtosis due to the segment trend in surface height.

#### 5.3.4.3 Conclusions for Section 5.3.4:

Our synthetic true SSH distribution was assumed to be an even mix of heights drawn from two Gaussian distributions, one with a mean of zero and a standard deviation of 1 m, and the other with a mean of 1 m and a standard deviation of 2 m.

The result of the Wiener deconvolution of the synthesized received distribution, made by convolving the true SSH distribution with the instrument impulse response distribution and adding noise, produced what is essentially a smoothed version of the true SSH distribution (Fig. 22 left for 8000 photons and Fig. 23 left for 800 photons). The Gaussian fits to the true and calculated distributions means and standard deviations are virtually identical, but of course, both miss the slight bi-modality and skewness of the true and calculated SSH distributions.

Using the Matlab `gmdistribution.fit` function on the calculated SSH distribution and assuming mixture distribution with 2 Gaussian components in 1 dimension yields for 8000 photons means of 0.0081 m and 1.0488 m versus the true values of 0 m and 1 m. The Expectation Maximization (EM) of `gmdistribution.fit` yields standard deviations for the two Gaussian components of 1.1481 m and 2.0062 m versus the true values of 1 m and 2 m. The `gmdistribution.fit` value mixture ratios are 0.5430 and 0.4570 versus the true values of 0.50 and 0.50.

For 800 photons the EM process yields means of -0.0553 m and 0.8430 m versus the true values of 0 m and 1 m. The Expectation Maximization of `gmdistribution.fit` yields standard deviations for the two Gaussian components of 1.0533 m and 2.0559 m versus the true values of 1 m and 2 m. The `gmdistribution,fit` value mixture ratios are 0.4670 and 0.5330 versus the true values of 0.50 and 0.50.

These results with Wiener convolution and analysis by fitting a 2-component Gaussian Mixtures are promising. Clearly 8000 photons produces much better fidelity than 800 photons. This modeling approach gives us confidence that the analysis procedure is capable of an accurate estimate of surface statistics. Further testing with synthetic data, MABEL data and ATLAS simulator data will be needed fully understand the capabilities of these tools. For example, a more precise test of capability might be to use an idealized synthetic surface histogram that was more nearly perfect, having been derived analytically or drawn as we have here, but from a very large number of samples (e.g., 800,000). Pulse noise would then be added corresponding to various sample sizes. Wiener deconvolution results could then be compared to the perfectly idealized surface histogram and errors attributed solely to the processing procedure, with no error associated with the initial synthesized surface.

In running the Matlab Wiener deconvolution prototype scheme, we found it to be stable over a wide range of imposed noise values and several Gaussian mixtures. For very high assumed signal to noise ratios, it more closely reproduces the true SSH PDF (e.g., Figs. 22 and 23) seemingly accepting as signal what looks to us like noise due to low sample counts. For low signal to noise ratios, the Wiener deconvolution scheme produced a smoothed version of the synthetic SSH distribution, throwing out the noise due to low sample counts. While we think the method of signal to noise estimation used here is reasonable, it must be tested with real data. In whatever way we estimate the signal to noise ratio, the Wiener deconvolution scheme appears to be a robust way of handling it. It does an excellent job of reproducing the overall mean and variance of the true SSH PDF (Figs. 22 and 23).

Fitting a Gaussian mixture model to the data also appears to work well but we should experiment with larger numbers of synthetic photon counts to see what improvements can be made to the accuracy of the component means and variances. We also need to see how the mixture means and higher moments (Eqn. 17) improve with higher photon counts. Because we have treated the Matlab routine `gmdistribution.fit` as a black box, we also need to learn more about how the EM method works and would be applied in a standalone code. The scheme can be compared to the minimum squared error approach used for GLAS and we can see if that existing routine can be used for ATLAS to derive Gaussian mixtures representing the ocean surface height distribution.

### 5.3.5 Applying *a priori* SSB Estimate

The *a priori* SSB estimate of Section 5.3.3 can be applied to the mean SSH and DOT (=SSH-EGM2008 Geoid) for comparison to in situ cal/val or other altimeters. The impact of this SSB on the other moments is TBD.

### 5.3.6 Expected Uncertainties in Means of Sea Surface Height

The ocean products of ATL12 are the distributions of sea surface height over ocean segments typically 5 to 7 km long and including about 8,000 candidate surface reflected photons. The height distributions are characterized up through their 4<sup>th</sup> moments (mean, standard deviation, skewness, and kurtosis) using the 2-Gaussian mixture approach. In this subsection, we examine the magnitude of the expected uncertainties in the mean of the surface height distribution. For the open ocean, we consider uncertainty in the mean height due to:

1. Signal-to-noise considerations in a distribution of photon heights.
2. Uncertainties in the mean impulse response.
3. Subsurface scattering.

These are borrowed from and consistent with the ATL07 Sea Ice ATBD except due the low rate of photon returns (about 1 photon per pulse) over the ocean surface, we exclude first-photon bias. We also do not consider sea state bias discussed in previous chapters because we are calculating SSB directly and the errors in this calculation will have to be determined during the ICESat-2 cal/val process.

#### 5.3.6.1 Signal-to-noise considerations and the dominant effect of surface wave roughness

We expect the largest contributions to uncertainty in the mean sea surface height to be due to surface roughness and at least over short averaging lengths in daytime, background noise. The total number of photons

( $NP_{tot}$ ) in a height window,  $W$ , is the sum of the number of signal photons, the background rate ( $B_s$ ) and the number of pulses ( $N_{pulses}$ ) within that window:

$$NP_{tot} = NP_{signal} + NP_{bkg}$$

Background photons are uniformly distributed within the height window and thus the standard deviation,  $\sigma_{bkg}$ , can be written as,

$$\sigma_{bkg} = W (12)^{-1/2} = 0.2887 W,$$

where the factor .2887 is the standard deviation of a uniform random variable on a unit interval. The number of background photons  $NP_{bkg}$  in the window ( $W$ ) is a Poisson variable with a mean value given by:

$$NP_{bkg} = 2 N_{pulses} B_s (W/c)$$

If the distribution of the received signal photons is approximately Gaussian, the variance depends on the transmit-pulse width ( $\sigma_{pulse}$ ) and the surface roughness ( $\sigma_{rough}$ ):

$$\sigma_{signal}^2 = \sigma_{rough}^2 + \sigma_{pulse}^2$$

The expected composite variance of surface height can then be written as:

$$\sigma_{surf}^2 = \frac{NP_{signal} \sigma_{signal}^2 + NP_{bkg} \sigma_{bkg}^2}{NP_{signal} + NP_{bkg}}$$

Except for the roughness, all of the quantities in this equation can be estimated from the data: the background and signal photon counts can be estimated from the total number of photons and the background rate. For a relatively smooth flat surface, the expected variance in the estimation of surface height in a window of  $N_{pulses}$  can be calculated using:

$$\hat{\sigma}_{surf}^2 = \frac{\sigma_{surf}^2}{NP_{total}}$$

Ultimately ICESat-2 ocean data will likely extend into the marginal ice zone (MIZ) for where the data will be analyzed for short along-track distances and smooth water. From the ATBD for Sea Ice (ATL07), over a flat lead with mean returns of  $\sim 1$  photon per pulse for 100 pulses (70-m of smooth open water) with a nominal reflectance of 0.2 and no background noise, the expected uncertainty is 1.0 cm due entirely to uncertainty due to pulse width. With a 3 MHz background rate the uncertainty increases to 1.1 cm. Even at short distances, the contribution of background noise is small.

In true open ocean conditions the dominant source of uncertainty in the mean height of the sea surface over each ocean segment will be the roughness of the surface due to waves.

$$\hat{\sigma}_{surf} = \frac{\sigma_{surf}}{\sqrt{NP_{total}}} \approx \frac{\sigma_{waves}}{\sqrt{NP_{total}}}$$

For a typical situation with a significant wave height ( $SWH=4 \sigma_{waves}$ ) equal to 2 m,  $\sigma_{waves}$  equals 0.5 m, and over a typical ocean segment with 8,000 photons, the uncertainty in the ocean segment mean sea surface height,  $\hat{\sigma}_{surf}$ , will be 0.56 cm. Over 8,000 pulses,  $\hat{\sigma}_{surf}$  associated with surface roughness will remain less than 1 cm for SWH less than 3.6 m. For larger SWH, ocean segments will need to be aggregated to maintain 1 cm uncertainty in mean sea surface height.

### 5.3.6.2 Uncertainties in the mean impulse response

In our processing we, account for the impact of the instrument impulse response

(IIP) on the distributions of surface heights by deconvolving from the received height distributions the impulse response estimated from the transmit echo pulse (TEP). To the extent that the TEP represents the impulse response this should eliminate uncertainty due to the IIP. Uncertainties due to a mismatch between the TEP and true IIP will have to be inferred by examination of the TEP in the on-orbit data, which remains to be done.

### 5.3.6.3 Uncertainties due to subsurface scattering.

Because the blue-green laser of ATLAS penetrates water, true subsurface returns have always been a concern, and the higher subsurface density of photons may be due in part to true subsurface scattering in the ocean. However, we see similarly enhanced subsurface densities over, clear deep ocean waters and even over land where penetration and backscatter shouldn't occur. Consequently present thinking expressed in the ATL03 Known Issues is that the subsurface noise level is due to forward scattering delays in the atmosphere of surface reflected photons.

Whatever their cause, some subsurface photon heights are being included in the surface height histogram, creating what we think may be an order 1-3 cm bias in average SSH. To reduce the sensitivity to subsurface returns, the present developmental code first makes a simple estimate of the high and low histogram limits and then uses these to determine separate above surface and subsurface noise levels, *tailnoisephigh* and *tailnoiselow*. The ultimate high limit is then chosen where the smoothed histogram falls below a factor *Th\_Nc\_f* (e.g., *Th\_Nc\_f* = 1.5) times *tailnoisephigh* and low limit is chosen where the smoothed histogram falls below the same factor times *tailnoiselow*. This method of reducing subsurface returns will be in future releases. We also plan to use a histogram for surface finding based on height departures from a smoothed high confidence photon surface to eliminate subsurface returns from under the crests of waves.

## 5.4 Ancillary Information

### 5.4.1 Solar Background Photon Rate and Apparent Surface Reflectance (ASR)

See section 3.1.1.5. The solar background rate is taken from ATL03 (*backgrd\_atlas/bckgrd\_rate*) and simply averaged over the length of the height segment to produce *backgr\_seg*.

The apparent surface reflectance should be taken from ATL09 (??/??/*asr*) at the 25 Hz rate and simply averaged over the length of the height segment to produce *asr\_seg*.

### 5.4.2 Additional Ancillary Data

Variables from the ATL03 *geolocation/* and *geophys\_corr/* groups will also simply averaged over each ocean segment and saved. Segment averages of the following variables, corresponding to the heights stored in *A<sub>fine</sub>* will be returned in ATL12. Those variables include

*neutat\_delay\_total*  
*ref\_azimuth*  
*ref\_elev*  
*seg\_dist\_x*  
*solar\_azimuth*  
*solar\_elevation*  
*geoid*  
*dac*  
*tide\_earth*  
*tide\_load*  
*tide\_oc\_pole*  
*tide\_ocean*  
*tide\_equilibrium*  
*tide\_pole*

Also, the first of the geosegment ids (*segment\_id*) for each ocean segment will be returned in ATL12 as *first\_geoseg*.

The percentages of each *surf\_type* of the photons from Fine Select in the ocean segment will also be returned as *surf\_type\_prcnt*. This will be a 5-element variable for each ocean segment with each element corresponding to the percentage of photons from each of the 5 surface types.

.

## 5.5 Output Parameters

Table 6 ATL12 Output (See Appendix A for full product specifications)

Product Label	Units	Description	Symbol
<b>sea_surface_heights</b>			
h	meters	Mean sea surface height relative to the WGS84 ellipsoid	<b>SSH</b>
h_var	meters <sup>2</sup>	Variance of best fit probability density function (meters <sup>2</sup> )	<b>SSHvar</b>
h_skewness		Skewness of photon sea surface height histogram	<b>SSHskew</b>
h_kurtosis		Excess kurtosis of sea surface height histogram	<b>SSHkurt</b>
mix_m1		Fraction of component 1 in 2-component Gaussian mixture	<b>m1</b>
mix_mu1	meters	Mean of component 1 in 2-component Gaussian mixture	<b>mu1</b>
mix_sig1	meters	Standard deviation of component 1 in 2-component Gaussian mixture	<b>Sig1</b>
mix_m2		Fraction of component 1 in 2-component Gaussian mixture	<b>m2</b>
mix_mu2	meters	Mean of component 1 in 2-component Gaussian mixture	<b>mu2</b>
mix_sig2	meters	Standard deviation of component 1 in 2-component Gaussian mixture	<b>Sig2</b>
t_seg	seconds	Mean time of surface photons in segment	<b>t_seg</b>
delt_seg		Time duration segment	<b>t_seg</b>
lat_seg	degrees	Mean latitude of surface photons in segment	<b>lat_seg</b>
lon_seg	degrees	Mean longitude of surface photons in segment	<b>lon_seg</b>
length_seg	meters	Length of segment (m)	<b>length_seg</b>
n_pulse_seg		Number of laser pulses in segment	<b>n_pls_seg</b>
binsize	meters	Bin size for Y and sshx	<b>binsize</b>
meanoffit2	meters	Mean of linear fit removed from surface photon height	<b>meanoffit2</b>
P0	meters	Constant of linear fit versus along-track distance to surface photon height over the ocean segment	<b>P0</b>
slope_seg		Slope of linear fit versus along-track distance to surface photon height over the ocean segment	<b>P1</b>
Y	m <sup>-1</sup>	Probability density function of photon surface height	<b>Y</b>
Ymean	meters	Mean=first moment of Y, should be $\sim 0 = h - \text{meanoffit2}$	<b>Ymean</b>
Yvar	meters <sup>2</sup>	Variance = second moment (m <sup>2</sup> ) of Y	<b>Yvar</b>

<i>Yskew</i>		Skewness = (third moment of $Y$ )/ $Yvar^{3/2}$	<b><i>Yskew</i></b>
<i>Ykurt</i>		Excess Kurtosis = (fourth moment of $Y$ )/ $Yvar^2$ -3	<b><i>Ykurt</i></b>
<i>bin_ssbias</i>	meters	Sea state bias estimated from the correlation of photon return rate with along track 10-m bin averaged surface height (4.3.1)	<b><i>binSSBias</i></b>
<i>SWH</i>	meters	Significant wave height estimated as 4 times the standard deviation of along track 10-m bin averaged surface height	<b><i>SWH</i></b>
<i>xbin</i>	meters	Center of 1 x 700 element array of 10-m bins	<b><i>xbin</i></b>
<i>htybin</i>	meters	1 x 700 element array of 10-m bin average heights from SSB calculation	<b><i>htybin</i></b>
<i>xrbin</i>	photon m <sup>-1</sup>	1 x 700 element array of 10-m bin average photon rate from SSB calculation	<b><i>xrbin</i></b>
<b>Height_segment_stat</b>			
<i>n_ttl_photon</i>		Number of photons in the ±15-m ocean downlink band	<b><i>n_ttl_photon</i></b>
<i>n_photons</i>		Number of surface photons found for the segment	<b><i>n_photon</i></b>
<i>Photon_rate</i>	m <sup>-1</sup>	Photon count rate, averaged over the segment	<b><i>r_surf</i></b>
<i>Photonns_rate</i>	m <sup>-1</sup>	Noise photon count rate, averaged over the segment	<b><i>r_noise</i></b>
<i>backgr_seg</i>	m <sup>-1</sup>	<i>backgrd_atlas/bckgrd_rate</i> from ATL03 averaged over the segment	<b><i>backgr_seg</i></b>
<i>first_pce_mframe_cnt</i>		First Major Frame ID in the SSH segment	<b><i>first_pce_mframe_cnt</i></b>
<i>first_tx_pulse</i>		First Transmit pulse in along-track segment	<b><i>first_tx_pulse</i></b>
<i>fpb_corr</i>	meters	Estimated first-photon bias correction to mean segment height = 0 pending findings to the contrary for the ocean	<b><i>fpb_corr</i></b>
<i>fpb_corr_stdev</i>	meters	Estimated error in <i>fpb_corr</i> = 0 pending findings to the contrary	<b><i>fpb_corr_stdev</i></b>
<i>Last_pce_mframe_cnt</i>		Last Major Frame ID in the SSH segment	<b><i>Last_pce_mframe_cnt</i></b>
<i>last_tx_pulse</i>		Last Transmit pulse in along-track segment	<b><i>last_tx_pulse</i></b>
<i>orbit_number =</i>		Unique identifying number for each planned ICESat-2 orbit	<b><i>orbit_number</i></b>
<i>segment_id</i>		A 7 digit number identifying the first along-track ATL03 geolocation segment number in the ocean height segment	<b><i>segment_id</i></b>
<i>ss_corr</i>	meters	Subsurface scattering correction, placeholder = zero pending further findings to the contrary	<b><i>ss_corr</i></b>

<i>ss_corr_stdev</i>	meters <sup>2</sup>	Estimated error of subsurface scattering correction, placeholder = zero pending further findings to the contrary	<b><i>ss_corr_stdev</i></b>
<i>neutat_delay_total_seg</i>	meters	Ocean segment average of total neutral atmosphere delay correction (wet + dry)	<b><i>neutat_delay_total_seg</i></b>
<i>ref_azimuth_seg</i>	deg	Ocean segment average of azimuth of the unit pointing vector for the reference photon in the local ENU frame in radians. The angle is measured from North and positive towards East	<b><i>ref_azimuth_seg</i></b>
<i>ref_elev_seg</i>	deg	Ocean segment average of elevation of the unit pointing vector for the reference photon in the local ENU frame in radians. The angle is measured from the East-North plane and positive towards Up	<b><i>ref_elev_seg</i></b>
<i>seg_dist_x_seg</i>	meters	Ocean segment average of the along-track distance from the equator crossing to the start of the 20-m geolocation segments included in the ocean segment	<b><i>seg_dist_x_seg</i></b>
<i>layer_flag_seg</i>		The layer flag from ATL09 that is in effect over 50% of the ocean segment, 0 indicating absence of clouds and forward scattering, and 1 indicating possibility of forward scattering as in ATL09	<b><i>layer_flag_seg</i></b>
<i>depth_ocn_seg</i>	meters	The average of depth ocean of geo-segments used in the ocean segment.	<b><i>depth_ocn_seg</i></b>
<i>solar_azimuth_seg</i>	deg	Ocean segment average of the azimuth of the sun position vector from the reference photon bounce point position in the local ENU frame. The angle is measured from North and is positive towards East. The average is provided in degrees.	<b><i>solar_azimuth_seg</i></b>
<i>solar_elevation_seg</i>	deg	Ocean segment average of the elevation of the sun position vector from the reference photon bounce point position in the local ENU frame. The angle is measured from the East-North plane and is positive towards Up. The average is provided in degrees.	<b><i>solar_elevation_seg</i></b>
<i>geoid_seg</i>	meters	Ocean segment average of geoid height above the WGS – 84 reference ellipsoid (range -107 to 86 m)	<b><i>geoid_seg</i></b>
<i>dac_seg</i>	meters	Ocean segment average of dynamic atmospheric correction (DAC) includes inverted barometer (IB) affect	<b><i>dac_seg</i></b>
<i>tide_earth_seg</i>	meters	Ocean segment average of solid earth tides	<b><i>tide_earth_seg</i></b>
<i>tide_load_seg</i>	meters	Ocean segment average of local displacement due to ocean loading (-6 to 0 cm)	<b><i>tide_load_seg</i></b>
<i>tide_oc_pole_seg</i>	meters	Ocean segment average of oceanic surface rotational deformation due to polar motion (-2 to +2 mm)	<b><i>tide_oc_pole_seg</i></b>
<i>tide_ocean_seg</i>	meters	Ocean segment average of ocean tides including diurnal and semi-diurnal (harmonic analysis)	<b><i>tide_ocean_seg</i></b>
<i>tide_equilibrium_seg</i>	meters	Long period equilibrium tides	<b><i>tide_equilibrium_seg</i></b>

<i>tide_pole_seg</i>	meters	Ocean segment average of solid pole tide - Rotational deformation due to polar motion (-1.5 to 1.5 cm)	<i>tide_pole_seg</i>
<i>first_geoseg</i>		The first of the geosegment ids ( <b><i>segment_id</i></b> ) for each ocean segment	<i>first_geoseg</i>
<i>surf_type_prcnt</i>		The percentages of each <b><i>surf_type</i></b> of the photons in the ocean segment as a 5-element variable with each element corresponding to the percentage of photons from each of the 5 surface types	<i>surf_type_prcnt</i>

## 5.6 Synthetic Test Data

The first task in the creation of the developmental software has been the creation of a synthetic data set. This is not part of ATLAS processing per se, but is a good tool for algorithm testing and development.

The procedure is imbedded in a developmental Matlab code (WienerTest\_GaussMixandNoise2.m). Here, the percent sign indicates a plane text description of the procedural step and is a non-executable comment in the Matlab code. Matlab executable lines are highlighted in yellow. The program begins with parts (A) through (E) which establish an artificial surface height histogram consisting of a mixture of 2 normal distributions convolved with a real impulse response distribution taken from MABEL data by Ron Kwok. A representative amount of noise is then added to this to synthesize a received surface height with a known underlying true surface distribution.

(A) Establish the instrument impulse response distribution from MABEL data (XmitHist000)

(B) Make a Gaussian mixture representing the ssh distribution (sshhist)

(C) Compute noise (Noise) as the rRMSdifference from the analytic Gaussian mixture and sshist in the tails (+2sig to +3 sig)

(D) Convolve the SSH distribution with the instrument impulse response distribution to produce the received distribution (rechist)

(E) Add random Poisson (or pulse) noise due to discrete nature of photon counts representative of what we might expect for a given bin size and total number of photon counts.

% -----

**% Begin Matlab code:**

% In this test program we will:

```

% (A) Establish the instrument impulse response distribution from Mabel data (XmitHist000)
% (B) Make a Gaussian mixture representing the ssh distribution (sshhist)
% (C) Compute noise (Noise) as the rms difference from the analytic gaussian mixture
% and sshist in the tails (+-2sig to +-3 sig)
% (D) Convolve the ssh ditribution with the instrument impulse response distribution to produce
% the received distribution (rechist)
% (E) Add random Poisson (or pulse) noise due to discrete nature of photon
% counts representative of what we might expect for a given binsize and
% total number of photon counts (NptsMix)
% photons.
%
% -----
% (A) load and plot Instrument impulse response Histogram
% -----
% -----
cd
/Users/jamie/Documents/ICESat2_SDT/ICESat2_OceanATBD_Development/PhotonSourceDistrib
ution
load XmitHist000
meanXmit00=sum(XmitHist000(:,1).*XmitHist000(:,2))/sum(XmitHist000(:,2))
stdXmit00=sqrt(sum(XmitHist000(:,1).*XmitHist000(:,1).*XmitHist000(:,2))/sum(XmitHist000(:,
2))))

% XmitHist000 is a raw histogram and XmitHist000(:,2) are the total number of photons in each
% 0.01-m bin convert. We convert it to a probability density function, the integral
% of which is 1.0. Binsize in all histograms/pdfs will be 0.01 m.
% XmitHist000 bins are relative to the mean delay is zero.
binsize=0.01;
totalxmit=sum(XmitHist000(:,2));
XmitHist_fraction=(XmitHist000(:,2)/totalxmit);
XmitHist000(:,2)=XmitHist_fraction/binsize;
checkintegralXMIT=sum(XmitHist000(:,2)*binsize);
meanXmit00=sum(XmitHist000(:,1).*XmitHist000(:,2))/sum(XmitHist000(:,2))
stdXmit00=sqrt(sum(XmitHist000(:,1).*XmitHist000(:,1).*XmitHist000(:,2))/sum(XmitHist000(:,
2))))

% plot
figure
plot(XmitHist000(:,1),XmitHist000(:,2))
title('Xmit Pulse Delay Rel to Mean in Equiv Surface Height')
ylabel('Occurences as Fraction of Total per meter')

```

```

xlabel('Height Delay (m)')
print -dpng XmitHistogram_GM_8k.png

%-----
% (B) Make a sequence sea surface height consisting of a mix of two normally
% distributed random numbers with Means MuMix, standard deviations SigmaMix
% and percent mixing ratios RatioMix, and number of points total NptsMix
% -----
% -----
MuMix=[1,0]
SigmaMix=[2,1]
RatioMix=[50,50]
NptsMix=8000
ssh=makeGaussianMix(MuMix,SigmaMix,RatioMix,NptsMix);
meanssh=mean(ssh)
MeanfromMixValues=sum(RatioMix.*MuMix/sum(RatioMix))
stdssh=std(ssh)
StdfromMixValues=sqrt(sum(RatioMix.*(SigmaMix.^2)/sum(RatioMix)))
lssh=length(ssh)

% Compute histogram of ssh using bin size = 0.01 m running from -3 Std to +3
% Std of the ssh mix. The output of hist is a raw histogram and we convert it to
% a probability density function, the integral of which is 1.0 by dividing by the
% total number of points (=length of ssh) and the binsize
%
Nsigs=3;
sshx=round(meanssh)-Nsigs*round(stdssh):binsize:round(meanssh)+Nsigs*round(stdssh);
sshhist=hist(ssh,sshx);
sshhist_fraction=(sshhist/lssh);
sshhist=sshhist_fraction/binsize;
checkintegralSSH=sum(sshhist*binsize)
%
meansshhist=sum(sshx.*sshhist)/sum(sshhist)
stdsshhist=sqrt(sum((sshx-meansshhist).*(sshx-meansshhist).*sshhist)/sum(sshhist))
totalssh=sum(sshhist)
Nbins=length(sshhist);

% -----
% (C) Compute noise (Noise) as the rms difference from the analytic gaussian mixture
% (gaussfit) and sshist in the tails (+-2sig to +-3 sig)
% -----
% -----

```

```

gaussfit=(1/stdssh)*(1/sqrt(2*pi))*exp(-0.5*((sshx-meanssh).^2)/stdssh^2);
NoiseAll=std(sshhist-gaussfit)

% because gaussfit is a pdf we divide histogram values by bin size for
% comparison. Noise values should probably be multiplied by bin size for
% computation as noise in histograms ?Noise=binsize*NoiseInTails?
DiffFromNorm=(sshhist)-gaussfit;
DiffFromNormInTails=[DiffFromNorm(1:round(0.5*Nbins/Nsigs)),DiffFromNorm(end-
round(0.5*Nbins/Nsigs))];
NoiseInTails=std(DiffFromNormInTails')

figure
plot(sshx,sshhist, sshx,gaussfit,'-g')
title(['Simulated True Sea Surface Height Distribution, 2-GaussMix ',num2str(NptsMix),'
Photons'])
ylabel('Occurrences as Fraction of Total per meter')
xlabel('Height (m)')
print -dpng Sim_SSH_Distriburtion_GM_8k.png

% -----
% (D) Convolve the instrument impulse response and simulated true height histograms
% to get a simulated received height ssh distribution rcvhist
% -----
% -----
% ----- Matlab Routine conv.m -----
% conv Convolution and polynomial multiplication.
% C = conv(A, B) convolves vectors A and B. The resulting vector is
% length MAX([LENGTH(A)+LENGTH(B)-1,LENGTH(A),LENGTH(B)]). If A and B are
% vectors of polynomial coefficients, convolving them is equivalent to
% multiplying the two polynomials.
%
% C = conv(A, B, SHAPE) returns a subsection of the convolution with size
% specified by SHAPE:
% 'full' - (default) returns the full convolution,
% 'same' - returns the central part of the convolution
% that is the same size as A.
% 'valid' - returns only those parts of the convolution
% that are computed without the zero-padded edges.
% LENGTH(C)is MAX(LENGTH(A)-MAX(0,LENGTH(B)-1),0).
% -----
% NOTE: conv.m does a raw convolution, i.e., simple sums of products. To

```

```
% replicate a true convolution integral with proper scaling, the results of
% conv.m must be multiplied by the bin size so that the scale of the
% resulting convolution is of the same order as the scale on the two
% histograms convolved.
% Also the length of the convolution should equal length of the ssh
% histogram plus the length Xmit histogram minus 1
%-----
```

```
tic
rcvhist=conv(sshhist,XmitHist000(:,2))*binsize;
cleanrcvhist=rcvhist;
toc
```

```
lrcvhist=length(rcvhist)
lxmithist=length(XmitHist000(:,2))
lsshhist=length(sshhist)
halfwidthrcvhist=(lxmithist+lsshhist-2)/2
if 2*halfwidthrcvhist+1==lrcvhist
    message=['length of rcvhist is consistent']
end
```

```
% If the impulse response distribution were symmetric conv.m would pad the length of the sshhist
% by (lxmithist-1)/2 at each end. The Xmit histogram is not symmetric. The minimum x-axis index
% of the received histogram should be the minimum index of the true surface height histogram plus
% the minimum negative bin index of the impulse response histogram and the maximum x-axis
% index of the received histogram should be the maximum index of the true histogram plus
% the maximum (positive) bin index of the Xmit histogram.
% Therefore, we find the index of the zero bin,zbin,
% of XmitHist000 (which is the old XmitHist00 histogram interpolated to even cm bin indices)and
% add the bins with index 0 to zbin-1 before the first bin of the ssh histogram and
% add the bins with index zbin+1 to end after the last bin of the ssh histogram
```

```
zbin=find(XmitHist000(:,1)==0);
xaddend=XmitHist000(zbin+1:end,1)+sshx(end)*ones(1,length(XmitHist000(zbin+1:end,1)));
xaddbegin=XmitHist000(1:zbin-1,1)+sshx(1)*ones(1,length(XmitHist000(1:zbin-1,1)));
xrechist=[xaddbegin,sshx,xaddend];
```

```
figure
plot(xrechist,rcvhist)
title('Simulated Convolved Sea Surface Height Distribution')
ylabel('Occurrences as Fraction of Total per meter')
xlabel('Height (m)')
```

```

% -----

% -----
% -----
% (E) Add random Poisson (or pulse) noise due to discrete nature of photon
% counts representative of what we might expect for a given binsize and
% total number of photon counts (NptsMix)
% -----
sumrchhist=sum(rcvhist*binsize)
noisy=rcvhist;
% make Poisson distributed photon counts in histogram to represent received + pulse noise
for inoise=1:length(rcvhist)
    noisy(inoise)=randpoisson_JM(NptsMix*binsize*cleanrcvhist(inoise));
end

% NOTE %
%randpoisson_JM.m is a Matlab subroutine to generate random numbers drawn
% from a Poisson distribution:

function X = randpoisson_JM(np)
x=1:round(np+1)*10;
p= poisspdf(x,np);
m=1;
X = zeros(m,1); % Preallocate memory
for i = 1:m
    u = rand;
    I = find(u < cumsum(p));
    if isempty(I)
        X(i)=0;
    else
        X(i) = min(I);
    end
end
end

% poisspdf Poisson probability density function.
% Y = poisspdf(X,LAMBDA) returns the Poisson probability density
% function with parameter LAMBDA at the values in X.
% The size of Y is the common size of X and LAMBDA. A scalar input
% functions as a constant matrix of the same size as the other input.
% Note that the density function is zero unless X is an integer.

```

```
% Convert back to PDF
Noise=std(noisey/(NptsMix*binsize)-rcvhist);
rcvhist=noisey/(NptsMix*binsize);
sumnoisyrcvhist=sum(rcvhist*binsize)

figure
plot(xrechist,rcvhist)
title(['Simulated Received Sea Surface Height Distribution + Pulse Noise= ',num2str(Noise)])
ylabel('Occurences as Fraction of Total per meter')
xlabel('Height (m)')
% -----
% rcvhist is the simulated received histogram at the histogram bins centered at xrechist. It
is shown in blue in Figure 17 for 8000 photons (left) and 800 photons (right).
```

## 5.7 Numerical Computation Considerations

*TBD – as needed specific considerations on method of code computation*

## 5.8 Programmer/Procedural Considerations

*TBD- provide information related to output parameters that were not in the algorithm description*

## 5.9 Calibration and Validation

There are three types of open ocean calibration and validation:

- 1) Direct comparison of sea surface height or dynamic ocean topography with satellite radar altimetry from TOPEX/Poseidon and CryoSat-2. This may be possible to automate so that the project personnel can do it, but funding is being sought outside the ICESat-2 and NASA Cryosphere program for Cal/Val.
- 2) Comparison of changes in DOT with in situ measurements of dynamic heights from hydrography plus ocean bottom pressure from in situ gauges or GRACE-FO. This will have to be done for the open ocean perhaps funded outside the Cryosphere program.
- 3) Direct comparison to in situ precision GPS measurements. Buoys are being built with NOPP funding to do this as an add-on to similar measurements for NASA Oceanography's SWOT cal/val effort.

## **6.0 BROWSE PRODUCTS**

*These browse figures show images that allow user to easily evaluate if the data would be useful and of quality for their research and will aid in the quick approval or disapproval of products prior to public distribution.*

### **6.1 Data Quality Monitoring**

#### **6.1.1 Line plots** (each strong beam)

- a) mean sea surface height for each segment
- b) standard deviation of height distribution and associated SWH for each segment
- c) skewness of height distribution for each segment
- d) kurtosis of height distribution for each segment

#### **6.1.2 Histograms** (each strong beam)

- a) Line plots of parameters of 2-Gaussian fit for each segment
- b) TBD quality measure of each 2-Gaussian fit

## 7.0 DATA QUALITY

### 7.1 Statistics

Calculate the following statistics for each open ocean granule and broken down by strong beam ground track – so there is one set for each ground track.

- Aggregate histogram and mean/standard deviation of each of the following parameters

#### 7.1.1 Per orbit statistics

Table 7 ATL12 Output Variables for Per Orbit Statistics

Product Label	Description	Symbol
<b>sea_surface_heights</b>		
h	Mean sea surface height	<i>SSH</i>
h_var	Variance of best fit probability density function (meters <sup>2</sup> )	<i>SSHvar</i>
h_skewness	Skewness of photon sea surface height histogram	<i>SSHskew</i>
h_kurtosis	Excess kurtosis of sea surface height histogram	<i>SSHkurt</i>
<i>mix_m1</i>	Fraction of component 1 in 2-component Gaussian mixture	<i>m1</i>
<i>mix_mu1</i>	Mean of component 1 in 2-component Gaussian mixture	<i>mu1</i>
<i>mix_sig1</i>	Standard deviation of component 1 in 2-component Gaussian mixture	<i>Sig1</i>
<i>mix_m2</i>	Fraction of component 1 in 2-component Gaussian mixture	<i>m2</i>
<i>mix_mu2</i>	Mean of component 1 in 2-component Gaussian mixture	<i>mu2</i>
<i>mix_sig2</i>	Standard deviation of component 1 in 2-component Gaussian mixture	<i>Sig2</i>
<i>delt_seg</i>	Time duration segment	<i>t_seg</i>
<i>lat_seg</i>	Mean latitude of surface photons in segment	<i>lat_seg</i>
<i>lon_seg</i>	Mean longitude of surface photons in segment	<i>lon_seg</i>
<i>length_seg</i>	Length of segment (m)	<i>length_seg</i>
<i>P0</i>	Constant of linear fit versus along-track distance to surface photon height over the ocean segment	<i>P0</i>
<i>slope_seg</i>	Slope of linear fit versus along-track distance to surface photon height over the ocean segment	<i>P1</i>
<i>n_pulse_seg</i>	Number of laser pulses in segment	<i>n_pls_seg</i>
<i>meanoffit2</i>	Mean of linear fit removed from surface photon height	<i>meanoffit2</i>
<i>Y</i>	Probability density function of photon surface height	<i>Y</i>
<i>Ymean</i>	Mean=first moment of Y, should be $\sim 0 = h - \text{meanoffit2}$	<i>Ymean</i>
<i>Yvar</i>	Variance = second moment (m <sup>2</sup> ) of Y	<i>Yvar</i>

<i>Yskew</i>	Skewness = (third moment of <i>Y</i> ) / $Yvar^{3/2}$	<b><i>Yskew</i></b>
<i>Ykurt</i>	Excess Kurtosis = (fourth moment of <i>Y</i> ) / $Yvar^2 - 3$	<b><i>Ykurt</i></b>
<i>binSSBias</i>	Sea state bias estimated from the correlation of photon return rate with along track 10-m bin averaged surface height (4.3.1)	<b><i>binSSBias</i></b>
<i>SWH</i>	Significant wave height estimated as 4 times the standard deviation of along track 10-m bin averaged surface height	<b><i>SWH</i></b>
<b>Height_segment_stat</b>		
<i>n_ttl_photon</i>	Number of photons in the ±15-m ocean downlink band	<b><i>n_ttl_photon</i></b>
<i>n_photons</i>	Number of surface photons found for the segment	<b><i>n_photon</i></b>
<i>Photon_rate</i>	Photon count rate, averaged over the segment	<b><i>r_surf</i></b>
<i>Photonns_rate</i>	Noise photon count rate, averaged over the segment	<b><i>r_noise</i></b>
<i>backgr_seg</i>	<i>backgrd_atlas/bckgrd_rate</i> from ATL03 averaged over the segment	<b><i>backgr_seg</i></b>
<i>first_pce_mframe_cnt</i>	First Major Frame ID in the SSH segment	<b><i>first_pce_mframe_cnt</i></b>
<i>first_tx_pulse</i>	First Transmit pulse in along-track segment	<b><i>first_tx_pulse</i></b>
<i>layer_flag_seg</i>	The layer flag from ATL09 that is in effect over 50% of the ocean segment, 0 indicating absence of clouds and forward scattering, and 1 indicating possibility of forward scattering as in ATL09	<b><i>layer_flag_seg</i></b>
<i>depth_ocn_seg</i>	The average of <i>depth_ocn</i> of geo-segments used in the ocean segment.	<b><i>depth_ocn_seg</i></b>
<i>orbit_number =</i>	Unique identifying number for each planned ICESat-2 orbit	<b><i>orbit_number</i></b>
<i>ss_corr</i>	Subsurface scattering correction, placeholder = zero pending further findings to the contrary	<b><i>ss_corr</i></b>
<i>ss_corr_stdev</i>	Estimated error of subsurface scattering correction, placeholder = zero pending further findings to the contrary	<b><i>ss_corr_stdev</i></b>
<i>neutat_delay_total_seg</i>	Ocean segment average of total neutral atmosphere delay correction (wet + dry)	<b><i>neutat_delay_total_seg</i></b>
<i>seg_dist_x_seg</i>	Ocean segment average of the along-track distance from the equator crossing to the start of the 20-m geolocation segments included in the ocean segment	<b><i>seg_dist_x_seg</i></b>
<i>solar_azimuth_seg</i>	Ocean segment average of the azimuth of the sun position vector from the reference photon bounce point position in the local ENU frame. The angle is measured from North and is positive towards East. The average is provided in degrees.	<b><i>solar_azimuth_seg</i></b>
<i>solar_elevation_seg</i>	Ocean segment average of the elevation of the sun position vector from the reference photon bounce point position in the local ENU frame. The angle is measured from the East-North plane and is positive towards Up. The average is provided in degrees.	<b><i>solar_elevation_seg</i></b>

<i>geoid_seg</i>	Ocean segment average of geoid height above the WGS – 84 reference ellipsoid (range -107 to 86 m)	<b><i>geoid_seg</i></b>
<i>dac_seg</i>	Ocean segment average of dynamic atmospheric correction (DAC) includes inverted barometer (IB) affect	<b><i>dac_seg</i></b>
<i>tide_earth_seg</i>	Ocean segment average of solid earth tides	<b><i>tide_earth_seg</i></b>
<i>tide_load_seg</i>	Ocean segment average of local displacement due to ocean loading (-6 to 0 cm)	<b><i>tide_load_seg</i></b>
<i>tide_oc_pole_seg</i>	Ocean segment average of oceanic surface rotational deformation due to polar motion (-2 to +2 mm)	<b><i>tide_oc_pole_seg</i></b>
<i>tide_ocean_seg</i>	Ocean segment average of ocean tides including diurnal and semi-diurnal (harmonic analysis) and longer period tides (dynamic and self-consistent equilibrium)	<b><i>tide_ocean_seg</i></b>
<i>tide_equilibrium_seg</i>	Long period equilibrium tides	<b><i>tide_equilibrium_seg</i></b>
<i>tide_pole_seg</i>	Ocean segment average of solid pole tide - Rotational deformation due to polar motion (-1.5 to 1.5 cm)	<b><i>tide_pole_seg</i></b>
<i>surf_type_prcnt</i>	The percentages of each <b><i>surf_type</i></b> of the photons in the ocean segment as a 5-element variable with each element corresponding to the percentage of photons from each of the 5 surface types	<b><i>surf_type_prcnt</i></b>

## **8.0 TEST DATA**

This section describes the test data sets that have been used to derive and verify the performance of the ATL12 code for surface finding, deconvolution of the instrument impulse response, and Gaussian mixture determination.

### **8.1 In Situ Data Sets**

**Table 8 ATL12 Test Data**

Instrument	Date	Location
MABEL	April 2012	Fram Strait and Greenland Sea
MABEL	July 2014	North Pacific

### **8.2 Simulated Test Data**

Development of ATL12 used the simulated data set described in Section 5.6 Synthetic Data. For these synthetic data we started with a synthetic sea surface height record comprised of a known 2-Gaussian mixture that we convolved with a known instrument impulse response and added random measurement noise. We exercised the developmental Matlab code and the ASAS PGE code on this data to see that they output the same 2-Gaussian mixture that was the basis of the synthetic ocean surface

## **9.0 CONSTRAINTS, LIMITATIONS, AND ASSUMPTIONS**

In this section, we list notable constraints, limitations, and assumptions important to ATL12 that affect the coverage, quality and interpretation of the sea surface height retrievals and our objectives for the ATL12. These topics have been discussed throughout the ATBD. In order to compare with other open ocean topography measures, the overarching objective for the ATL12 product is that it should be a solid description of sea surface height probability distribution over each strong beam ground track (and weak beam ground track where available). This objective and the constantly changing wave-covered character of the ocean surface impose the primary constraint on the ATL12 product. To achieve standard errors in mean sea surface height better than 1-cm under typical sea states, we accumulate the distributions over distances of 5 to 7 km. This is far longer than the ultimate spatial resolution of the ICESat-2 instrument, which we in fact use in the ATL12 analysis for sea state bias estimation. Users can aggregate the ATL 12 distributions to obtain greater statistical significance, and we do this to produce the ocean gridded product, ATL19. Where applicable we and other users can go back to ATL03 photon heights and derive specialized ocean products using ATL12 statistics as a guide and benchmark.

### **9.1 Constraints**

The following are constraints imposed by the inherent capability of the instrument.

- At 532 nm, clouds will affect visibility of the open ocean. First impressions looking at preliminary ICESat-2 data the lidar appears able detect the ocean surface through at least thin clouds better than expected.
- The reflectance of the ocean surface is lower than the other surfaces ICESat-2 operates over with the result that only on the order of one photon per pulse is returned from the surface. Thus, longer path lengths are required to accumulate desired statistical significance of ocean height measurements than would be required for other surfaces. On the other hand, we don't have to worry about detector saturation and first photon bias over the ocean.

### **9.2 Limitations**

These limitations stem from on our current understanding of the altimetric returns from the sea ice cover.

- Subsurface Scattering - Quantification of the impact of subsurface scattering on height retrievals due to multiple scattering from bubbles or particles in the water remains to be addressed. For the central parts of the deep ocean, these effects are likely reduced by the scarcity of scatterers in the water. We might also expect that just as surface waves reduce the reflectance of the surface, they may also reduce the transmittance of subsurface returns up through the ocean surface, a benefit offsetting the generation of bubbles by wind waves. Preliminary analysis of ICESat-2 deep ocean data suggests long, but low energy negative tails in the raw height distribution that are mainly removed in the trimming of the histogram in the fine surface finding step. Subsurface scattering will be most important in coastal regions where sediment and biological productivity increase the density of scatterers. Gaining a better understanding the

subsurface return problem will be a high priority for future ICESat-2 oceanography.

- Sea State Bias – ICESat-2 will be unique in estimating what we think will be the main source of sea state bias by calculating the correlation of photon return rate and surface height at scales resolving the energy containing surface waves. This constitutes what is termed EM-bias in other altimeters. Because we don't use retracking in the traditional sense or assume a Gaussian surface distribution, we anticipate ICESat-2 will not suffer from sea state bias due to these factors, and the ICESat-2 sea state bias is wholly due to EM-bias. We will assess this assumption as part of the validation process.

### **9.3 Assumptions**

These are assumptions made by the retrieval routines that will have to be tested.

- Ocean Surface Height retrievals – As discussed above key assumptions are that our fine surface finding clips off the negative histogram tail due to subsurface return and that what is commonly termed EM-bias is the sole source of sea state bias in our analysis of ICESat-2 over the ocean.

## 10.0 REFERENCES

- Arnold, D. V., W. K. Melville, R. H. Stewart, J. A. Kong, W. C. Keller, and E. Lamarre (1995), Measurements of electromagnetic bias at Ku and C bands, *J. Geophys. Res.*, *100*(C1), 969-980.
- Carrère, L., and F. Lyard (2003), Modeling the barotropic response of the global ocean to atmospheric wind and pressure forcing - comparisons with observations.
- Chambers, D. P., S. A. Hayes, J. C. Ries, and T. J. Urban (2003), New TOPEX sea state bias models and their effect on global mean sea level, *J. Geophys. Res.*, *108*(C10), 3305.
- Chapron, B., V. Kerbaol, D. Vandemark, and T. Elfouhaily (2000), Importance of peakedness in sea surface slope measurements and applications, *J. Geophys. Res.*, *105*(C7), 17195-17202.
- Cox, C., and W. Munk (1954), Measurement of the Roughness of the Sea Surface from Photographs of the Sun's Glitter, *J. Opt. Soc. Am.*, *44*(11), 838-850.
- Elfouhaily, T., D. R. Thompson, B. Chapron, and D. Vandemark (2000), Improved electromagnetic bias theory, *J. Geophys. Res.*, *105*(C1), 1299-1310.
- Gaspar, P., F. Ogor, P.-Y. Le Traon, and O.-Z. Zanife (1994), Estimating the sea state bias of the TOPEX and POSEIDON altimeters from crossover differences, *J. Geophys. Res.*, *99*(C12), 24981-24994.
- Hausman, J., and V. Zlotnicki (2010), Sea State Bias In Radar Altimetry Revisited, , *Marine Geodesy*, *33*(S1), 336---347.
- Markus, T., et al. (2016), The Ice, Cloud, and land Elevation Satellite-2 (ICESat-2): Science 1 requirements concept, and implementation., *Remote Sensing of the Environment*, in press.
- Menzies, R. T., D. M. Tratt, and W. H. Hunt (1998), Lidar In-Space Technology Experiment Measurements of Sea Surface Directional Reflectance and the Link to Surface Wind Speed, *Appl. Opt.*, *37*(24), 5550-5559.
- Plant, W. J. (2015a), Short wind waves on the ocean: Wavenumber-frequency spectra, *J. Geophys. Res. Oceans*, *120*, 2147-2158.
- Plant, W. J. (2015b), Short wind waves on the ocean: Long-wave and windspeed dependences, *J. Geophys. Res. Oceans*, *120*, 6436-6444.
- Urban, T. J., and B. E. Schutz (2005), ICESat sea level comparisons, *Geophys. Res. Lett.*, *32*(23), L23S10.
- Vandemark, D., B. Chapron, T. Elfouhaily, and J. W. Campbell (2005), Impact of high-frequency waves on the ocean altimeter range bias, *J. Geophys. Res.*, *110*(C11), C11006.
- Wu, J. (1972), Sea-Surface Slope and Equilibrium Wind-Wave Spectra, *Physics of Fluids*, *15*(5), 741-747.



## **ACRONYMS**

### Acronym List

ASA	ATLAS Science Algorithm Software
ATLAS	ATLAS Advance Topographic Laser Altimeter System
GSFC	Goddard Space Flight Center
ICESat-2 MIS	ICESat-2 Management Information System
IIP	Instrument Impulse Response
MIZ	Marginal Ice Zone
PSO	Project Science Office
PSO	ICESat-2 Project Support Office
SDMS	Scheduling and Data Management System
SIPS	Science Investigator-led Processing System
TEP	Transmit Echo Pulse

## **GLOSSARY**

## APPENDIX A: ICESat2 Data Products

### ICESat-2 Data Products

File ID/Level	Product Name	Concept	Short Description	Frequency
00/0	Telemetry Data	Full rate Along-track with channel info	Raw ATLAS telemetry in Packets with any duplicates removed	Files for each APID for some defined time period
01/1A	Reformatted Telemetry	Full rate Along-track with channel info	Parsed, partially reformatted, time ordered telemetry. Proposed storage format is NCSA HDF5.	Uniform time TBD minutes (1 minute?)
02/1B	Science Unit Converted Telemetry	Full rate Along-track with channel info	Science unit converted time ordered telemetry. Reference Range/Heights determined by ATBD Algorithm using Predict Orbit and s/c pointing. All photon events per channel per pulse. Includes Atmosphere raw profiles.	Uniform time TBD minutes (1 minute?)
03/2A	Global Geolocated Photon Data	Full rate Along-track with channel info	Reference Range/Heights determined by ATBD Algorithm using POD and PPD. All photon events per pulse per beam. Includes POD and PPD vectors. Classification of each photon by several ATBD Algorithms.	Uniform time TBD minutes (1 minute?)
04/2A	Calibrated Backscatter Profiles	3 profiles at 25 Hz rate (based on 400 pulse mean)	Along-track backscatter data at full instrument resolution. The product will include full 532 nm (14 to -1.0 km) calibrated attenuated backscatter profiles at 25 times per second for vertical bins of approximately 30 meters. Also included will be calibration coefficient values for the polar region.	Per orbit
05/2B	Photon Height Histograms	Fixed distances Along-track for each beam	Histograms by prime Classification by several ATBD Algorithms. By beam	Uniform time TBD minutes (30 minutes?)
06/L3	Antarctica Ice Sheet Height / Greenland Ice Sheet Height	Heights calculated with the ice sheet algorithm, as adapted for a dH/dt calculation	Surface heights for each beam, along and across-track slopes calculated for beam pairs. All parameters are calculated for the same along-track increments for each beam and repeat.	There will be TBD files for each ice sheet per orbit

<b>File ID/Level</b>	<b>Product Name</b>	<b>Concept</b>	<b>Short Description</b>	<b>Frequency</b>
07/ L3	Arctic Sea Ice Height/ Antarctic Sea Ice Height	Along-track heights for each beam ~50-100m (uniform sampling); separate Arctic and Antarctic products	Heights of sea ice and open water samples (at TBD length scale) relative to ellipsoid after adjusted for geoidal and tidal variations, and inverted barometer effects. Includes surface roughness from height statistics and apparent reflectance	There will be files for each pole per orbit
08/ L3	Land Water Vegetation Heights	Uniform sampling along-track for each beam pair and variable footprint	Heights of ground including inland water and canopy surface at TBD length scales. Where data permits, include estimates of canopy height, relative canopy cover, canopy height distributions (decile bins), surface roughness, surface slope and aspect, and apparent reflectance. (Inland water > 50 m length -TBD)	Per half (TBD) orbit
09/ L3	ATLAS Atmosphere Cloud Layer Characteristics	Based on 3 profiles at a 25 hz rate. (400 laser pulses are summed for each of the 3 strong beams.)	Cloud and other significant atmosphere layer heights, blowing snow, integrated backscatter, optical depth	Per day
10/ L3	Arctic Sea Ice Freeboard / Antarctic Sea Ice Freeboard	Along-track all beams. Freeboard estimate along-track (per pass); separate Arctic/ Antarctic products	Estimates of freeboard using sea ice heights and available sea surface heights within a ~TBD km length scale; contains statistics of sea surface samples used in the estimates.	There will be files for each polar region per day
11/ L3	Antarctica Ice Sheet H(t) Series/ Greenland Ice Sheet H(t) Series	Height time series for pre-specified points (every 200m) along-track and Crossovers.	Height time series at points on the ice sheet, calculated based on repeat tracks and/or crossovers	There will be files for each ice sheet for each year
12/ L3	Ocean Height	Along-track heights per beam for ocean including coastal areas	Height of the surface 10 Hz/700 m (TBD) length scales. Where data permits, include estimates of height distributions (decile bins), surface roughness, surface slope, and apparent reflectance	Per half orbit
13/ L3	Inland Water Height	Along-track height per beam	Along-track inland ground and water height extracted from Land/Water/ Vegetation product. TBD data-derived	TBD files Per day

			surface indicator or mask. Includes roughness, slope and aspect.	
--	--	--	--	--

File ID/Level	Product Name	Concept	Short Description	Frequency
14/L4	Antarctica Ice Sheet Gridded/ Greenland Ice Sheet Gridded	Height time series interpolated onto a regular grid for each ice sheet. Series (5-km posting interval)	Height maps of each ice sheet for each year of the mission, based on all available ICESat-2 data.	Per ice sheet per year
15/L4	Antarctica Ice Sheet dh/dt Gridded/ Greenland Ice Sheet dh/dt Gridded	Images of dh/dt for each ice sheet, gridded at 5 km.	Height-change maps of each ice sheet, with error maps, for each mission year and for the whole mission.	Per ice sheet for each year of mission, and for the mission as a whole
16/ L4	ATLAS Atmosphere Weekly	Computed statistics on weekly occurrences of polar cloud and blowing snow	Polar cloud fraction, blowing snow frequency, ground detection frequency	Per polar region Gridded 2 x 2 deg. weekly
17/ L4	ATLAS Atmosphere Monthly	Computed statistics on monthly occurrences of polar cloud and blowing snow	Global cloud fraction, blowing snow and ground detection frequency	Per polar region Gridded 1 x 1 deg. Monthly
18/L4	Land Height/ Canopy Height Gridded	Height model of the ground surface, estimated canopy heights and canopy cover gridded on an annual basis. Final high resolution DEM generated at end of mission	Gridded ground surface heights, canopy height and canopy cover estimates	Products released annually at a coarse resolution (e.g. 0.5 deg. tiles, TBD). End of mission high resolution (~1-2km)
19/ L4	Ocean MSS	Gridded monthly	Gridded ocean height product including coastal areas. TBD grid size. TBD merge with Sea Ice SSH	Monthly

20/ L4	Arctic and Antarctic Gridded Sea Ice Freeboard/	Gridded monthly; separate Arctic and Antarctic products	Gridded sea ice freeboard. (TBD length scale)	Aggregate for entire month for each polar region
--------	---	---	---	--

File ID/Level	Product Name	Concept	Short Description	Frequency
21/ L4	Arctic Gridded Sea Surface Height within Sea Ice/ Antarctic Gridded Sea Surface Height within Sea Ice	Aggregate for entire month (all sea surface heights within a grid) separate Arctic and Antarctic products	Gridded monthly sea surface height inside the sea ice cover. TBD grid	Aggregate for entire month for each polar region
Experimental	Arctic Sea Ice Thickness / Antarctic Sea Ice Thickness	Per Pass Thickness samples (from 10-100m freeboard means) for every 10 km (TBD) segment (all beams) where leads are available; (per pass)	Sea ice thickness estimates derived from the sea ice freeboard product. External input: snow depth and density for each pass.	There will be files for each polar region per day
Experimental	Arctic Gridded monthly Sea Ice Thickness / Antarctic Gridded monthly Sea Ice Thickness	Aggregate for entire month (all thickness observations within a grid) plus Thickness (corrected for growth)	Gridded sea ice thickness product; centered at mid-month. Include thickness with or without adjustment for ice growth (based on time differences between freeboard observation).	Gridded monthly (all thickness observations within a grid) for each polar region
Experimental	Lake Height	Along reference track per beam in Pan-Arctic basin (>50-60 deg N).	Extracted from Product 08 and 13, for lakes >10 km <sup>2</sup> , with slope and aspect. Ice on/off flag. TBD water mask developed from existing masks.	Monthly along track product, no pointing
Experimental	Snow Depth	Along reference track per beam for Pan-Arctic basin (>50-60 deg N).	Extracted from Product 08 and 13 along track repeat heights, with slope and aspect. Snow detection flag.	Monthly along track product, no pointing



## APPENDIX B: Sea State Bias Computations for a Photon Counting Lidar

For ICESat-2, we are looking over all the received surface photon heights to get a received height distribution and then deconvolving the instrument impulse response to get the surface height distribution. If we are getting a disproportionate share of photons back from the wave crests or troughs because of a difference in reflectance between crests and troughs, the correlation of height and reflectance (or in this case rate of photon returns) and the sea state bias it causes are unknown to us. However, if as a separate step we take advantage of the fine spatial resolution of ICESat-2 to obtain along-track distance bin average estimates of height and photon return rate unbiased by the number of photons in the bins, and over bins that are short compared to the dominate surface wavelength, we can estimate the sea state bias in the surface height distribution using the relation of *Arnold et al.* [1995]. To do this we need to consider the *Arnold et al.* relation in terms of bin averages rather than aggregate photon averages.

First we establish the relation between average height computed over all surface photons and the average taken over all photons grouped in  $K$  along-track distance bins. The photon average sea surface height is the sum the heights of  $N$  surface reflected photons divided by  $N$ :

$$H_{\text{photonavg}} = \frac{1}{N} \sum_{i=1}^N \eta_i \quad (\text{B1})$$

However, if we express  $N$  as the sum over all  $K$  along-track bins of the number of photons grouped into each bin,  $r_j$ , we see that:

$$N = \sum_{j=1}^K r_j \quad (\text{B2})$$

Similarly, we can group the heights into the contributions from each bin

$$\sum_{i=1}^N \eta_i = \sum_{j=1}^K \sum_{l=1}^{r_j} \eta_l \quad (14- \text{B3})$$

where  $\eta_l$  is the height of the  $l^{\text{th}}$  photon in a bin with a total of  $r_j$  photons in it. Therefore, the average height over all photon heights is equal to the bin average heights weighted by the relative share of photons in each bin, combining (12-14)

$$\frac{1}{N} \sum_{i=1}^N \eta_i = \frac{1}{N} \sum_{j=1}^K \sum_{l=1}^{r_j} \eta_l = \frac{\sum_{j=1}^K \sum_{l=1}^{r_j} \eta_l}{\sum_{j=1}^K r_j} \quad (15- \text{B4})$$

In the relation of *Arnold et al.*, [1995] (9), we replace the backscatter coefficient of  $\sigma_i^0$ , by the number of photons per bin  $r_l$  as an expression of the energy returned from the surface in each bin.

SSB is the photon average or photon weighted bin average minus the true average of surface heights over all the distance bins,  $\sum_{j=1}^K \eta_j / K$  :

$$SSB = \frac{1}{N} \sum_{i=1}^N \eta_i - \frac{\sum_{j=1}^K \eta_j}{K} = \frac{\sum_{j=1}^K \sum_{l=1}^{r_j} \eta_l}{\sum_{j=1}^K r_j} - \frac{\sum_{j=1}^K \eta_j}{K} \quad (B5)$$

where  $\eta_j$  is the true average of height in the  $j^{\text{th}}$  bin not biased by the number photons, and so the second term on the right is  $\mu_\eta$ , the true arithmetic mean of surface height averaged over  $K$  bins.

$$\mu_\eta = \frac{\sum_{j=1}^K \eta_j}{K} \quad (B6)$$

The number of samples in along-track bin  $j$ , is  $r_j$ , and though the sample rate with each sample,  $\rho_j$ , is potentially different for each sample, we take  $\rho_j$  as the average sample rate in each  $\delta_x$  wide bin such that

$$\delta_x \rho_j = r_j \quad (B7)$$

The average of photon heights in each bin is

$$\bar{\eta}_j = \frac{1}{r_j} \sum_{l=1}^{r_j} \eta_l \quad (B8)$$

So

$$r_j \bar{\eta}_j = \sum_{l=1}^{r_j} \eta_l \quad (B9)$$

and (B5) becomes

$$SSB = \frac{\sum_{j=1}^K r_j \bar{\eta}_j}{\sum_{j=1}^K r_j} - \frac{\sum_{j=1}^K \eta_j}{K} \quad (B10)$$

and with (B6), (B10) becomes

$$SSB = \frac{\sum_{j=1}^K r_j \bar{\eta}_j}{\sum_{j=1}^K r_j} - \mu_\eta = \frac{\sum_{j=1}^K r_j \bar{\eta}_j - \sum_{j=1}^K r_j \mu_\eta}{\sum_{j=1}^K r_j} = \frac{\sum_{j=1}^K r_j (\bar{\eta}_j - \mu_\eta)}{\sum_{j=1}^K r_j} \quad (B11)$$

This looks like the same relation as (9) by *Arnold et al.* [1995] but it is a little unclear if Arnold et al meant to use the backscatter coefficient in his equation or the variation in backscatter coefficient about the mean. To check this for our relation we break height and return rate in  $\frac{\sum_{j=1}^K \sum_{l=1}^{r_j} \eta_l}{\sum_{j=1}^K r_j}$  into mean, ( $\mu$ ) and time varying (primed) components. Speaking

of the along-track bin quantities,  $\bar{\eta}_j = \mu_\eta + \eta_j'$  and  $r_j = \mu_{r_j} + r_j'$ . From (B9):

$$\frac{1}{N} \sum_{i=1}^N \eta_i = \frac{1}{N} \sum_{j=1}^K \sum_{l=1}^{r_j} \eta_l = \frac{\sum_{j=1}^K \sum_{l=1}^{r_j} \eta_l}{\sum_{j=1}^K r_j} = \frac{\sum_{j=1}^K r_j \bar{\eta}_j}{\sum_{j=1}^K r_j} \quad (B12)$$

If the along-track bins are small enough so that the sea surface height variation within a bin is much smaller than the variation of height between bins (bins are small compared to the wavelength of the dominant waves), we can assume that the average of photon heights within bin,  $\bar{\eta}_j$ , equals the true average of height within a bin,  $\eta_j$ , and the true average height is equal to the average of  $\bar{\eta}_j$  over all bins.

$$\mu_\eta = \frac{\sum_{j=1}^K \eta_j}{K} = \frac{\sum_{j=1}^K \bar{\eta}_j}{K} \quad (B13)$$

This assumption is equivalent to saying the bias due to variation of the number of photons within bins is small compared to the bias due to the differences in the number of photons among bins. Similarly, the average photon rate,  $\mu_\rho$ , is

$$\mu_\rho = \frac{\sum_{j=1}^K r_j}{K} \quad (\text{B14})$$

Applying (B9) to (B4) and breaking into mean and varying parts

$$\begin{aligned} \frac{1}{N} \sum_{i=1}^N \eta_i &= \frac{\sum_{j=1}^K \sum_{l=1}^{r_j} \eta_l}{\sum_{j=1}^K r_j} = \frac{\sum_{j=1}^K r_j \bar{\eta}_j}{\sum_{j=1}^K r_j} = \frac{\sum_{j=1}^K r_j \eta_j}{\sum_{j=1}^K r_j} = \frac{\sum_{j=1}^K (r_j \eta_j + \mu_r \mu_\eta)}{\sum_{j=1}^K r_j} \\ &= \frac{\sum_{j=1}^K (r_j \eta_j + r_j \mu_\eta + \mu_r \eta_j + \mu_r \mu_\eta)}{\sum_{j=1}^K r_j} \\ &= \frac{\sum_{j=1}^K (r_j \eta_j + \mu_r \mu_\eta)}{\sum_{j=1}^K r_j} + \frac{K \mu_r \mu_\eta}{\sum_{j=1}^K r_j} = \frac{\sum_{j=1}^K (r_j \eta_j)}{\sum_{j=1}^K r_j} + \mu_\eta \end{aligned} \quad (\text{B15})$$

So in fact the product in the SSB expression of *Arnold et al.* (1995) is the product of the variations in distance bin photon rate and photon height:

$$SSB = \frac{\sum_{j=1}^K (r_j \eta_j)}{\sum_{j=1}^K r_j} \quad (\text{B16})$$

Alternatively, consider breaking down (B11)

$$SSB = \frac{\sum_{j=1}^K r_j \bar{\eta}_j}{\sum_{j=1}^K r_j} - \mu_\eta = \frac{\sum_{j=1}^K r_j \bar{\eta}_j - \sum_{j=1}^K r_j \mu_\eta}{\sum_{j=1}^K r_j} = \frac{\sum_{j=1}^K r_j (\bar{\eta}_j - \mu_\eta)}{\sum_{j=1}^K r_j} \quad (\text{B17})$$

with,  $\bar{\eta}_j = \mu_\eta + \eta_j'$  and  $r_i = \mu_r + r_j'$ .

$$SSB = \frac{\sum_{j=1}^K r_j \bar{\eta}_j}{\sum_{j=1}^K r_j} - \mu_\eta = \frac{\sum_{j=1}^K (r_j' + \mu_r)(\eta_j' + \mu_\eta)}{\sum_{j=1}^K r_j} - \mu_\eta = \frac{\sum_{j=1}^K (r_j' \eta_j')}{\sum_{j=1}^K r_j} + \mu_\eta - \mu_\eta = \frac{\sum_{j=1}^K (r_j' \eta_j')}{\sum_{j=1}^K r_j} \quad (B18)$$

consistent with (B16).

We propose that there is a sea state bias in the higher moments also. If we consider higher sample  $n^{\text{th}}$  moments of height

$$M(n) = \frac{\sum_{j=1}^K (\eta_j - \mu_\eta)^n}{K} = \frac{\sum_{j=1}^K g_j(n)}{K} \quad (B19)$$

As with (B15):

$$\begin{aligned} M(n) &= \frac{1}{N} \sum_{i=1}^N g_i(n) = \frac{\sum_{j=1}^K \sum_{l=1}^{r_j} g_j(n)}{\sum_{j=1}^K r_j} = \frac{\sum_{j=1}^K r_j \bar{g}_j(n)}{\sum_{j=1}^K r_j} = \frac{\sum_{j=1}^K r_j g_j(n)}{\sum_{j=1}^K r_j} = \frac{\sum_{j=1}^K (r_j' + \mu_r)(g_j(n) + \mu_g)}{\sum_{j=1}^K r_j} \\ &= \frac{\sum_{j=1}^K (r_j' g_j(n) + r_j' \mu_g + \mu_r g_j(n) + \mu_r \mu_g)}{\sum_{j=1}^K r_j} \\ &= \frac{\sum_{j=1}^K (r_j' g_j(n) + \mu_r \mu_g)}{\sum_{j=1}^K r_j} = \frac{\sum_{j=1}^K (r_j' g_j(n)')}{\sum_{j=1}^K r_j} + \frac{K \mu_r \mu_g}{\sum_{j=1}^K r_j} = \frac{\sum_{j=1}^K (r_j' g_j(n)')}{\sum_{j=1}^K r_j} + \mu_g \end{aligned}$$

Thus, the  $(\eta_j - \mu_\eta)^n$ ,  $n^{\text{th}}$  moment, would have a similar derivation for their sea state bias,  $SSBM(n)$ :

$$SSBM(n) = \frac{\sum_{j=1}^K r_j ((\eta_j - \mu_\eta)^n - \text{avg}(\eta_j - \mu_\eta)^n)}{\sum_{j=1}^K r_j} \quad (\text{B20})$$

## APPENDIX C: Expectation-Maximization (EM) Procedure

From Appendix E of ATBD ATL07

EM algorithm for estimating the parameters of two-component normal mixtures  
 The EM algorithm estimates the parameters of a two-component normal mixture that best describe a distribution of random variables (*Dempster et al., 1977; Bilmes, 1998*).  
 The two-component mixture model:

$$f(x_i) = \alpha\phi_i(x_i; \mu_1, \sigma_1) + (1 - \alpha)\phi_2(x_i; \mu_2, \sigma_2)$$

$$\phi_i(x; \mu_i, \sigma_i) = \frac{1}{\sqrt{2\pi\sigma_i}} e^{-\frac{(x-\mu_i)^2}{2\sigma_i^2}} \quad (\text{Normal Distribution})$$

The EM steps to compute the parameters of the mixture model with  $T$  random variates  $x_t(\alpha, \mu_1, \sigma_1, \mu_2, \sigma_2)$  are:

1. Initialize with:  $\alpha, \mu_1, \sigma_1, \mu_2, \sigma_2$
2. Expectation (E) step: compute:

$$\gamma_i = \frac{\alpha\phi_i(x_t; \mu_1, \sigma_1)}{\alpha\phi_i(x_t; \mu_1, \sigma_1) + (1 - \alpha)\phi_2(x_t; \mu_2, \sigma_2)}$$

for  $t = 1, \dots, T$ .

3. Maximization (M) step. compute:

$$\mu_1 = \frac{\sum_{t=1}^T \gamma_t x_t}{\sum_{t=1}^T \gamma_t}, \quad \sigma_1^2 = \frac{\sum_{t=1}^T \gamma_t (x_t - \mu_1)^2}{\sum_{t=1}^T \gamma_t}$$

$$\mu_2 = \frac{\sum_{t=1}^T (1 - \gamma_t) x_t}{\sum_{t=1}^T (1 - \gamma_t)}, \quad \sigma_2^2 = \frac{\sum_{t=1}^T (1 - \gamma_t) (x_t - \mu_2)^2}{\sum_{t=1}^T (1 - \gamma_t)}, \text{ and}$$

$$\alpha = \sum_{t=1}^T \frac{\gamma_t}{T}$$

Iterate E and M steps until parameters converge.

## 11.0 REFERENCES

- Arnold, D. V., W. K. Melville, R. H. Stewart, J. A. Kong, W. C. Keller, and E. Lamarre (1995), Measurements of electromagnetic bias at Ku and C bands, *J. Geophys. Res.*, *100*(C1), 969-980.
- Carrère, L., and F. Lyard (2003), Modeling the barotropic response of the global ocean to atmospheric wind and pressure forcing - comparisons with observations.
- Chambers, D. P., S. A. Hayes, J. C. Ries, and T. J. Urban (2003), New TOPEX sea state bias models and their effect on global mean sea level, *J. Geophys. Res.*, *108*(C10), 3305.
- Chapron, B., V. Kerbaol, D. Vandemark, and T. Elfouhaily (2000), Importance of peakedness in sea surface slope measurements and applications, *J. Geophys. Res.*, *105*(C7), 17195-17202.
- Cox, C., and W. Munk (1954), Measurement of the Roughness of the Sea Surface from Photographs of the Sun's Glitter, *J. Opt. Soc. Am.*, *44*(11), 838-850.
- Elfouhaily, T., D. R. Thompson, B. Chapron, and D. Vandemark (2000), Improved electromagnetic bias theory, *J. Geophys. Res.*, *105*(C1), 1299-1310.
- Gaspar, P., F. Ogor, P.-Y. Le Traon, and O.-Z. Zanife (1994), Estimating the sea state bias of the TOPEX and POSEIDON altimeters from crossover differences, *J. Geophys. Res.*, *99*(C12), 24981-24994.
- Hausman, J., and V. Zlotnicki (2010), Sea State Bias In Radar Altimetry Revisited, , *Marine Geodesy*, *33*(S1), 336---347.
- Markus, T., et al. (2016), The Ice, Cloud, and land Elevation Satellite-2 (ICESat-2): Science 1 requirements concept, and implementation., *Remote Sensing of the Environment*, in press.
- Menzies, R. T., D. M. Tratt, and W. H. Hunt (1998), Lidar In-Space Technology Experiment Measurements of Sea Surface Directional Reflectance and the Link to Surface Wind Speed, *Appl. Opt.*, *37*(24), 5550-5559.
- Plant, W. J. (2015a), Short wind waves on the ocean: Long-wave and windspeed dependences, *J. Geophys. Res. Oceans*, *120*, 6436-6444.
- Plant, W. J. (2015b), Short wind waves on the ocean: Wavenumber-frequency spectra, *J. Geophys. Res. Oceans*, *120*, 2147-2158.
- Urban, T. J., and B. E. Schutz (2005), ICESat sea level comparisons, *Geophys. Res. Lett.*, *32*(23), L23S10.
- Vandemark, D., B. Chapron, T. Elfouhaily, and J. W. Campbell (2005), Impact of high-frequency waves on the ocean altimeter range bias, *J. Geophys. Res.*, *110*(C11), C11006.
- Wu, J. (1972), Sea-Surface Slope and Equilibrium Wind-Wave Spectra, *Physics of Fluids*, *15*(5), 741-747.